haematologica
Journal of the Ferrata Storti Foundation

A novel *KMT2A::AFF1*-derived fusion circRNA regulates mitochondrial metabolism in t(4;11) B-cell acute lymphoblastic leukemia

by Doron Tolomeo, Michela Bardini, Santina Venuto, Grazia Visci, Angelo Lonoce, Lucrezia Calamo, Ingrid Cifola, Marco Severgnini, Maria Mastrodonato, Daniela Semeraro, Luigia Valsecchi, Mario Mauri, Roberta La Starza, Martina Lucarelli, Amalia Azzariti, Simona Serrati, Anna Ferrari, Giorgia Simonetti, Giovanni Martinelli, Nicola Santoro, Monica Fumagalli, Gaia Di Timoteo, Ilaria Saltarella, Martina Milani, Orietta Spinelli, Nicoletta Bertorello, Giovanni Cazzaniga, Grazia Fazio and Clelia Tiziana Storlazzi

Received: December 30, 2025.
Accepted: July 31, 2026.

Citation: Doron Tolomeo, Michela Bardini, Santina Venuto, Grazia Visci, Angelo Lonoce, Lucrezia Calamo, Ingrid Cifola, Marco Severgnini, Maria Mastrodonato, Daniela Semeraro, Luigia Valsecchi, Mario Mauri, Roberta La Starza, Martina Lucarelli, Amalia Azzariti, Simona Serratì, Anna Ferrari, Giorgia Simonetti, Giovanni Martinelli, Nicola Santoro, Monica Fumagalli, Gaia Di Timoteo, Ilaria Saltarella, Martina Milani, Orietta Spinelli, Nicoletta Bertorello, Giovanni Cazzaniga, Grazia Fazio and Clelia Tiziana Storlazzi.
A novel KMT2A::AFF1-derived fusion circRNA regulates mitochondrial metabolism in t(4;11) B-cell acute lymphoblastic leukemia.
Haematologica. 2026 Aug 13. doi: 10.3324/haematol.2025.300437 [Epub ahead of print]

A novel *KMT2A::AFF1*-derived fusion circRNA regulates mitochondrial metabolism in t(4;11) B-cell acute lymphoblastic leukemia

Doron Tolomeo[1*], Michela Bardini[2*], Santina Venuto[1], Grazia Visci[1], Angelo Lonoce[1], Lucrezia Calamo[1], Ingrid Cifola[3], Marco Severgnini[3], Maria Mastrodonato[1], Daniela Semeraro[1], Luigia Valsecchi[2], Mario Mauri[4], Roberta La Starza[5], Martina Lucarelli[5], Amalia Azzariti[6], Simona Serratì[6], Anna Ferrari[7], Giorgia Simonetti[7], Giovanni Martinelli[8], Nicola Santoro[9], Monica Fumagalli[2], Gaia Di Timoteo[10], Ilaria Saltarella[11], Martina Milani[12], Orietta Spinelli[12], Nicoletta Bertorello[13], Giovanni Cazzaniga[2,14], Grazia Fazio[2,14#], Clelia Tiziana Storlazzi[1#]

1. Department of Biosciences, Biotechnologies, and Environment, University of Bari Aldo Moro, Bari, Italy

2. Tettamanti Center, Fondazione IRCCS San Gerardo dei Tintori, Monza, Italy

3. Institute for Biomedical Technologies (ITB), National Research Council (CNR), Segrate, Italy.

4. School of Medicine and Surgery, University of Milano-Bicocca, Milan, Italy

5. Hematology and Bone Marrow Transplantation Section, Department of Medicine and Surgery, University of Perugia, Centro di Ricerche EmatoOncologiche, Azienda di Perugia, Perugia, Italy

6. IRCCS Istituto Tumori "Giovanni Paolo II", Bari, Italy

7. Biosciences Laboratory, IRCCS Istituto Romagnolo per lo Studio dei Tumori (IRST) "Dino Amadori", Meldola (FC), Italy

8. Department of Hematology and Oncology Sciences, Institute of Hematology "L. and A. Seràgnoli", S. Orsola University Hospital, Bologna, Italy

9. Pediatric Oncology AOUC of Policlinico of Bari, Bari, Italy

10. Department of Biology and Biotechnology Charles Darwin, Sapienza University of Rome, Rome, Italy

11. Department of Precision and Regenerative Medicine and Ionian Area (DIMEPRE-J), Section of Pharmacology, School of Medicine, University of Bari Aldo Moro, Bari, Italy

12. Hematology and Bone Marrow Transplant Unit, Ospedale Papa Giovanni XXIII, Bergamo, Italy

13. Pediatric Onco-Hematology Department, Regina Margherita Children's Hospital, Turin, Italy

14. School of Medicine and Surgery, University of Milano-Bicocca, Milan, Italy.

* equally contributing first authors

# equally contributing last authors

Correspondence to: Prof. Clelia Tiziana Storlazzi (cleliatiziana.storlazzi@uniba.it), PhD, Department of Biosciences, Biotechnology, and Environment, University of Bari Aldo Moro, Via E. Orabona no.4, 70125 Bari (Italy)

Dr. Doron Tolomeo (doron.tolomeo@uniba.it), PhD, Department of Biosciences, Biotechnology, and Environment, University of Bari Aldo Moro, Via E. Orabona no.4, 70125 Bari (Italy)

Running heads: A novel *KMT2A::AFF1* f-circRNA impacts mitochondrial metabolism in B-ALL

Data availability statement: Raw sequence data and gene counts are available in the GEO repository under Accession Number GSE304109. Data used for the analyses are available upon reasonable request.

Funding statement: This work was supported by Unione Europea "National Center for Gene Therapy and Drugs based on RNA Technology", PNRR missione 4 – componente 2 – investimento 1.4, cod. prog. CN00000041- CUP H93C22000430007" to CTS.

Permission to reproduce material from other sources: Not applicable

Clinical trial registration: Not applicable

Author Contributions: DT, MB, GF, and CTS conceived the study and wrote the manuscript, with the assistance of GC. MB, GC, and GF provided established cell lines for the study. GF, DT, LV, and SV performed cell culturing. DT and SV carried out cell transfection assays. IS performed cell electroporation experiments. GF performed total RNA sequencing. IC and MS analyzed RNA sequencing data and performed bioinformatics analyses. AL, GV, DT, and LC performed semiquantitative PCR experiments. DT and SV performed RT-qPCR experiments and cell death analysis. MMau carried out confocal microscopy analyses. LV and MB performed Seahorse profiling and interpreted the data. DT performed subcellular fractionation under the supervision of GDT. DS and MMas performed electron transmission microscopy analysis. SS and AA performed extracellular vesicle isolation and RNA extraction. GF, GC, NS, MF, RLS, ML, AF, GS, MMi, OS, NB, and GM provided patient biological samples and clinical data. All authors read and approved the final manuscript.

Conflict of Interest: The authors affiliated to the IRCCS Istituto Tumori "Giovanni Paolo II", Bari, are responsible for the views expressed in this article, which do not necessarily represent the institute.

Abstract

The t(4;11) translocation, which drives *KMT2A::AFF1* fusion gene expression, is associated with poor prognosis in pediatric and adult B-cell Acute Lymphoblastic Leukemia (B-ALL). *KMT2A::AFF1* fusion circular RNAs (f-circRNAs) have been identified in B-ALL, though their contribution to leukemia has not yet been outlined. We identified a novel recurrent *KMT2A::AFF1*-derived back-splicing junction joining *AFF1* exon 7 to *KMT2A* exon 3 (AK_7_3) in SEM, RS4;11, and ALL-PO B-ALL cell lines, all of which carry the t(4;11)(q24;q23)/*KMT2A::AFF1* translocation. This sequence was observed in RT-PCR products encompassing two splicing variants of *KMT2A* exon 4, which are also present in the linear *KMT2A::AFF1* chimera. AK_7_3 was also found in 12/18 pediatric and 17/24 adult t(4;11)-positive B-ALL patients, including three paired diagnosis/relapse samples, whereas it was absent in 23 t(4;11)-negative B-ALL patients. Whole-transcriptome analysis of AK_7_3-knockdown SEM cells identified upregulated genes involved in oxidative stress response and regulation of apoptosis. Cell death analysis confirmed the pro-apoptotic impact of AK_7_3 silencing. Confocal analyses, Seahorse bioenergetic profiling, and electron microscopy revealed an overproduction of reactive oxygen species, increased mitochondrial membrane potential, mitochondrial respiration, and dysmorphic mitochondria after AK_7_3 knockdown in *KMT2A::AFF1* cell lines.

In summary, we identified AK_7_3 as a novel f-circRNA back-splicing junction recurrent in t(4;11)-positive B-ALL patients at both diagnosis and relapse. Our data provide evidence for a functional role of this molecule as an anti-apoptotic agent that affects mitochondrial function, suggesting its potential involvement in *KMT2A::AFF1*-driven B-ALL leukemogenesis.

Keywords: B-ALL, t(4;11), fusion circular RNA, *KMT2A*, *AFF1*, mitochondrial metabolism

Introduction

Circular RNAs (circRNAs) recently emerged as a large class of non-coding RNAs with key roles in cancer development and progression[1]. Back-splicing events generate circular transcripts with higher cellular stability than their cognate linear counterparts. The functions of these molecules, as well as the regulatory mechanisms underlying their biogenesis, remain only partially elucidated. Specifically, circRNAs may function as microRNA (miRNA) sponges, transcriptional regulators of oncogenes and tumor suppressor genes, or protein-coding transcripts. Interestingly, some circRNAs have recently been reported to induce recurrent chromosomal rearrangements involving the *Lysine methyltransferase 2A* gene (*KMT2A*, previously known as *MLL*), a gene frequently rearranged in acute leukemias[2].

CircRNAs can also be generated by the back-splicing of linear fusion transcripts[3], resulting in fusion-circular RNAs (f-circRNAs). In hematological malignancies, particularly in acute myeloid leukemia (AML), f-circRNAs originating from back-splicing of *PML::RARA* and *KMT2A::MLLT3* linear fusion transcripts have been reported in patients and cell lines and have been shown to have pro-proliferative and oncogenic properties[4]. Moreover, f-circRNAs originating from the *KMT2A::AFF1* fusion gene, arising from the reciprocal t(4;11) chromosomal translocation, and joining the *KMT2A* gene (mapped on chromosome 11q23.3) to the *AFF1* gene (*ALF transcription elongation factor 1*, mapped on chromosome 4q21.3-q22.1), were recently identified from RNA-seq data in B-cell precursor acute lymphoblastic leukemia (B-ALL) patients[5]. While the *KMT2A::AFF1* fusion is rare in AML (0.8%) and exceptionally rare in T-cell ALL, it is almost exclusively associated with B-ALL (56.5%), accounting for 82.7%, 48.3%, and 40.6% of infant, adult, and pediatric patients, respectively[6, 7]. Clinically, the presence of a *KMT2A* gene rearrangement in

B-ALL is a poor prognostic factor, associated with chemoresistance, early relapse, and a dismal outcome[8]. In particular, the *KMT2A::AFF1* fusion protein drives leukemogenesis by deregulating genes with oncogenic potential, such as *HOXA*, *MEIS1*, *MYC*, and *BCL2*[9]. Therefore, a comprehensive understanding of the transcriptional consequences of t(4;11) is essential for elucidating the disease biology and improving the therapeutic management of B-ALL.

A previous study identified a specific *KMT2A::AFF1* f-circRNA isoform joining *AFF1* exon 2 to *KMT2A* exon 11 in the RS4;11 B-ALL cell line, as well as six distinct *KMT2A::AFF1* f-circRNAs in patients[5]. However, these findings lacked wet-lab validation by RT-PCR and Sanger sequencing in patients. Furthermore, the recurrence of *KMT2A::AFF1* f-circRNAs in t(4;11)-positive samples, as well as their functional role in leukemogenesis, remains unexplored, leaving a knowledge gap regarding the biological significance of these molecules.

In this context, we aimed to explore and validate the expression of f-circRNAs in *KMT2A::AFF1*-positive B-ALL cell lines and primary clinical samples, using several complementary experimental approaches to understand their function and to gain new insights into the pathogenic mechanisms underlying *KMT2A::AFF1*-rearranged B-ALL. Importantly, we identified a back-splicing junction for candidate *KMT2A::AFF1* f-circRNAs, which we validated in pediatric and adult B-ALL patients. By knocking down this back-splicing junction in two cell line models, we unraveled the biological effects of its downregulation in *KMT2A::AFF1* B-ALL, suggesting a potential role in mitochondrial function and apoptosis regulation.

Methods

Cell lines

Three *KMT2A::AFF1* positive B-ALL cell lines were used in this study: SEM (derived from a pediatric patient at relapse), ALL-PO (derived from an infant patient at diagnosis), and RS4;11 (derived from an adult patient at relapse). SEM harbors the *KMT2A::AFF1* (5'→3') linear fusion transcript, joining *KMT2A* exon 9 (NM_001412597.1) to *AFF1* exon 4 (NM_005935.4)[10, 11]. RS4;11 shows the fusion of *KMT2A* exon 10 to *AFF1* exon 4[12], and ALL-PO two splicing variants joining *KMT2A* exons 10 or 11 to *AFF1* exon 4 (personal communication). The B-ALL cell line NALM6, lacking the t(4;11) translocation, was used as a negative control. SEM (ACC 546), RS4;11 (ACC 508), and NALM6 (ACC 128) cell lines were purchased from DSMZ (Braunschweig, Germany) (https://webshop.dsmz.de/), whereas the ALL-PO cell line was previously established by serial transplantation in SCID mice[13]. All cell lines were grown in RPMI-1640 complete medium (Euroclone, Pero, Italy) supplemented with 10% Fetal Bovine Serum (FBS) (Euroclone), except ALL-PO cells, which were grown in Advanced RPMI-1640 medium (Thermo Fisher Scientific, Waltham, Massachusetts, USA).

Patient samples

The study included 65 subjects: 18 pediatric and 24 adult *KMT2A::AFF1*-positive B-ALL patients, as well as 20 pediatric and three adult B-ALL patients without the fusion, used as control samples (Online Supplementary Table S1). Pediatric patients were enrolled in the AIEOP-BFM studies (EudraCT Number AIEOP-BFM ALL 2009: 2007-004270-43 and AIEOP-BFM ALL 2017: 2016-001935-12); adult patients were enrolled in the TRINEG-ALL, INTHEMA, NILG-ALL 09/00 and 10/17, GIMEMA ALL2418, and Hemaomics studies. For one patient (no. 45), three follow-up samples were analyzed. For two pediatric (nos. 3 and 7) and one adult (no. 43)

patients, paired diagnosis/relapse samples were available. For patients nos. 3 and 7, relapse was defined by molecular analysis of minimal residual disease (MRD) by RT-qPCR using patient-specific IG/TR markers and/or the *KMT2A::AFF1* genomic breakpoint, with MRD levels of 7.8×10^{-1} and 1.8×10^{0}, respectively. The study was conducted in compliance with the Declaration of Helsinki and was approved by the local Ethics Committee of San Gerardo Hospital, Monza, Italy (Prot. No. 1369/2010 and 2941/2019 and the related local informed consent ASG-MA-052A for adult subjects); Comitato Etico della Romagna (CEROM), Meldola (FC), Italy (Prot. No. 5244/2019, 5710/2020, 5805/2019, 106/2021); Comitato Etico Indipendente di Area Vasta Emilia Centro (CE-AVEC), Bologna, Italy (Prot. No. 112/2014/U/Tess); Comitato etico ASST Papa Giovanni XXIII, Bergamo, Italy (NILG-ALL 09/00 Prot. No. 298, NILG-ALL 10/17 Prot. No. 122, and GIMEMA ALL2418 Prot. No. 1800). All subjects involved provided signed informed consent.

Additional methods used in this study are described in the *Online Supplementary Appendix.*

Statistical analysis

RT-qPCR data were analyzed using the REST relative expression software tool[14]. Total RNA-seq data were analyzed using the DESeq2 Bioconductor/R package and the Wald test for two-group comparisons, with the Benjamini-Hochberg (BH) method for multiple testing correction, as stated in the "Total RNA-sequencing library preparation and bioinformatics data analysis" paragraph (see *Online Supplementary Appendix*).

Data obtained from confocal microscopy, cell death analysis and Seahorse profiling were analyzed with unpaired t-test, and data were expressed as mean ± standard

deviation (SD) of technical/biological replicates. Bar graphs were generated with GraphPad Prism software.

Results

Identification of *KMT2A::AFF1* f-circRNA in B-ALL cell lines

To investigate the occurrence of any f-circRNAs arising from *KMT2A::AFF1*, we used divergent primers flanking the linear RNA fusion junction, with the forward primer mapping on the *AFF1* exon 7 and a reverse primer on the *KMT2A* exon 5 (Figure 1A), in RT-PCR assays on RNAs from B-ALL cell lines and on a commercial pooled bone marrow (BM) RNA sample. A 374 bp product was obtained from both RNase R-treated and untreated RNA from the SEM cell line harboring the t(4;11) translocation, whereas no product was detectable on RNAs from the *KMT2A::AFF1*-negative NALM6 B-ALL cell line or the commercial BM, regardless of the RNase R treatment (Figure 1B). Sanger sequencing disclosed the presence of a junction between *AFF1* exon 7 and *KMT2A* exon 3 (Figure 1B). As this fusion junction is not compatible with a linear reciprocal *AFF1::KMT2A* (5'→3') transcript product, considering the exons involved, this sequence, hereafter referred to as AK_7_3, corresponds to a back-splicing junction of a novel f-circRNA. RT-qPCR assays on SEM cell line showed that the expression level of the back-splicing fusion junction does not decrease after RNase R treatment, unlike what we observed for the linear *KMT2A::AFF1* and the *GAPDH* reference transcript under the same conditions (Figure 1C), therefore corroborating the circular nature of the targeted transcript, and, thus, the identification of a novel f-circRNA.

Interestingly, the 374 bp sequenced PCR product revealed that *KMT2A* exon 3 was spliced to a shorter variant of exon 4, compared to that of the NM_001412597.1

isoform (137 bp instead of 2,654 bp in length) already described in the literature[15] and reported in the latest release of the UCSC Genome Browser (T2T CHM13v2.0/hs1) in the *KMT2A* transcript variant with Accession Number XM_054368833.1 (Figure 1B, D).

Notably, the AK_7_3 back-splicing junction was also identified in an alternative f-circRNA, harboring a canonical *KMT2A* exon 3::exon 4 splicing junction (Figure 1 E).

We extended our PCR analyses, using a different primer combination (see the Online Supplementary Methods section), to two additional B-ALL cell lines, both harboring the t(4;11) translocation: the adult RS4;11 cell line and the pediatric ALL-PO cell line, revealing f-circRNAs involving the same AK_7_3 back-splicing junction (Online Supplementary Figure S1A, B).

Similarly to what was observed in the SEM cells, the co-existence of two f-circRNA isoforms with the same AK_7_3 back-splicing junction but two different *KMT2A* exon 3::exon 4 splicing junctions was evidenced also in RS4;11 and ALL-PO by additional RT-PCR experiments (see Online Supplementary Methods section) (Online Supplementary Figure S1C,D). Of note, a *5'KMT2A::3'AFF1* linear fusion transcript isoform harboring the shorter *KMT2A* exon 4 variant was also validated in the three cell lines, by RT-PCR and Sanger sequencing (Online Supplementary Figure S2).

AK_7_3 expression quantification in the three *KMT2A*-rearranged (*KMT2A*-r) cell lines revealed the highest expression in the SEM cell line (Online Supplementary Figure S3A). RT-qPCR assays on nuclear and cytoplasmic RNA fractions evidenced that AK_7_3 was localized in the cytoplasmic compartment for all the cell lines analyzed (Online Supplementary Figure S3B, D).

Furthermore, to test the potential wrapping of AK_7_3 in secreted extracellular vesicles (EVs), we performed RT-PCR analysis of RNA samples extracted from EVs released by SEM and RS4;11 cells. The results excluded the presence of the f-circRNAs containing AK_7_3, as well as of the linear *KMT2A::AFF1* transcripts, in EVs from both cell lines (Online Supplementary Figure S3E).

AK_7_3 is selectively expressed in B-ALL patients with the t(4;11) translocation

We tested the occurrence of the *KMT2A::AFF1* back-splicing junction in 42 t(4;11)-positive B-ALL patients (18 pediatric and 24 adult cases), including paired diagnosis/relapse samples when available (Online Supplementary Table S1).

We found that AK_7_3 was present in 12 out of 18 (66.6%) diagnostic or relapse samples from pediatric B-ALL patients and in 17 out of 24 (70.8%) diagnostic or relapse samples from adult B-ALL patients harboring the t(4;11) translocation (Figure 2; Online Supplementary Figure S4, S5).

For two pediatric patients (nos. 3 and 7), the paired diagnostic and relapse samples were available. In both these patients, the percentage of leukemic blasts was similar at diagnosis and relapse (94% and 84%, respectively, for patient no. 3; 65% and 80%, respectively, for patient no. 7) (Online Supplementary Table S1), and the paired diagnostic and relapse samples presented with stable clonality (as the same IG/TR clonal markers identified at diagnosis were also found at relapse, data not shown). Interestingly, in both cases, AK_7_3 expression persisted at relapse, albeit at lower levels than in their corresponding diagnostic samples (Figure 2). In contrast, in the adult patient no. 43, no AK_7_3 expression was detected at either diagnosis or relapse, while patient no. 45 resulted positive for AK_7_3 at diagnosis, but was negative in all three follow-up samples collected within 1 year from diagnosis (Figure

2, Online Supplementary Table S1). At the same time point, the linear *KMT2A::AFF1* transcript was assessed as positive at a lower level (10^{-3}) relative to its diagnostic sample (RT-qPCR analysis, data not shown).

Furthermore, we investigated the occurrence of the two f-circRNA splicing variants in patients carrying AK_7_3. Our results indicated that all AK_7_3-positive patients were carriers of the canonical *KMT2A* exon 3::exon 4 splicing junction (Online Supplementary Figures S6A, S7). Conversely, the short *KMT2A* exon 4 variant was observed only in a portion of patients (20 out of 29, 69%); in detail, we did not find it in the relapse of the pediatric patient no.3 (3r), the pediatric patients nos. 15, 16, 18, and the adult patients no. 45, 49, 54, 59, and 60 (Supplementary Figures S6B, S8, S9). Interestingly, the RT-qPCR analysis of 20 pediatric and three adult B-ALL patients not carrying the t(4;11) translocation, including samples with a normal karyotype or harboring the t(12;21) translocation or other rearrangements (Online Supplementary Table S1, and data not shown), indicated that the AK_7_3 back-splicing junction selectively occurs only in t(4;11)-positive B-ALL patients (Figure 2). Globally, these results suggest that f-circRNAs harboring AK_7_3 were specifically expressed in the vast majority of t(4;11)-positive B-ALL patients.

In vitro AK_7_3 knockdown affects the expression of genes involved in oxidative stress response, regulation of apoptosis, and mitochondrial metabolism.

To investigate the functional role of f-circRNAs harboring AK_7_3, we performed its knockdown (KD) in the SEM cell line with two custom-designed DsiRNAs, and compared the effects with those of cells transfected with a commercial negative control DsiRNA (DS-NC1). To identify the best interfering strategy, SEM cells were alternatively transfected with one of the two DsiRNAs (7_3a or 7_3b), as well as with

a 1:1 combo of the two molecules (7_3a+7_3b), followed by RT-qPCR on extracted total RNA. The 7_3a was the most effective DsiRNA in inducing strong downregulation of AK_7_3 expression as compared to 7_3b and the combination of the two molecules (Online Supplementary Figure S10A), without affecting the *KMT2A::AFF1* linear RNA (Online Supplementary Figure S10B). It was consequently selected for further functional studies.

Three independent biological replicates of SEM cells transfected with 7_3a DsiRNA ($SEM^{AK\_7\_3\ KD}$) and with a negative control (SEM^{NC}) were profiled for gene expression changes by using total RNA-seq technology. From the sequencing, we obtained at least 40M read pairs/sample, with a mean of 78% of reads uniquely mapping to the human genome. First, we evaluated the expression of the *KMT2A::AFF1* linear fusion transcript in $SEM^{AK\_7\_3\ KD}$ cells and SEM^{NC} cells to confirm the absence of difference in transcript expression after AK_7_3 silencing. Reads-per-million (RPM) counts over the *KMT2A::AFF1* linear junction were 0.744, 0.753, 0.632, and 0.493, 0.445, 0.705 for the three replicates of $SEM^{AK\_7\_3\ KD}$ and SEM^{NC}, respectively, suggesting that the two conditions did not show any difference in the linear fusion transcript expression (p=0.827, Mann-Whitney U-test).

Principal component analysis (PCA) showed good sample separation according to the treatment received (7_3a DsiRNA vs. DS-NC1) (Figure 3A). Differential expression analysis identified 58 differentially expressed genes (DEGs), including 53 up- and five down-regulated genes, in $SEM^{AK\_7\_3\ KD}$ cells vs. SEM^{NC} cells (Figure 3B; Online Supplementary Table S2). To explore the functional processes affected by AK_7_3 silencing, we performed functional enrichment analysis of these DEGs on Gene Ontology Biological Process (GO-BP) terms and several pathway collections (Online Supplementary Table S3). Interestingly, we found that up-regulated genes enrich

terms related to cellular response to oxidative stress, regulation of intrinsic apoptotic signaling pathway, translation, ribosome biogenesis, rRNA processing, MYC targets, as well as some metabolic pathways, such as metabolism of amino acids and derivatives, metabolism of RNA, metabolism of proteins (Figure 3C-D). On the other hand, the five down-regulated genes are mainly involved in RNA processing and mRNA trans-splicing (Figure 3C). Overall, these findings suggest that AK_7_3-silenced cells may be more sensitive to oxidative stress than control cells and may experience a general metabolic stress.

Upon detailed analysis of DEGs enriched for these processes, we identified genes previously implicated in ALL apoptosis mechanisms, such as *FAU* and *OAZ1*, whose expression increased after AK_7_3 silencing (Figure 3E).

Interestingly, among the 53 up-regulated DEGs, we identified eight genes annotated in the Broad Institute Human MitoCarta 3.0 database as encoding mitochondrial-localized proteins, namely *COX7A2, SLIRP, TUFM, HSPE1, ROMO1, CHCHD2, ATP5MC2,* and *ATP5MK* (Table 1), and localized in the mitochondrial matrix, inner membrane, or intermembrane space. They are involved in oxidative phosphorylation complexes, mtRNA metabolism, translation, protein import, and homeostasis. Specifically, in our functional enrichment analysis, we found that they participate in several functions, including cellular response to oxidative stress (*ROMO1, CHCHD2*) and organonitrogen compound biosynthetic process (*ATP5MK, ATP5MC2, TUFM*) (Figure 3E). *TUFM* and *HSPE1* also enriched the *MYC* target hallmark gene set (Online Supplementary Table S3). Moreover, we found that AK_7_3 silencing up-regulates eight known *KMT2A* target genes, namely *ARHGDIB, CD74, HLA-B, LGALS1, OAZ1, RPL31, RPL36,* and *RPS21* (Table 2).

The over-expression of *ROMO1*, *OAZ1*, *FAU*, and *COX7A2* caused by AK_7_3 silencing was validated by RT-qPCR assays in $SEM^{AK\_7\_3\ KD}$ vs. SEM^{NC} (Online Supplementary Figure S11) and, also, on an additional cellular model generated from the RS4;11 cell line ($RS4;11^{AK\_7\_3\ KD}$ vs. $RS4;11^{NC}$) which corroborated the results obtained in SEM cells (Online Supplementary Figure S12A, B).

Globally, these results suggest that f-circRNAs harboring AK_7_3 may play a functional role in the oxidative stress response, mitochondrial metabolism, and apoptosis regulation.

AK_7_3 knockdown in *KMT2A::AFF1* positive cell lines stimulates cell apoptosis, increases ROS production, and mitochondrial activity.

To validate the effects of AK_7_3 silencing in B-ALL disclosed by RNA-seq profiling in the SEM cells, we performed apoptosis analysis on $SEM^{AK\_7\_3\ KD}$ cells vs. SEM^{NC} by measuring cytoplasmic histone-associated DNA fragments. Our results showed a significant increase in apoptosis in $SEM^{AK\_7\_3\ KD}$ cells as compared to control cells (Figure 4A).

To investigate whether f-circRNAs harboring AK_7_3 may have a functional effect on t(4;11)-positive B-ALL cell metabolism, we performed confocal microscopy analyses and Seahorse bioenergetic profiling. After confirming AK_7_3 silencing by RT-qPCR (Online Supplementary Figure S13A, B), we analyzed reactive oxygen species (ROS) production and mitochondrial membrane potential (MMP) by confocal microscopy. We observed that $SEM^{AK\_7\_3\ KD}$ cells have a 1.5-fold higher production of intracellular ROS than SEM^{NC} cells, consistent with an increased oxidative phosphorylation state upon knocking down AK_7_3 expression in t(4;11)-positive B-ALL cells (Figure 4B; Online Supplementary Figure S13C). This also correlates with

a 1.5-fold increase in MMP, a marker of mitochondrial activity (Figures 4C; Online Supplementary Figure S13D), with no significant change in mitochondrial mass (Figure 4D), suggesting that AK_7_3 silencing in SEM cells leads to mitochondrial hyperactivation.

Finally, to further analyze mitochondrial function, we performed Seahorse bioenergetic profiling of $SEM^{AK\_7\_3\ KD}$ and SEM^{NC} cells with the Mito Stress Test, which enables real-time measurements of key mitochondrial parameters, including oxygen consumption rate (OCR) and ATP production. The OCR profiles clearly showed that AK_7_3 knockdown increased mitochondrial activity when compared to controls (Figures 4E; Online Supplementary Figure S13E). The basal and maximal respiration, the spare respiratory capacity, as well as the total ATP produced by mitochondria were significantly increased in $SEM^{AK\_7\_3\ KD}$ cells as compared to control, in two independent biological replicates (Figures 4F, G; Online Supplementary Figure S13F, G). Overall, these data suggest that AK_7_3 silencing affects mitochondrial function in t(4;11)-positive SEM cells, by increasing oxidative phosphorylation and enhancing mitochondrial activity.

To further corroborate these findings, we used the second knockdown model obtained in the RS4;11 cell line. Confocal analyses of $RS4;11^{AK\_7\_3\ KD}$ and $RS4;11^{NC}$ cells confirmed a ROS hyperproduction and an increased MMP, compatible with an altered mitochondrial function upon AK_7_3 silencing (Online Supplementary Figure S12C, G).

AK_7_3 knockdown is associated with dysmorphic mitochondria in SEM cells

To investigate the origin of the enhanced respiration of $SEM^{AK\_7\_3\ KD}$ cells, we analyzed their mitochondrial structure. In untreated SEM cells, transmission electron

microscopy (TEM) analysis revealed mitochondria with a regular shape and numerous cristae (Figures 5A, B). In the SEM^{NC} cells, mitochondrial morphology was similar to that of the untreated cell line; however, some mitochondria exhibited a larger intracristal space (Figures 5C, D). In the $SEM^{AK\_7\_3\ KD}$ cells, some mitochondria showed matrix rarefaction and reduced cristae, while others were characterized by an altered and more expanded intracristal space (Figure 5E). Swollen mitochondria with lost and damaged matrix material and fragmented cristae were also observed (Figure 5F).

Discussion

In the present work, we identified a novel recurrent f-circRNA back-splicing junction (AK_7_3) in the *KMT2A::AFF1*-positive SEM, RS4;11, and ALL-PO B-ALL cell lines, as well as in the vast majority of diagnostic or relapse samples from pediatric (67%) and adult (71%) t(4;11)-positive B-ALL patients harboring different *KMT2A::AFF1* splicing isoforms or t(4;11) translocations with varying breakpoints in *KMT2A* or *AFF1* genes. The back-splicing junction is shared by two f-circRNA splicing isoforms harboring different *KMT2A* exon 4 variants. Interestingly, AK_7_3 expression persisted at relapse in two pediatric patients, albeit at lower levels than in diagnostic samples, suggesting a potential biological role in treatment resistance and disease recurrence. However, AK_7_3 was absent (or below the RT-qPCR detection limit) in sequential MRD samples obtained during follow-up from one adult patient. The AK_7_3 was not expressed in *KMT2A::AFF1*-negative B-ALL patients, indicating that it is specifically associated with the *KMT2A::AFF1* fusion gene.

We observed that AK_7_3 knockdown in SEM cells altered ROS production, mitochondrial activity, and apoptosis regulation, as evidenced by both transcriptomic

enrichment analysis and functional studies. ROS overproduction after AK_7_3 knockdown in SEM and RS4;11 cells was accompanied by increased mitochondrial membrane potential. Additionally, we observed swelling of dysmorphic mitochondria in $SEM^{AK\_7\_3\ KD}$ cells. Concordantly, among the DEGs up-regulated by AK_7_3 silencing, we found the *Reactive oxygen species modulator 1* (*ROMO1*) and *Cytochrome c oxidase subunit 7A2* (*COX7A2*), which encode mitochondrial-localized proteins and have been reported to regulate ROS levels in cells[16]. These findings were validated by RT-qPCR in both SEM and RS4;11 KD models and suggest that the f-circRNAs harboring AK_7_3 may exert a protective role on leukemic cells by limiting ROS accumulation and by attenuating oxidative phosphorylation. This mechanism could help cancer cells to maintain adequate ROS levels at low to moderate concentrations, thereby activating tumor-promoting processes[17]. Indeed, a high level of ROS in the cytoplasm reflects a high rate of oxidative phosphorylation; on the other hand, hyperproduction of ROS (and their accumulation within cells) is known to trigger apoptosis by damaging proteins, nucleic acids, lipids, membranes, and organelles[18-22]. This scenario is supported by transcriptomic profiling of AK_7_3-silenced SEM cells, which revealed the up-regulation of several processes related to oxidative stress response, apoptotic signaling pathway, MYC targets, and amino acid, RNA, and protein metabolic pathways. Taken together, these findings suggest that AK_7_3-silenced cells experience oxidative and general metabolic stress, ultimately leading to apoptosis. Therefore, we hypothesize that f-circRNAs harboring AK_7_3 enable leukemia cells to survive under stressful conditions and to avoid apoptosis induced by high ROS levels or impaired mitochondrial function, thereby conferring a survival advantage.

The potential involvement of f-circRNAs harboring AK_7_3 in apoptosis is noteworthy and supported by the up-regulation of tumor suppressor genes involved in programmed cell death, such as *FAU* (*Ubiquitin-like and ribosomal protein S30 fusion*)[23] and *OAZ1* (*Ornithine decarboxylase antizyme 1*), observed in AK_7_3-silenced cells, and validated by RT-qPCR in both SEM and RS4;11 KD models. Interestingly, *OAZ1,* previously reported to induce erythroid differentiation and cell apoptosis in chronic myeloid leukemia, is also a target gene of *KMT2A*[24]. Further investigations into the mechanisms by which f-circRNAs harboring AK_7_3 regulate genes involved in apoptotic pathways are warranted, given recent evidence that Venetoclax, a BCL2 inhibitor, suppresses tumor cells in *KMT2A*-r B-ALL *in vitro* (SEM and RS4;11) and *in vivo*[25] models.

Although we observed a reduction in AK_7_3 expression at relapse as compared to diagnosis in two pediatric B-ALL patients, the analysis was performed on samples with varying blast percentages; thus, it is challenging to directly associate RNA expression (not DNA) with the absolute number of leukemic cells. Nevertheless, we find it very interesting that, in both cases, the diagnostic IG/TR markers were maintained at relapse, as were both the linear *KMT2A::AFF1* and the f-circRNAs harboring AK_7_3. Although the limited number of paired-case observations here hampers hypotheses regarding its potential role in leukemia progression, these findings suggest that f-circRNAs harboring AK_7_3 may be involved in B-ALL initiation and treatment resistance.

AK_7_3 showed enrichment in the cytoplasmic fraction in SEM, RS4;11, and ALL-PO cell lines, suggesting a functional role in this subcellular compartment, possibly acting as a microRNA sponge. Moreover, the observed impact of AK_7_3 knockdown on mitochondrial activity may indicate a specific colocalization of f-

circRNA and mitochondria. Indeed, the lack of AK_7_3 secretion in EVs released by SEM and RS4;11 cell lines may support this hypothesis. The same result was also obtained for the linear *KMT2A::AFF1* fusion transcript, whose absence in secreted EVs was evaluated *in vitro* here for the first time. Further investigations into the mitochondrial sublocalization of f-circRNAs harboring AK_7_3 are mandatory, as mitochondrial circRNAs have been shown to play a role in cell energy metabolism, particularly in cancer, where they indirectly upregulate key glycolytic enzymes[26]. Indeed, during progression, cancer cells must reprogram their energy metabolism to continuously fuel cell growth and division under fluctuating oxygen and glucose levels[27].

In summary, our results suggest that f-circRNAs warrant greater consideration in studies of *KMT2A*-r leukemia, as we demonstrate a functional role for the f-circRNAs harboring AK_7_3 in regulating apoptosis and mitochondrial metabolism in B-ALL, independent of the *KMT2A::AFF1* linear transcript effects on downstream pathways.

References

1. Kristensen LS, Jakobsen T, Hager H, Kjems J. The emerging roles of circRNAs in cancer and oncology. Nat Rev Clin Oncol. 2022;19(3):188-206.
2. Conn VM, Gabryelska M, Toubia J, et al. Circular RNAs drive oncogenic chromosomal translocations within the MLL recombinome in leukemia. Cancer Cell. 2023;41(7):1309-1326.e10.
3. Visci G, Tolomeo D, Agostini A, Traversa D, Macchia G, Storlazzi CT. CircRNAs and Fusion-circRNAs in cancer: New players in an old game. Cell Signal. 2020;75:109747.
4. Guarnerio J, Bezzi M, Jeong JC, et al. Oncogenic role of fusion-circRNAs derived from cancer-associated chromosomal translocations. Cell. 2016;165(2):289-302.
5. Dal Molin A, Tretti Parenzan C, Gaffo E, et al. Discovery of fusion circular RNAs in leukemia with KMT2A::AFF1 rearrangements by the new software CircFusion. Brief Bioinform. 2023;24(1):bbac589.
6. Meyer C, Larghero P, Almeida Lopes B, et al. The KMT2A recombinome of acute leukemias in 2023. Leukemia. 2023;37(5):988-1005.
7. Forgione MO, McClure BJ, Eadie LN, Yeung DT, White DL. KMT2A rearranged acute lymphoblastic leukaemia: unravelling the genomic complexity and heterogeneity of this high-risk disease. Cancer Lett. 2020;469:410-418.
8. Chan AKN, Chen CW. Rewiring the epigenetic networks in MLL-rearranged leukemias: epigenetic dysregulation and pharmacological interventions. Front Cell Dev Biol. 2019;7:81.
9. Harman JR, Thorne R, Jamilly M, et al. A KMT2A-AFF1 gene regulatory network highlights the role of core transcription factors and reveals the regulatory logic of key downstream target genes. Genome Res. 2021;31(7):1159-1173.
10. Marschalek R, Greil J, Löchner K, et al. Molecular analysis of the chromosomal breakpoint and fusion transcripts in the acute lymphoblastic SEM cell line with chromosomal translocation t(4;11). Br J Haematol. 1995;90(2):308-320.
11. Greil J, Gramatzki M, Burger R, et al. The acute lymphoblastic leukaemia cell line SEM with t(4;11) chromosomal rearrangement is biphenotypic and responsive to interleukin-7. Br J Haematol. 1994;86(2):275-283.
12. Ragusa D, Makarov EM, Britten O, Moralli D, Green CM, Tosi S. The RS4;11 cell line as a model for leukaemia with t(4;11)(q21;q23): revised characterisation of cytogenetic features. Cancer Rep (Hoboken). 2019;2(5):e1207.
13. Gobbi A, Di Berardino C, Scanziani E, et al. A human acute lymphoblastic leukemia line with the T(4;11) translocation as a model of minimal residual disease in SCID mice. Leuk Res. 1997;21(11-12):1107-1114.
14. Pfaffl MW, Horgan GW, Dempfle L. Relative expression software tool (REST) for group-wise comparison and statistical analysis of relative expression results in real-time PCR. Nucleic Acids Res. 2002;30(9):e36.
15. Nam DK, Honoki K, Yu M, Yunis JJ. Alternative RNA splicing of the MLL gene in normal and malignant cells. Gene. 1996;178(1-2):169-175.
16. Amini MA, Talebi SS, Karimi J. Reactive Oxygen Species Modulator 1 (ROMO1), a new potential target for cancer diagnosis and treatment. Chonnam Med J. 2019;55(3):136-143.
17. Nakamura H, Takada K. Reactive oxygen species in cancer: Current findings and future directions. Cancer Sci. 2021;112(10):3945-3952.

18. Redza-Dutordoir M, Averill-Bates DA. Activation of apoptosis signalling pathways by reactive oxygen species. Biochim Biophys Acta. 2016;1863(12):2977-2992.
19. An X, Yu W, Liu J, Tang D, Yang L, Chen X. Oxidative cell death in cancer: mechanisms and therapeutic opportunities. Cell Death Dis. 2024;15(8):556.
20. Brandl N, Seitz R, Sendtner N, Müller M, Gülow K. Living on the edge: ROS homeostasis in cancer cells and its potential as a therapeutic target. Antioxidants (Basel). 2025;14(8):1002.
21. Perillo B, Di Donato M, Pezone A, et al. ROS in cancer therapy: the bright side of the moon. Exp Mol Med. 2020;52(2):192-203.
22. Huang R, Chen H, Liang J, et al. Dual Role of Reactive Oxygen Species and their Application in Cancer Therapy. J Cancer. 2021;12(18):5543-5561.
23. Pickard MR, Mourtada-Maarabouni M, Williams GT. Candidate tumour suppressor Fau regulates apoptosis in human cells: an essential role for Bcl-G. Biochim Biophys Acta. 2011;1812(9):1146-1153.
24. Wu B, Wang X, Ma W, Zheng W, Jiang L. Assay of OAZ1 mRNA levels in chronic myeloid leukemia combined with application of leukemia PCR array identified relevant gene changes affected by antizyme. Acta Haematol. 2014;131(3):141-147.
25. Richter A, Lange S, Holz C, et al. Effective tumor cell abrogation via Venetoclax-mediated BCL-2 inhibition in KMT2A-rearranged acute B-lymphoblastic leukemia. Cell Death Discov. 2022;8(1):302.
26. Liu D, Zhou X, He Y, Zhao J. The Roles of CircRNAs in mitochondria. J Cancer. 2024;15(9):2759-2769.
27. Tufail M, Jiang CH, Li N. Altered metabolism in cancer: insights into energy pathways and therapeutic targets. Mol Cancer. 2024;23(1):203.

Table 1. DEGs encoding proteins with mitochondrial localization, according to the Broad Institute Human MitoCarta 3.0 database. For each gene, log2 fold-change and adjusted p-value found in the differential expression analysis of AK_7_3 silenced samples vs. controls are indicated.

Gene	Log2 FoldChange	Adjusted p-value	MitoCarta3.0 SubMitoLocalization	MitoCarta3.0 MitoPathways
COX7A2	0.231434	0.049689	MIM	OXPHOS > Complex IV > CIV subunits | OXPHOS > OXPHOS subunits
SLIRP	0.224695	0.070441	Matrix	Mitochondrial central dogma > mtRNA metabolism > mtRNA stability and decay | Mitochondrial central dogma > Translation
TUFM	0.148516	0.096403	Matrix	Mitochondrial central dogma > Translation > Translation factors
HSPE1	0.303352	0.094259	Matrix	Protein import, sorting and homeostasis > Protein homeostasis > Chaperones
ROMO1	0.333445	0.008967	MIM	Protein import, sorting and homeostasis > Protein import and sorting > TIM23 presequence pathway | Small molecule transport
CHCHD2	0.193623	0.022224	IMS	Mitochondrial dynamics and surveillance > Apoptosis
ATP5MC2	0.224376	0.001826	MIM	OXPHOS > Complex V > CV subunits | OXPHOS > OXPHOS subunits
ATP5MK	0.25209	0.078299	MIM	OXPHOS > Complex V > CV subunits | OXPHOS > OXPHOS subunits | Mitochondrial dynamics and surveillance > Cristae formation

Legend: MIM, mitochondrial inner membrane; IMS, intermembrane space; OXPHOS, oxidative phosphorylation.

Table 2. List of *KMT2A* target genes whose expression is affected by AK_7_3 f-circRNA silencing. For each gene, log2 fold-change and adjusted p-value found in the differential expression analysis of AK_7_3 silenced samples vs. controls are indicated.

***KMT2A* target gene**	**GSEA Gene Set**	**Log2 FoldChange**	**Adjusted p-value**	**Description**
RPL31	MULLIGHAN_MLL_SIGNATURE_1_DN	0.278791	0.024501	ribosomal protein L31
RPL36	MULLIGHAN_MLL_SIGNATURE_1_DN,MULLIGHAN_MLL_SIGNATURE_2_DN	0.214315	0.003025	ribosomal protein L36
LGALS1	MULLIGHAN_MLL_SIGNATURE_1_UP,MULLIGHAN_MLL_SIGNATURE_2_UP,ROSS_LEUKEMIA_WITH_MLL_FUSIONS	0.213424	0.069892	galectin 1
RPS21	MULLIGHAN_MLL_SIGNATURE_1_DN	0.213255	0.000292	ribosomal protein S21
CD74	GAUSSMANN_MLL_AF4_FUSION_TARGETS_D_UP	0.172509	0.004734	CD74 molecule
HLA-B	GAUSSMANN_MLL_AF4_FUSION_TARGETS_A_DN,GAUSSMANN_MLL_AF4_FUSION_TARGETS_A_UP	0.15167	0.08017	major histocompatibility complex, class I, B
OAZ1	MULLIGHAN_MLL_SIGNATURE_1_UP,MULLIGHAN_MLL_SIGNATURE_2_UP	0.150787	0.078848	ornithine decarboxylase antizyme 1
ARHGDIB	SCHRAETS_MLL_TARGETS_DN	0.14018	0.04015	Rho GDP dissociation inhibitor beta

Figures legends

Figure 1: RT-PCR assays using divergent primers revealed novel *KMT2A::AFF1* f-circRNAs in the SEM cell line. A) Schematic representation of the divergent primer map position on *KMT2A* and *AFF1*, taking into account the fusion junction of the linear *KMT2A::AFF1* transcript in the SEM cell line. B) Left panel: RT-PCR results showing the presence of the f-circRNA back-splicing junction product specifically in the SEM cell line RNA samples, both without and with RNase R treatment, and not in the other control samples (NALM6; and commercial pooled bone marrow (BM) RNA sample, regardless of the RNAse R treatment). NTC: Blank. Marker: 2-Log DNA ladder; right panel: partial chromatogram and sequence of the novel *KMT2A::AFF1* back-splicing junction. C) RT-qPCR analysis of AK_7_3, *KMT2A::AFF1* linear fusion transcript, and *GAPDH* transcript expression in SEM RNA samples treated (red) and untreated (blue) with RNase R. *KMT2A::AFF1* and *GAPDH* were used as positive controls of the digestion step. D) Schematic representation of the RT-PCR product reported in panel B, showing the presence of the alternative *KMT2A* exon 4, described in the *KMT2A* transcript variant with Accession Number XM_054368833.1. E) Schematic representation of the divergent primer map position on *KMT2A* and back-splicing junction of AK_7_3, to obtain the RT-PCR product in the right panel, corresponding to the sequence shown in the partial chromatogram, with the back-splicing junction and the *KMT2A* exon 3::exon 4 canonical splicing junction indicated respectively with the black and red vertical arrows.

Figure 2: AK_7_3 is expressed in diagnostic and relapse samples from pediatric and adult B-ALL patients. RT-qPCR assays showing relative expression levels of AK_7_3 in pediatric and adult B-ALL patients. The relapse samples (3r and 7r) showed a statistically significant reduction in expression compared with the paired samples at diagnosis (3o and 7o, respectively). The SEM cell line was used for normalizing the relative expression of AK_7_3 in patients. Results are shown as mean±SD. ****p<0.0001, *p<0.05 (REST 2009 software).

Figure 3: AK_7_3 silencing affects the B-ALL transcriptome. A) Principal Component Analysis (PCA) of the AK_7_3 silenced samples ($SEM^{AK\_7\_3\ KD}$) and negative controls (SEM^{NC}). B) Volcano plot of DEGs identified in AK_7_3 silenced samples vs. negative controls. The magnitude of changes (log_2 fold change, on the x-axis) is plotted against their statistical significance ($-log_{10}$ adjusted p-value, on the y-axis). C-D) Functional enrichment analysis of DEGs identified in $SEM^{AK\_7\_3\ KD}$ cells vs. SEM^{NC} controls. Bubble plots show selected Gene Ontology Biological Process (GO-BP) terms (panel C) and Reactome pathways (panel D) enriched for up- and down-regulated genes. Bubble size represents the number of DEGs involved in each enriched function with respect to the overall number of input DEGs (gene ratio values), while color gradient indicates statistical significance of the enrichment (adjusted p-values). E) The network plot shows DEGs enriching the GO-BP of interest. The bubble size of GO terms corresponds to the number of genes involved.

Figure 4: AK_7_3 knockdown in SEM cells affects apoptosis and mitochondrial metabolism. A) Cell death analysis of $SEM^{AK\_7\_3\ KD}$ cells vs. SEM^{NC}. The error bars were calculated on nine biological replicates. *p<0.05 (Unpaired t-test). B) Confocal

analysis of ROS in $SEM^{AK\_7\_3\ KD}$ cells vs. SEM^{NC} (48 hours after transfection) by using CellROX and Hoechst 33342. Bar graphs report the quantification of ROS (mean green signal/mean blue signal) normalized to SEM^{NC}. ****p<0.0001 (Unpaired t-test). C-D) Confocal analysis of mitochondrial membrane potential (MMP) in $SEM^{AK\_7\_3\ KD}$ cells vs. SEM^{NC} (72 hours after transfection) by using MitoTracker red/green and Hoechst 33342. Bar graphs report the quantification of mitochondrial activity (mean red signal/mean green signal) as a measure of mitochondrial activity (panel C), and mitochondrial mass (mean green signal/mean blue signal) as a measure of total mitochondria (panel D). Data were normalized to SEM^{NC}. ****p<0.0001 (Unpaired t-test), ns: not significant. E) Seahorse bioenergetic profiling of SEM cells 48 hours after transfection, by using Seahorse XF Mito Stress Test. F) Total ATP produced by mitochondrial respiration. The bar graph shows the mean OCR values for eight replicates. *p<0.05 (Unpaired t-test). G) Histograms showing the basal mitochondrial respiration (left panel), the maximal mitochondrial respiration (middle panel), and the spare respiratory capacity (right panel). The bar graph reports the mean OCR values calculated from eight replicates. **p<0.01; ****p<0.0001 (Unpaired t-test).

Figure 5: AK_7_3 knockdown induces dysmorphic mitochondrial ultrastructure *in vitro*. TEM images of mitochondria of (A, B) untreated SEM cells, (C, D) SEM^{NC} cells, and (E, F) $SEM^{AK\_7\_3\ KD}$ cells. In some mitochondria, the space between the outer and inner membranes is larger than in other mitochondria (arrow). Swollen mitochondria with fragmented cristae (arrowhead) are shown. Scale bar: (A, E) 500 nm; (B, C, D, F) 200 nm.

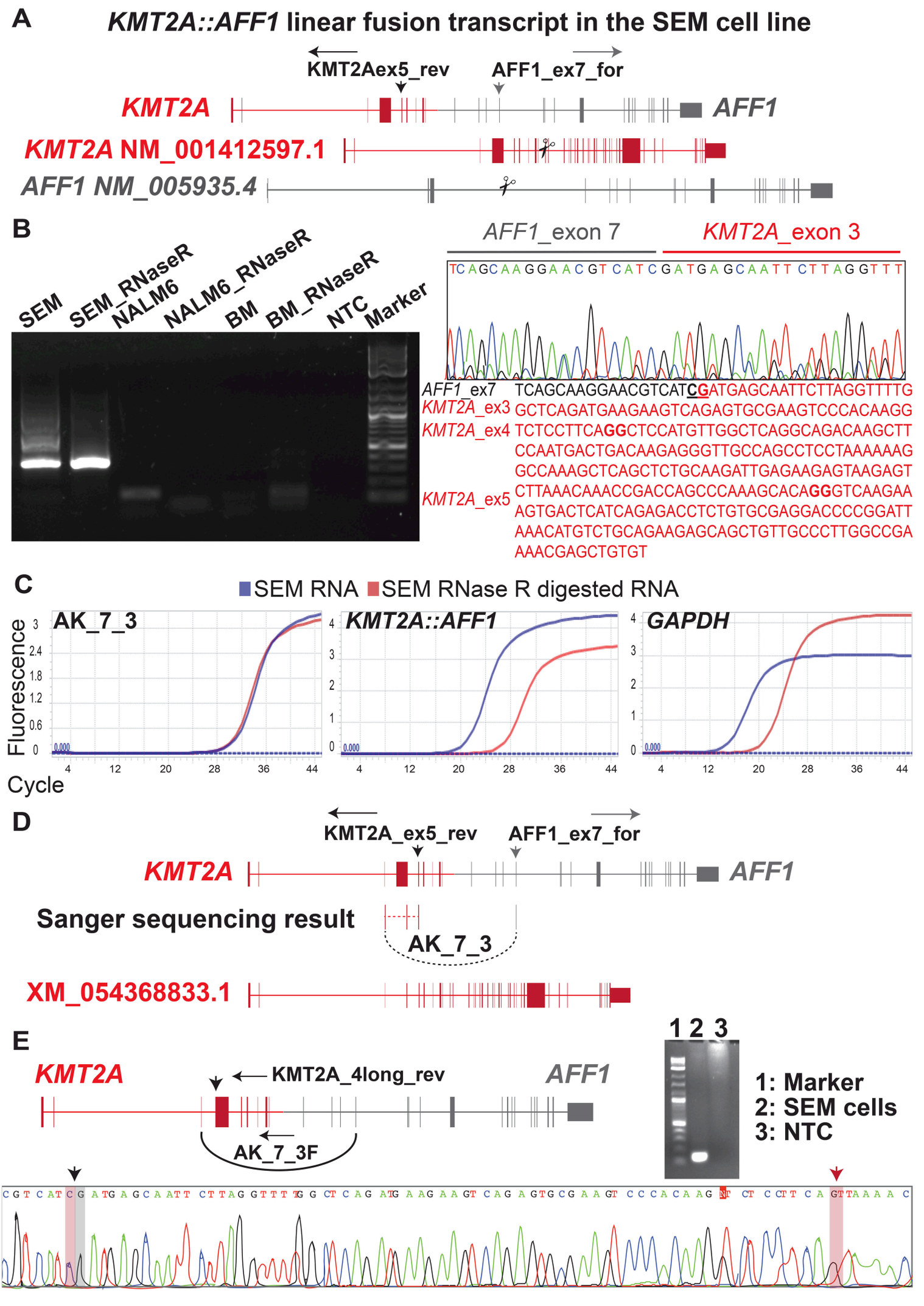
A
KMT2A::AFF1 linear fusion transcript in the SEM cell line
KMT2Aex5_rev
AFF1_ex7_for
KMT2A
AFF1
KMT2A NM_001412597.1
AFF1 NM_005935.4
B
SEM
SEM_RNaseR
NALM6
NALM6_RNaseR
BM
BM_RNaseR
NTC
Marker
AFF1_exon 7
KMT2A_exon 3
TCAGCAAGGAACGTCATCGATGAGCAATTCTTAGGTTTT
AFF1_ex7 TCAGCAAGGAACGTCATCGATGAGCAATTCTTAGGTTTTG
KMT2A_ex3 GCTCAGATGAAGAAGTCAGAGTGCGAAGTCCCACAAGG
KMT2A_ex4 TCTCCTTCAGGCTCCATGTTGGCTCAGGCAGACAAGCTT
CCAATGACTGACAAGAGGGTTGCCAGCCTCCTAAAAAAG
GCCAAAGCTCAGCTCTGCAAGATTGAGAAGAGTAAGAGT
KMT2A_ex5 CTTAAACAAACCGACCAGCCCAAAGCACAGGGTCAAGAA
AGTGACTCATCAGAGACCTCTGTGCGAGGACCCCGGATT
AAACATGTCTGCAGAAGAGCAGCTGTTGCCCTTGGCCGA
AAACGAGCTGTGT
C
SEM RNA
SEM RNase R digested RNA
AK_7_3
KMT2A::AFF1
GAPDH
Fluorescence
Cycle
D
KMT2A_ex5_rev
AFF1_ex7_for
KMT2A
AFF1
Sanger sequencing result
AK_7_3
XM_054368833.1
E
KMT2A
KMT2A_4long_rev
AFF1
AK_7_3F
1 2 3
1: Marker
2: SEM cells
3: NTC

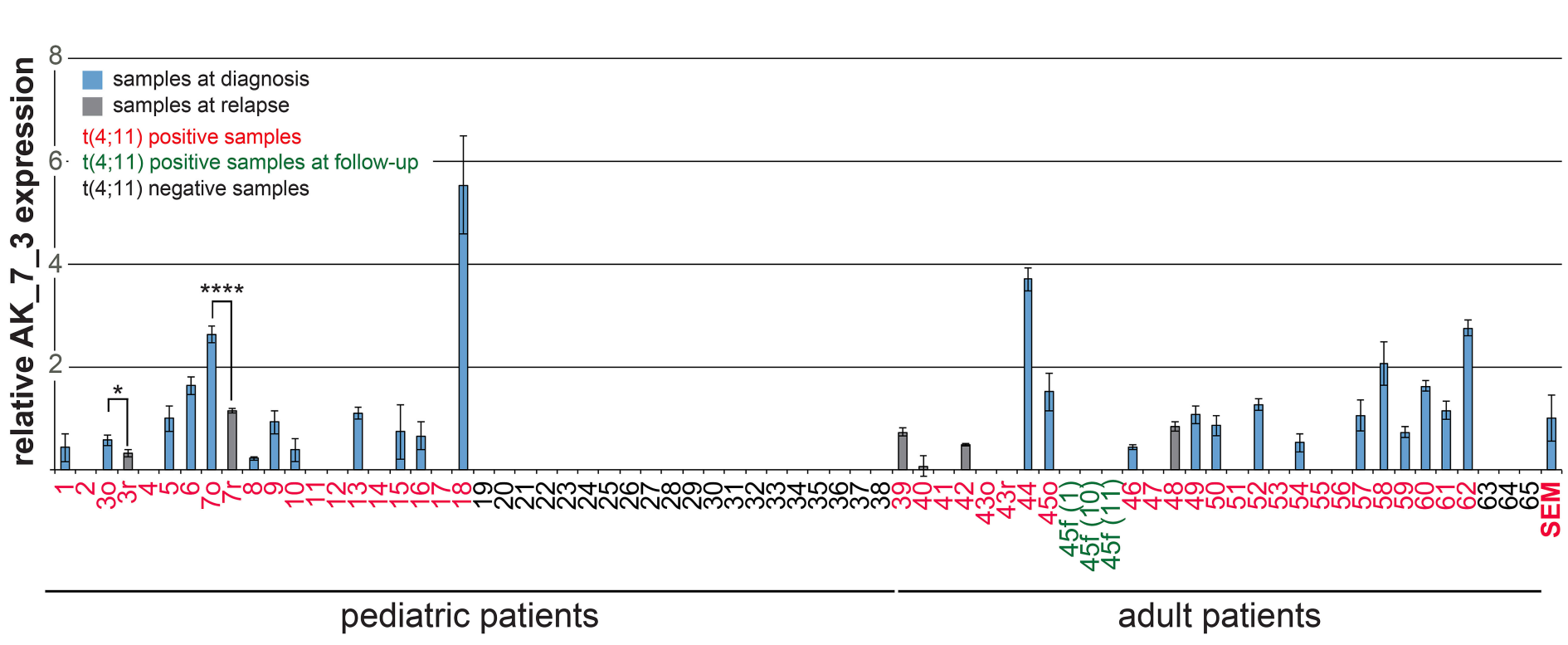
relative AK_7_3 expression
8
6
4
2
samples at diagnosis
samples at relapse
t(4;11) positive samples
t(4;11) positive samples at follow-up
t(4;11) negative samples
*
****
1 2 3o 3r 4 5 6 7o 7r 8 9 10 11 12 13 14 15 16 17 18 19 20 21 22 23 24 25 26 27 28 29 30 31 32 33 34 35 36 37 38 39 40 41 42 43o 43r 44 45o 45f (1) 45f (10) 45f (11) 46 47 48 49 50 51 52 53 54 55 56 57 58 59 60 61 62 63 64 65 SEM
pediatric patients
adult patients

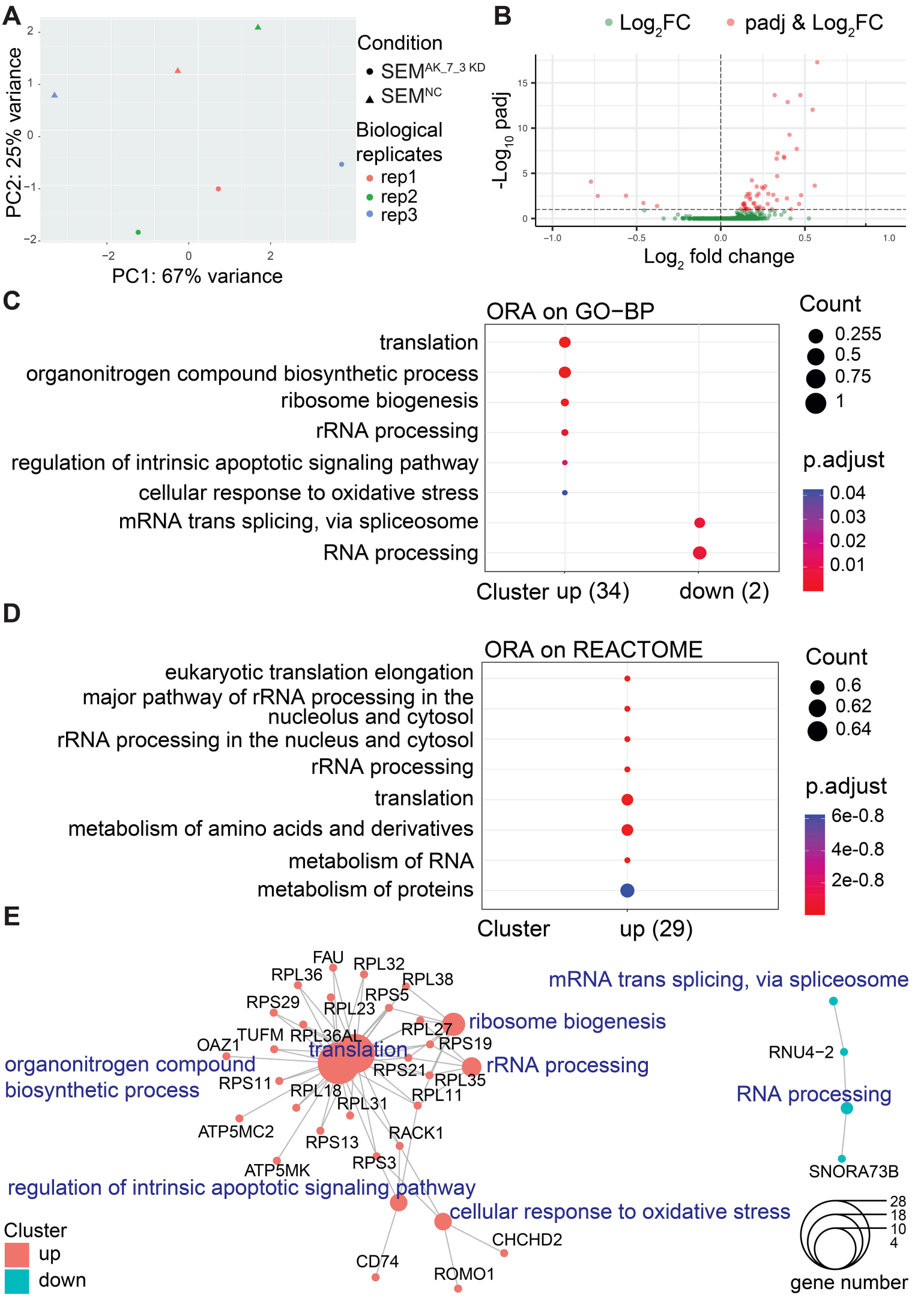
A
PC2: 25% variance
PC1: 67% variance
Condition
SEMAK_7_3 KD
SEMNC
Biological replicates
rep1
rep2
rep3
B
Log2FC
padj & Log2FC
-Log10 padj
Log2 fold change
C
ORA on GO−BP
translation
organonitrogen compound biosynthetic process
ribosome biogenesis
rRNA processing
regulation of intrinsic apoptotic signaling pathway
cellular response to oxidative stress
mRNA trans splicing, via spliceosome
RNA processing
Cluster up (34)
down (2)
Count
0.255
0.5
0.75
1
p.adjust
0.04
0.03
0.02
0.01
D
ORA on REACTOME
eukaryotic translation elongation
major pathway of rRNA processing in the nucleolus and cytosol
rRNA processing in the nucleus and cytosol
rRNA processing
translation
metabolism of amino acids and derivatives
metabolism of RNA
metabolism of proteins
Cluster
up (29)
Count
0.6
0.62
0.64
p.adjust
6e-0.8
4e-0.8
2e-0.8
E
FAU
RPL32
RPL36
RPL38
RPS5
RPS29
RPL23
ribosome biogenesis
RPL27
TUFM
RPL36AL
RPS19
OAZ1
translation
organonitrogen compound biosynthetic process
RPS21
rRNA processing
RPS11
RPL35
RPL18
RPL11
RPL31
ATP5MC2
RACK1
RPS13
ATP5MK
RPS3
regulation of intrinsic apoptotic signaling pathway
cellular response to oxidative stress
CHCHD2
CD74
ROMO1
mRNA trans splicing, via spliceosome
RNU4−2
RNA processing
SNORA73B
Cluster
up
down
28
18
10
4
gene number

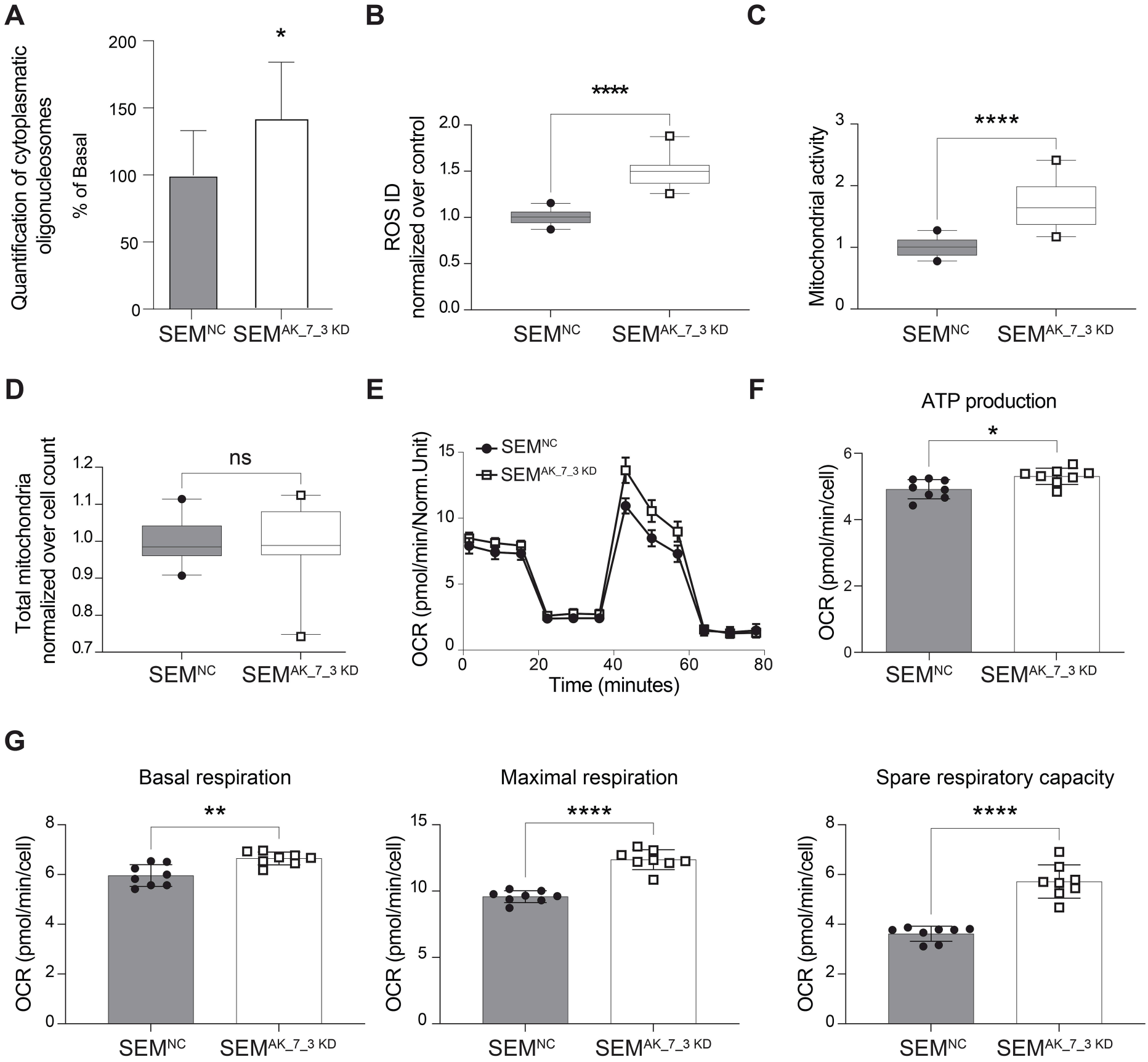
A
Quantification of cytoplasmatic oligonucleosomes
% of Basal
200
150
100
50
0
*
SEMNC
SEMAK_7_3 KD
B
ROS ID
normalized over control
2.0
1.5
1.0
0.5
0.0
****
SEMNC
SEMAK_7_3 KD
C
Mitochondrial activity
3
2
1
0
****
SEMNC
SEMAK_7_3 KD
D
Total mitochondria
normalized over cell count
1.2
1.1
1.0
0.9
0.8
0.7
ns
SEMNC
SEMAK_7_3 KD
E
OCR (pmol/min/Norm.Unit)
15
10
5
0
SEMNC
SEMAK_7_3 KD
0
20
40
60
80
Time (minutes)
F
ATP production
OCR (pmol/min/cell)
6
4
2
0
*
SEMNC
SEMAK_7_3 KD
G
Basal respiration
OCR (pmol/min/cell)
8
6
4
2
0
**
SEMNC
SEMAK_7_3 KD
Maximal respiration
OCR (pmol/min/cell)
15
10
5
0
****
SEMNC
SEMAK_7_3 KD
Spare respiratory capacity
OCR (pmol/min/cell)
8
6
4
2
0
****
SEMNC
SEMAK_7_3 KD

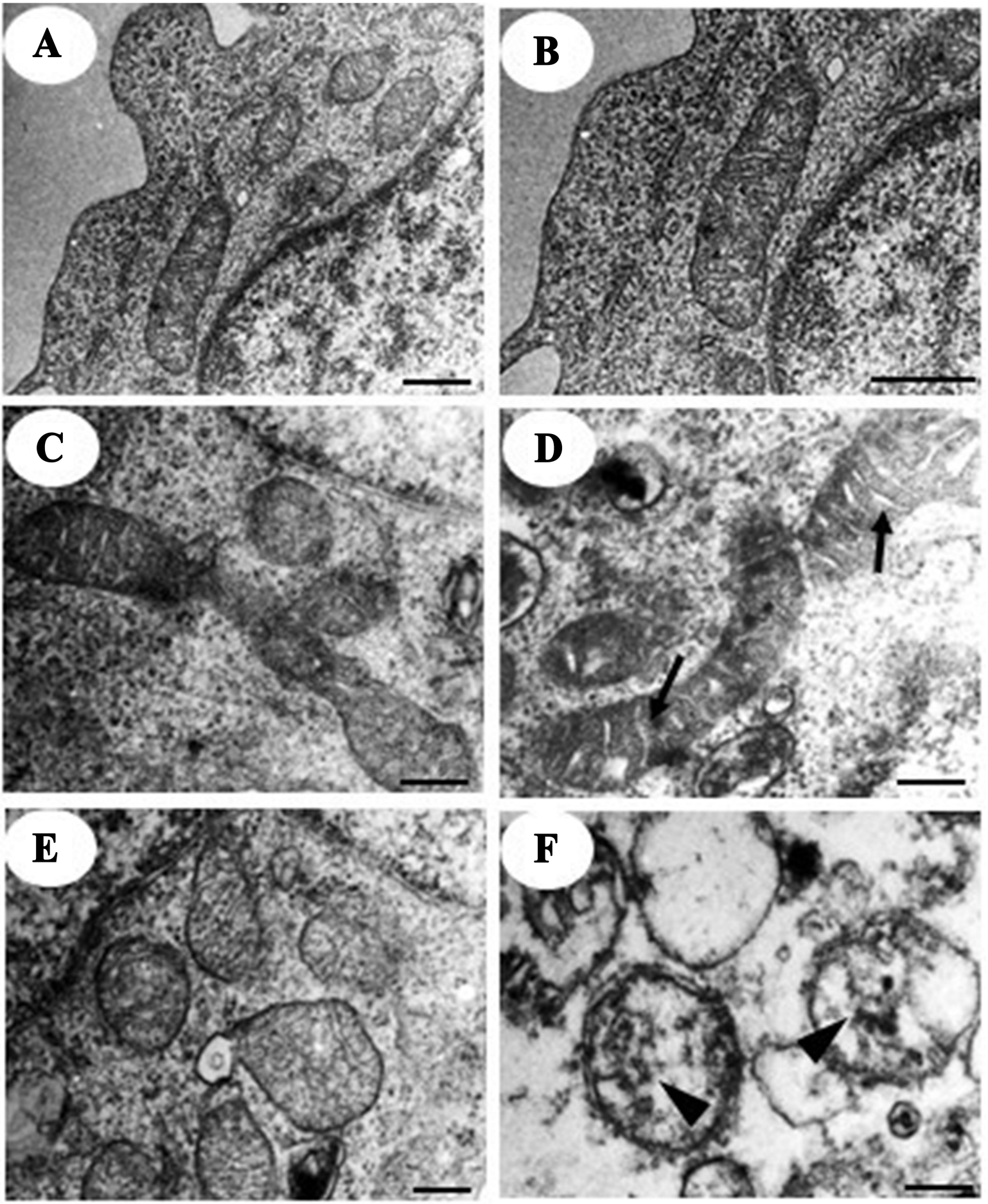
A
B
C
D
E
F

Supplementary Methods

RNA extraction from whole cell lysates, RNase R digestion, RT-PCR, RT-qPCR assays

Total RNA was extracted from cell lines using the RNeasy Mini kit (Qiagen, Hilden, Germany) and from Bone Marrow (BM) or Peripheral Blood (PB) samples of patients using the AllPrep DNA/RNA Mini Kit (Qiagen), the QIAamp RNA Blood Mini Kit (Qiagen), or TRIzol (Thermo Fisher Scientific), according to the manufacturers' protocols. RNA concentration was evaluated with the NanoPhotometer® N50 (Implen, München, Germany).

RNase R digestion was performed as previously described[1].

One microgram of RNA from each sample was reverse-transcribed using the SuperScript IV VILO Master Mix with ezDNase (Thermo Fisher Scientific). The final reaction volume was diluted 1:10, and 2.5 µl were used for PCR-based assays. Two-round RT-PCR experiments were performed on the T100 Thermal Cycler (Bio-Rad, Pleasanton, CA, USA) using the Platinum *Taq* DNA Polymerase (Thermo Fisher Scientific) as follows: initial denaturation at 94 ^{o}C for 3 min; 35 cycles of 94 ^{o}C for 30 s, 60 ^{o}C for 30 s, 72 ^{o}C for 45 s; and 72 ^{o}C for 5 min as final extension. Reaction products were stained with GelRed Nucleic Acid Gel Stain (Biotium, Fremont, CA, USA) and visualized after 1% agarose gel electrophoresis using the ChemiDoc XRS+ Gel Imaging System (Bio-Rad) and the 2-Log DNA ladder (Fisher Scientific, Hampton, NH, USA). RT-qPCR assays were carried out using the FastStart Essential DNA Green Master (Roche, Basel, Switzerland) on the LightCycler® 96 (Roche) with the following conditions: 95 ^{o}C for 10 min; 45 cycles of 95 °C for 10 s, 60 ^{o}C for 10 s, 72 °C for 10 s. Melting curve analysis was performed at 95 ^{o}C for 10 s, 65 ^{o}C for 1

min, and 92 ^{o}C for 1 s. All the samples were run in triplicate. Relative AK_7_3 expression was calculated using the $2^{-\Delta\Delta Ct}$ method, with the SEM/SEM^{NC} cell lines used as the calibrator and *GAPDH* as the reference gene, as previously described[2]. See below for the SEM^{NC} definition.

The 374 bp RT-PCR product obtained in the experiment reported in Figure 1A, B was obtained using a forward primer designed in *AFF1* exon 7 (AFF1_ex7_for) and a reverse primer in *KMT2A* exon 5 (KMT2A_ex5_rev). *KMT2A* exon numbering is in accordance with previous literature[3, 4].

Furthermore, the linear *KMT2A::AFF1* splicing variant, including the shortest isoform of exon 4, was validated by RT-PCR and Sanger sequencing using a forward primer designed in *KMT2A* exon 3 (KMT2A_ex3_for) and a reverse primer in *AFF1* exon 4 (AFF1_ex4_rev) (Online Supplementary Figure S2). To analyze the linear fusion RNA in RT-qPCR and on RNA samples from EVs, we used a forward primer designed in *KMT2A* exon 8 (KMT2A_ex8_for) and a reverse primer in *AFF1* exon 7 (AFF1 exon 7-R) (Figure 1C; Online Supplementary Figures S3E; S10B).

The 227 bp RT-PCR product reported in the Online Supplementary Figure S1A, as well as in the RT-qPCR experiments (Figure 2; Online Supplementary Figures S3A; S10 A; S12A, D; S13A, B), was obtained using a forward primer in *AFF1* exon 4 (AFF1_ex4_for) and a reverse primer designed on the back-splicing junction (AK_7_3R).

The 128 bp RT-PCR product (Figure 1E; Online Supplementary Figure S1C, S6A, S7) was amplified using a forward primer designed on the back-splicing junction (AK_7_3F) and a reverse primer in *KMT2A* exon 4 (KMT2A_4long_rev). This RT-PCR product corresponds to the f-circRNA obtained by the backsplicing of the *KMT2A::AFF1,* including the long isoform of *KMT2A* exon 4. Conversely, the RT-

PCR product corresponding to the f-circRNA obtained by backsplicing of *KMT2A::AFF1,* including the short isoform of *KMT2A* exon 4, was obtained by combining primers AK_7_3F and KMT2Aex5_rev (360 bp) (Online Supplementary Figure S1C; S6B). All primers, including those used for evaluating *ROMO1*, *OAZ1*, *FAU*, and *COX7A2* gene expression levels, are listed in the Online Supplementary Table S4.

RNA extraction from subcellular fractions

To assess subcellular enrichment of the AK_7_3 back-splicing junction, we performed RT-qPCR on nuclear and cytoplasmic RNA fractions using a customized protocol. Briefly, after rinsing with 1× PBS, 10×10^6 cells (vitality index > 85%) were suspended and incubated 10 min on ice in Buffer A (TrisHCl 200mM pH=8, NaCl 10mM, $MgCl_2$ 3mM, NP40 0,1%, Glycerol 10%, EDTA 0.2mM, DTT 1mM) supplemented with the Protease Inhibitor Mix HP (Serva Electrophoresis GmbH, Heidelberg, Germany). The cytoplasmic fraction was obtained by collecting the supernatant after 5 min of centrifugation at 2,000 rpm at 4 °C. To get the nuclear fraction, the pellet was washed twice with 300µL Buffer A and 5 min centrifugations at 2,000 rpm at 4 °C. After discarding the washing buffer, the pellet was suspended in 300µL Buffer C (TrisHCl 200mM, pH=8, NaCl 400mM, Glycerol 20%, DTT 1mM) supplemented with the Protease Inhibitor Mix HP (Serva Electrophoresis GmbH). After two thermal shocks (10 min at -20 °C, 3 min at +55 °C) and 15 min of centrifugation at 13,000 rpm at 4 °C, the supernatant containing the nuclear extract was obtained. Then, RNA was extracted from the cytoplasmic and nuclear fractions using TRIzol reagent (Thermo Fisher Scientific), according to the manufacturer's instructions. One microgram of

RNA from the cytosolic fractions and the same volume of the nuclear RNA samples were retrotranscribed as described above and used for RTqPCR assays.

RNA isolation from extracellular vesicles (EVs)

After two 1× PBS washes, B-ALL cell lines at 70% confluence were incubated for 48 hours in conditioned medium supplemented with Exosome-Depleted fetal bovine serum (EXO-FBS-250A-1, System Biosciences, Abingdon, UK). EV isolation was performed by using a differential centrifugation protocol[5]. Size distribution and concentration of EVs were measured by Nanoparticle Tracking Analysis (NTA) using the NanoSight instrument (NS300, Malvern Instruments LTD, Rome, Italy) and reported in the Online Supplementary Table S5. EV RNA isolation and quantification were performed as previously described[6].

AK_7_3 silencing by RNA interference

For AK_7_3 silencing by RNA interference, SEM cells were transfected with two Dicer-Substrate Short Interfering RNAs (DsiRNAs) specifically designed on the AK_7_3 back-splicing junction [7_3a: 5' rGrGrArArCrGrUrCrArUrCrGrArUrGrArGrCrArArUrUrCTT, and 7_3b: 5' rGrArArCrGrUrCrArUrCrGrArUrGrArGrCrArArUrUrCrUTA] (Integrated DNA Technologies, Inc., Coralville, IA, USA). A commercial non-targeting DsiRNA (DS-NC1) (Integrated DNA Technologies) was used as a negative control. The two cell lines are referred to as $SEM^{AK\_7\_3\ KD}$ and SEM^{NC} throughout the text. All transfections were performed using Lipofectamine RNAiMAX Transfection Reagent (Thermo Fisher Scientific), according to the manufacturer's instructions, and a reverse transfection was performed, followed by a forward transfection 24 hours later. As the

previously described approach was not successful in the RS4;11 cell line, we transfected these cells using the Neon Transfection system (Thermo Fisher Scientific), following a previously published protocol specifically optimized for this cell line (voltage: 1,750 V, width: 20 ms, 1 pulse)[7].

Total RNA-sequencing library preparation and bioinformatics data analysis

Three independent biological replicates of AK_7_3-silenced and DS-NC1 control cells from the SEM cell line were profiled for gene-expression changes using whole-transcriptome RNA sequencing (RNA-seq) 48 hours after forward transfection. After total RNA extraction, libraries were prepared using the Universal Plus Total RNA-seq library preparation kit with NuQuant (Tecan, Männedorf, Switzerland), targeting transcript depletion for globin genes with AnyDeplete (Tecan). The yields of the final libraries were assessed using a Qubit 4.0 fluorometer (Thermo Fisher Scientific), and qualitatively measured using a DNA1000 chip on an Agilent 2100 Bioanalyzer (Agilent Technologies, Santa Clara, CA, USA). Libraries were sequenced in 2×150-cycle runs on the Illumina NextSeq 2000 platform (Illumina, San Diego, CA, USA), to obtain at least 40 million read pairs per sample.

After FastQC (v.0.11.8) quality control, raw reads were trimmed to 100 bases and mapped to the human reference genome (hg38) using STAR (v.2.7.10a)[8]. Gene counts were calculated using the HTSeq package (version 0.11.1)[9], with the hg38 Encode-Gencode GTF (version 43) as the gene annotation file. Differential gene expression analysis was performed using the DESeq2 Bioconductor/R package (v.1.38.3)[10]. Genes with a low expression (sum of read counts across all samples < 10) were filtered out before testing for statistical significance. A |log2FC| > 0 and adjusted p-value (Benjamini-Hochberg (BH) correction) < 0.1 were used as cut-off to define statistically

significant differentially expressed genes (DEGs). The ClusterProfiler R package (v.4.6.2) was used to perform functional enrichment over-representation analysis (ORA) on Gene Ontology Biological Process (GO-BP) categories and biological pathway collections (KEGG, Reactome, and MSigDB hallmark gene sets)[11]. A false discovery rate (FDR, BH correction) threshold of < 0.05 was applied to all the annotation terms to define statistically significant enrichments.

Raw sequence data and gene counts are available in the GEO repository, under Accession Number GSE304109.

The presence of the *KMT2A::AFF1* linear fusion transcript in our RNA-seq data was assessed by STAR-Fusion[12], and sequencing reads mapped on the junction, divided by the number of total mapped reads for each sample, were used to calculate the expression of the fusion transcript as reads-per-million (RPM) count.

For *KMT2A* target gene analysis, 23 gene sets representing published *KMT2A* target gene expression signatures were downloaded from the GSEA Molecular Signatures Database (MSigDB, https://www.gsea-msigdb.org/gsea/msigdb/index.jsp), accounting for 2,129 total genes (gene sets used are listed in the Online Supplementary Table S6).

Apoptosis assay

Cells were seeded at 0.5×10^6 cells in a 12-well plate and transfected with either the AK_7_3-specific DsiRNA or the DS-NC1 negative control as described above. 48 hours after forward transfection, cells from nine biological replicates per condition were lysed using the Incubation buffer from the Cell Death Detection ELISA kit (Roche). Cytoplasmic protein concentration was evaluated by the Bradford assay (Thermo Fisher Scientific), according to the manufacturer's instructions, and 10 μg of protein per sample was used to measure the cytoplasmic oligonucleosome levels with

the Cell Death Detection ELISA kit, following the manufacturer's protocol. Each sample was analyzed as two technical replicates. The absorbance at 490 nm was measured, and the background absorbance (from wells containing the incubation buffer instead of the sample solution) was subtracted. The mean value from SEM^{NC} samples was used as a baseline to normalize the mean adsorbance obtained from silenced samples (reported as a percentage of cytoplasmic histone-associated DNA fragments).

Confocal laser scanning microscopy (CLSM)

Cells were seeded at 1×10^6 cells in a 6-well plate and transfected with either the AK_7_3-specific DsiRNA or the DS-NC1 negative control as described above. For Reactive Oxygen Species (ROS) analysis, 48 hours after transfection, cells were incubated for 30 min at 37 ^{o}C with 5 μM CellROX Green Reagent (Thermo Fisher Scientific) added to the culture medium. Cells were then washed with 1× PBS, fixed in 4% PFA for 10 min, and washed twice with 1× PBS. Samples were stained for 10 min with Hoechst 33342 dye (1 μg/mL) (Thermo Fisher Scientific), and the Fluoromount-G Mounting Medium (Sigma-Aldrich, St. Louis, Missouri, USA) was used to mount the slides.

For Mitochondrial Membrane Potential (MMP) analysis, cells were collected 72 hours after transfection, washed, and stained with 50 nM MitoTracker Red CMX and 25 nM MitoTracker Green (both from Thermo Fisher Scientific) in complete medium for 30 min, according to the manufacturer's instructions. Nuclei were stained for 15 min with Hoechst 33342 dye (blue) at a concentration of 1 μg/mL (Thermo Fisher Scientific). Cells were washed twice and then mounted on glass slides in 90% (v/v) glycerol/PBS. Images were acquired using an LSM 710 confocal laser-scanning microscope (Zeiss, Oberkochen, Germany) with a 63×, 1.4 NA oil-immersion objective and analyzed with

an in-house-optimized macro in ImageJ software (www.imagej.net). ROS and mitochondrial mass were quantified by measuring the integrated density of the green signal normalized to the total number of nuclei (blue signal). MMP was quantified by measuring the intensity difference of the red/green signal ratio. Data were obtained from at least ten fields per sample (approximately 200 cells per field).

Seahorse XF bioenergetic profiling analysis

The bioenergetic profile of $SEM^{AK\_7\_3\ KD}$ and SEM^{NC} cells was analyzed by using the Seahorse XF Pro analyzer (Agilent Technologies) and the Mito Stress Test kit (1.5 μM Oligomycin, 2.5 μM BAM15, and 0.5 μM Rotenone/Antimycin-A) (Agilent Technologies). Cells were collected after 48h transfection with AK_7_3 or DS-NC1 DsiRNA (from two independent biological replicates), as explained above, washed, counted, resuspended in complete RPMI Seahorse XF assay medium (Agilent Technologies), supplemented with glucose (10mM), pyruvate (1mM), and L-glutamine (2mM), and seeded at 6×10^4 cells/well in the Seahorse 96-well poly-D-lysine pre-coated plates (Sigma-Aldrich). Plates were centrifuged at 200 rcf without a brake for 1 min to facilitate cell adhesion, then incubated for 1 hour at 37 °C in the absence of CO_2. Seahorse analysis was performed at 37 °C in the absence of CO_2. The mean Oxygen Consumption Rate (OCR) was calculated from eight technical replicates and normalized to the number of nuclei per well, determined by Hoechst-33342 nuclear labeling and Operetta CLS imaging. Data were automatically analyzed with the Seahorse Wave Controller Software (v.2.6.1) and Wave Pro Software and Seahorse Analytics (Agilent Technologies). The parameters related to mitochondrial function (ATP production, basal respiration, maximal respiration, and spare respiratory capacity) were calculated according to the manufacturer's instructions.

Transmission electron microscopy (TEM)

48 hours after AK_7_3 or DS-NC1 DsiRNA transfection, cellular pellets (1×10^6 cells) were fixed in 3% buffered glutaraldehyde (TAAB Laboratories, Aldermaston, UK) at 4 °C for 1 hour and washed twice with PBS. Samples were then post-fixed with 1% osmium tetroxide in PBS at 4 °C for 30 min. After re-washing in 1X PBS, pellets were dehydrated in a graded series of acetone and embedded in Araldite 502 Epoxy Resin Kit (Electron Microscopy Science, Hatfield, PA, USA). Ultra-thin sections were mounted on nickel grids, stained with uranyl acetate and lead citrate, and observed with a Jeol Jem 1400 Flash electron microscope (Basiglio, Milan, Italy).

References

1. Panda AC, Gorospe M. Detection and Analysis of Circular RNAs by RT-PCR. Bio Protoc. 2018;8(6):e2775.
2. Livak KJ, Schmittgen TD. Analysis of relative gene expression data using real-time quantitative PCR and the 2(-Delta Delta C(T)) Method. Methods. 2001;25(4):402-408.
3. Meyer C, Larghero P, Lopes BA, Marschalek R. The KMT2A/MLL consensus gene structure: a comprehensive update for research and diagnostic implications. Leukemia. 2024;38(6):1403-1406.
4. Nilson I, Löchner K, Siegler G, et al. Exon/intron structure of the human ALL-1 (MLL) gene involved in translocations to chromosomal region 11q23 and acute leukaemias. Br J Haematol. 1996;93(4):966-972.
5. Théry C, Amigorena S, Raposo G, Clayton A. Isolation and characterization of exosomes from cell culture supernatants and biological fluids. Curr Protoc Cell Biol. 2006;Chapter 3(Unit 3.22).
6. Tolomeo D, Traversa D. circPVT1 and PVT1/AKT3 show a role in cell proliferation, apoptosis, and tumor subtype-definition in small cell lung cancer. Genes Chromosomes Cancer. 2023;62(7):377-391.
7. Beyer M, Krämer OH. RNA interference protocol to silence oncogenic drivers in leukemia cell lines. STAR Protoc. 2022;3(3):101512.
8. Dobin A, Davis CA, Schlesinger F, et al. STAR: ultrafast universal RNA-seq aligner. Bioinformatics. 2013;29(1):15-21.
9. Anders S, Pyl PT, Huber W. HTSeq--a Python framework to work with high-throughput sequencing data. Bioinformatics. 2015;31(2):166-169.

10. Love MI, Huber W, Anders S. Moderated estimation of fold change and dispersion for RNA-seq data with DESeq2. Genome Biol. 2014;15(12):550.
11. Yu G, Wang LG, Han Y, He QY. clusterProfiler: an R package for comparing biological themes among gene clusters. OMICS. 2012;16(5):284-287.
12. Haas BJ, Dobin A, Li B, Stransky N, Pochet N, Regev A. Accuracy assessment of fusion transcript detection via read-mapping and de novo fusion transcript assembly-based methods. Genome Biol. 2019;20(1):213.

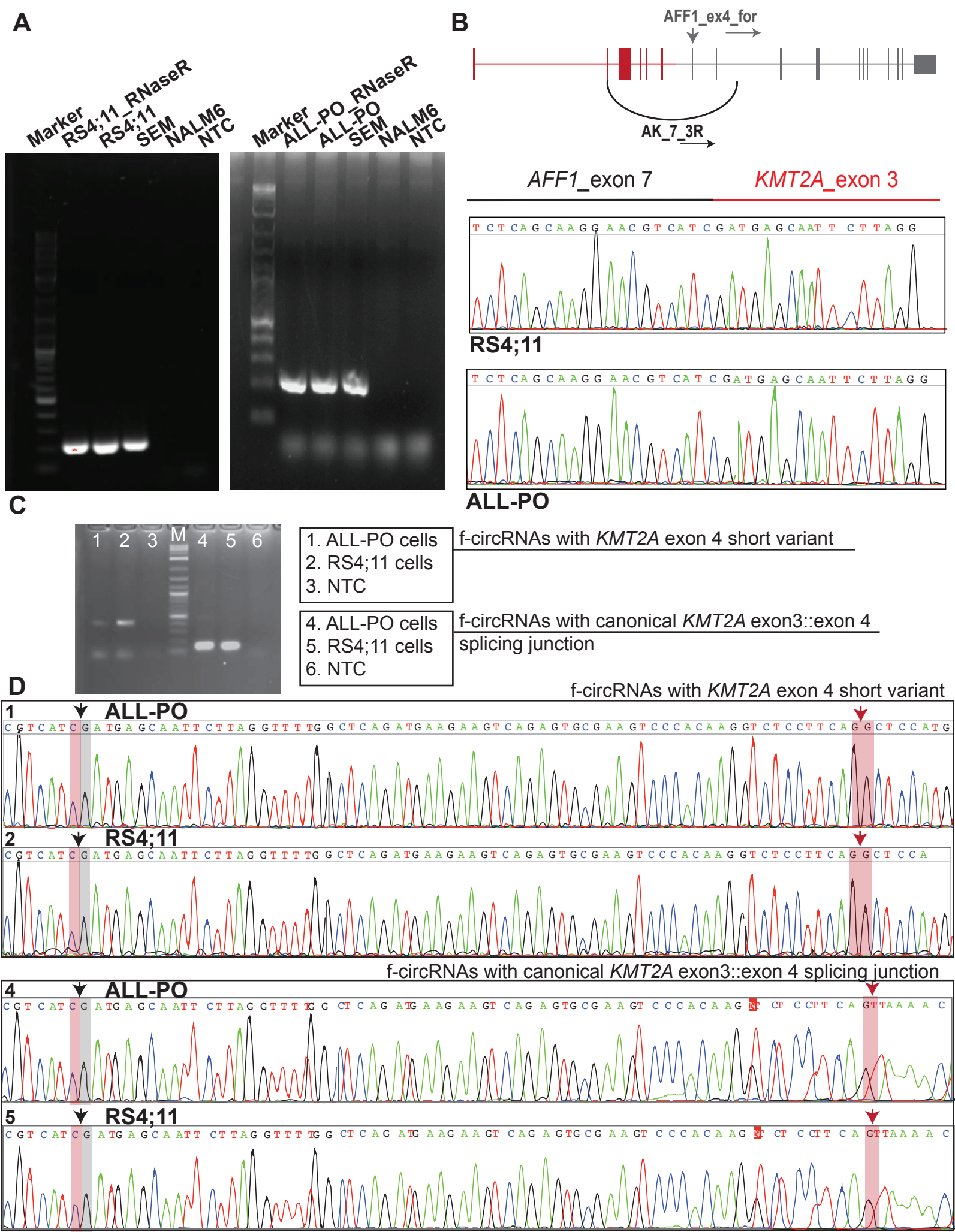
A
Marker
RS4;11_RNaseR
RS4;11
SEM
NALM6
NTC
Marker
ALL-PO_RNaseR
ALL-PO
SEM
NALM6
NTC
B
AFF1_ex4_for
AK_7_3R
AFF1_exon 7
KMT2A_exon 3
RS4;11
ALL-PO
C
1 2 3 M 4 5 6
1. ALL-PO cells
2. RS4;11 cells
3. NTC
f-circRNAs with KMT2A exon 4 short variant
4. ALL-PO cells
5. RS4;11 cells
6. NTC
f-circRNAs with canonical KMT2A exon3::exon 4 splicing junction
D
f-circRNAs with KMT2A exon 4 short variant
1 ALL-PO
2 RS4;11
f-circRNAs with canonical KMT2A exon3::exon 4 splicing junction
4 ALL-PO
5 RS4;11

Supplementary Figure S1: Molecular characterization of the AK_7_3 back-splicing junction in RS4;11, and ALL-PO cell lines. A) RT-PCR results showing the occurrence of the AK_7_3 in RS4;11 and ALL-PO cell line RNA samples, both with and without RNase R treatment. The SEM and NALM6 samples were used as positive and negative controls, respectively. NTC: Blank. Marker: 2-Log DNA ladder. B) Top: schematic representation of the divergent primer map position on *AFF1* and back-splicing junction of AK_7_3, to obtain the RT-PCR products in panel A; bottom: partial chromatograms of the Sanger sequencing products shown in panel A, showing the back-splicing junction, respectively, in RS4;11, and ALL-PO cell lines. C) RT-PCR results showing the occurrence of the AK_7_3 isoform harboring the short variant of *KMT2A* exon 4 (on the left) and the isoform harboring the canonical *KMT2A* exon3::exon 4 splicing junction (on the right) in ALL-PO and RS4;11 cell line RNA samples. NTC: Blank. M: marker, 2-Log DNA ladder. D) Partial chromatograms of the RT-PCR products shown in panel C, with the back-splicing and the *KMT2A* exon 3::exon 4 junctions indicated respectively with the black and red vertical arrows.

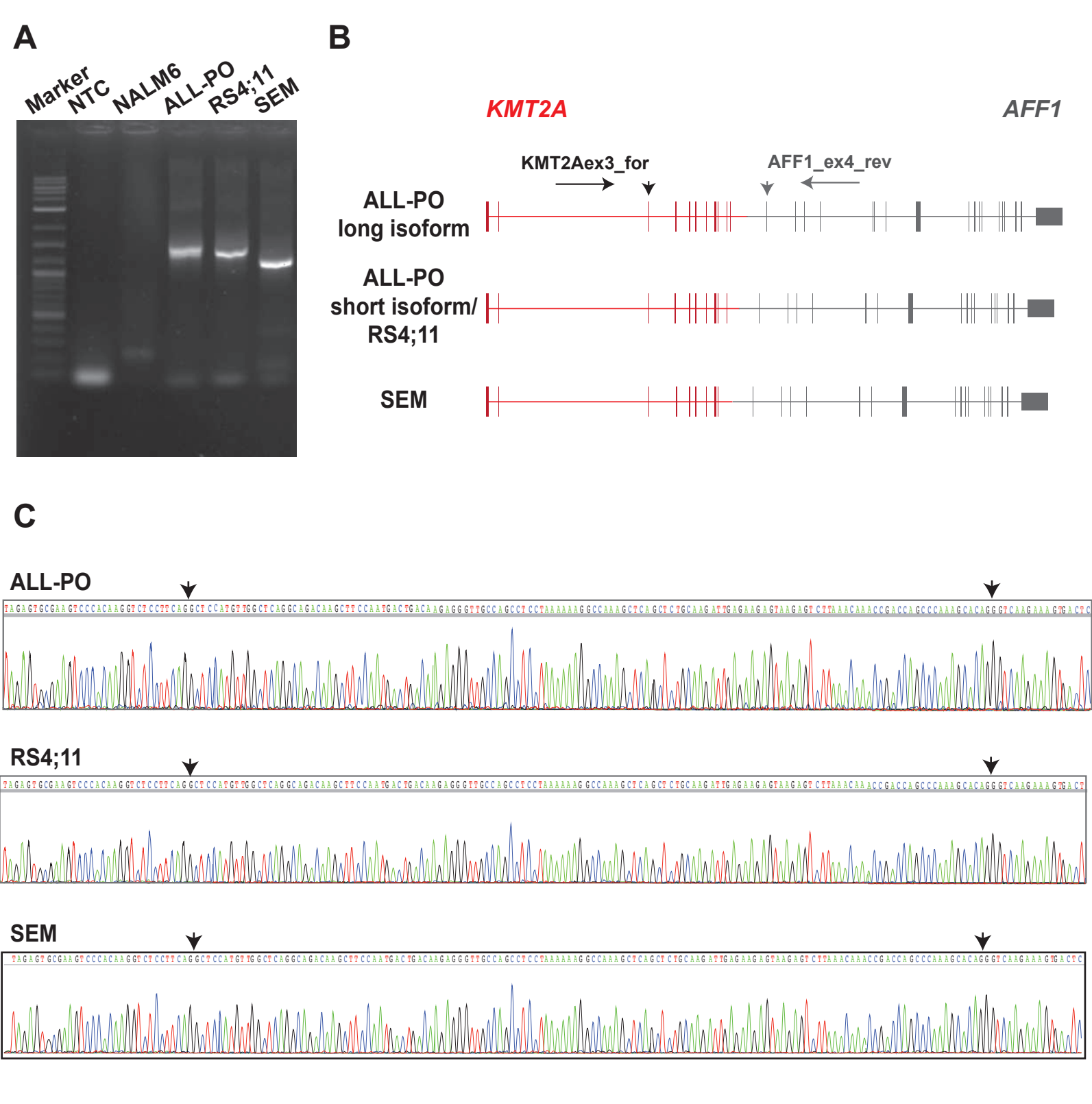
A
Marker
NTC
NALM6
ALL-PO
RS4;11
SEM
B
KMT2A
AFF1
KMT2Aex3_for
AFF1_ex4_rev
ALL-PO
long isoform
ALL-PO
short isoform/
RS4;11
SEM
C
ALL-PO
RS4;11
SEM

Supplementary Figure S2: ALL-PO, SEM, and RS4;11 cell lines express *KMT2A::AFF1* linear fusion transcript isoforms with a short variant of *KMT2A* exon 4. A) RT-PCR results showing the occurrence of the *KMT2A::AFF1* linear chimeric transcripts harboring the short variant of *KMT2A* exon 4 in ALL-PO (1,405/1,291 bp), RS4;11 (1,291 bp), and SEM (1,159 bp) cell line RNA samples. The NALM6 cells were used as a negative control. NTC: Blank. Marker: 2-Log DNA ladder. B) Schematic representation of the RT-PCR products obtained in panel A, along with the primer pair used for amplification. In ALL-PO cells, the two RT-PCR products correspond to different *KMT2A::AFF1* isoforms involving fusion of *AFF1* to *KMT2A* exon 10 or exon 11, respectively. C) Partial chromatograms of the Sanger sequencing products shown in panel A, showing the occurrence of the short variant of *KMT2A* exon 4, highlighted between the two black arrows.

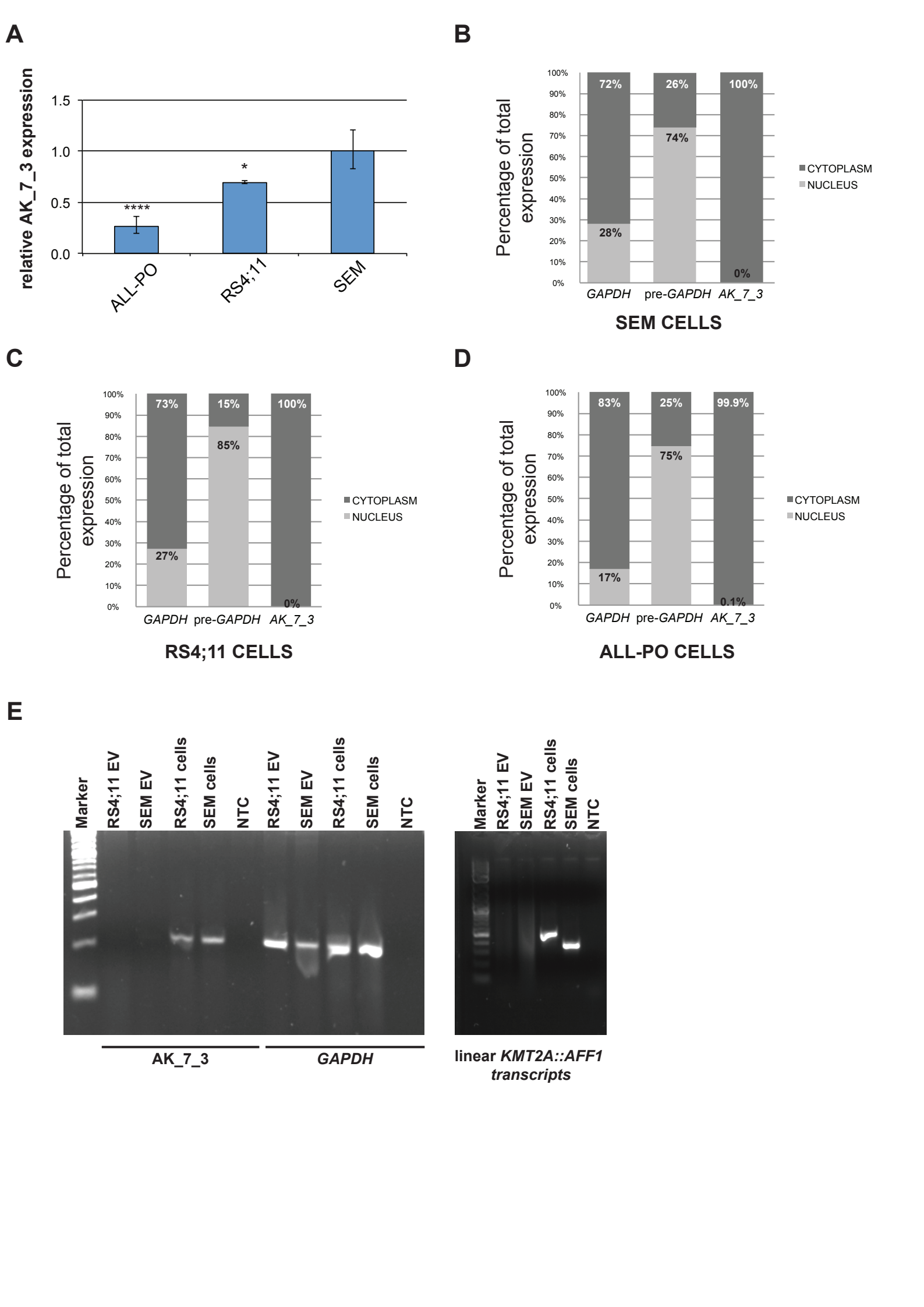
A
relative AK_7_3 expression
1.5
1.0
0.5
0.0
****
*
ALL-PO
RS4;11
SEM
B
Percentage of total expression
100%
90%
80%
70%
60%
50%
40%
30%
20%
10%
0%
72%
28%
26%
74%
100%
0%
GAPDH
pre-GAPDH
AK_7_3
CYTOPLASM
NUCLEUS
SEM CELLS
C
Percentage of total expression
73%
27%
15%
85%
100%
0%
GAPDH
pre-GAPDH
AK_7_3
CYTOPLASM
NUCLEUS
RS4;11 CELLS
D
Percentage of total expression
83%
17%
25%
75%
99.9%
0.1%
GAPDH
pre-GAPDH
AK_7_3
CYTOPLASM
NUCLEUS
ALL-PO CELLS
E
Marker
RS4;11 EV
SEM EV
RS4;11 cells
SEM cells
NTC
RS4;11 EV
SEM EV
RS4;11 cells
SEM cells
NTC
AK_7_3
GAPDH
Marker
RS4;11 EV
SEM EV
RS4;11 cells
SEM cells
NTC
linear KMT2A::AFF1 transcripts

Supplementary Figure S3: AK_7_3 quantification in cell lines, subcellular enrichment, and evaluation of its secretion in EVs. A) Relative expression (mean±SD) of the AK_7_3 f-circRNA back-splicing junction in the three B-ALL cell lines as assessed by RT-qPCR analysis. ****p<0.0001, *p<0.05 (REST 2009 software). B, C, and D) Subcellular localization of AK_7_3 in SEM (B), RS4;11 (C), and ALL-PO (D) cells, detected using cell fractionation. *GAPDH*: cytoplasmic marker; pre-*GAPDH*: nuclear marker. E) RT-PCR analysis of AK_7_3 (left panel) and linear *KMT2A::AFF1* fusion transcripts (right panel) in the RNA samples extracted from extracellular vesicles (EVs) or cells of SEM and RS4;11 cell lines. The *GAPDH* transcript (housekeeping gene) was used as a positive control.


Case 1
T C T CA G C A A G G A A C G T CA T C G A T G A G C A A T T C T T A G G
Case 3o
T C T CA G C A A G G A A C G T CA T C G A T G A G C A A T T C T T A G G
Case 3r
T C T CA G C A A G G A A C G T CA T C G A T G A G C A A T T C T T A G G
Case 5
T C T CA G C A A G G A A C G T CA T C G A T G A G C A A T T C T T A G G
Case 6
T C T CA G C A A G G A A C G T CA T C G A T G A G C A A T T C T T A G G
Case 7o
T C T CA G C A A G G A A C G T CA T C G A T G A G CA T T C T T A G G
Case 7r
T C T CA G C A A G G A A C G T CA T C G A T G A G CA T T C T T A G G
Case 8
T C T CA G C A A G G A A C G T CA T C G A T G A G C A A T T C T T A G G
Case 9
T C T CA G C A A G G A A C G T CA T C G A T G A G C A A T T C T T A G G
Case 10
T C T CA G C A A G G A A C G T CA T C G A T G A G C A A T T C T T A G G
Case 13
T C T CA G C A A G G A A C G T CA T C G A T G A G C A A T T C T T A G G
Case 15
T C T CA G C A A G G A A C G T CA T C G A T G A G C A A T T C T T A G G
Case 16
T C T CA G C A A G G A A C G T CA T C G A T G A G C A A T T C T T A G G
Case 18
T C T CA G C A A G G A A C G T CA T C G A T G A G C A A T T C T T A G G

Supplementary Figure S4: AK_7_3 back-splicing sequences in t(4;11)-positive pediatric B-ALL patients. Partial chromatograms, obtained from Sanger sequencing of the RT-qPCR products, showing the AK_7_3 back-splicing junctions (red arrows) found in pediatric B-ALL patients. The diagnostic and relapse samples from patients nos. 3 and 7 are indicated, respectively, by (o) and (r).


Case 39
T C T C A G C A A G G A A C G T C A T C G A T G A G C A A T T C T T A G G
Case 40
T C T C A G C A A G G A A C G T C A T C G A T G A G C A A T T C T T A G G
Case 42
T C T C A G C A A G G A A C G T C A T C G A T G A G C A A T T C T T A G G
Case 44
T C T C A G C A A G G A A C G T C A T C G A T G A G C A A T T C T T A G G
Case 45o
T C T C A G C A A G G A A C G T C A T C G A T G A G C A A T T C T T A G G
Case 46
T C T C A G C A A G G A A C G T C A T C G A T G A G C A A T T C T T A G G A
Case 48
T C T C A G C A A G G A A C G T C A T C G A T G A G C A A T T C T T A G G
Case 49
T C T C A G C A A G G A A C G T C A T C G A T G A G C A A T T C T T A G G
Case 50
T C T C A G C A A G G A A C G T C A T C G A T G A G C A A T T C T T A G G
Case 52
T C T C A G C A A G G A A C G T C A T C G A T G A G C A A T T C T T A G G
Case 54
T C T C A G C A A G G A A C G T C A T C G A T G A G C A A T T C T T A G G
Case 57
T C T C A G C A A G G A A C G T C A T C G A T G A G C A A T T C T T A G G
Case 58
T C T C A G C A A G G A A C G T C A T C G A T G A G C A A T T C T T A G G
Case 59
T C T C A G C A A G G A A C G T C A T C G A T G A G C A A T T C T T A G G
Case 60
T C T C A G C A A G G A A C G T C A T C G A T G A G C A A T T C T T A G G
Case 61
T C T C A G C A A G G A A C G T C A T C G A T G A G C A A T T C T T A G G
Case 62
T C T C A G C A A G G A A C G T C A T C G A T G A G C A A T T C T T A G G

Supplementary Figure S5: AK_7_3 back-splicing sequences in t(4;11)-positive adult B-ALL patients. Partial chromatograms, obtained from Sanger sequencing of the RT-qPCR products, showing the AK_7_3 back-splicing junctions (red arrows) found in adult B-ALL patients. The diagnostic sample of patient no. 45 is indicated with (o).

A

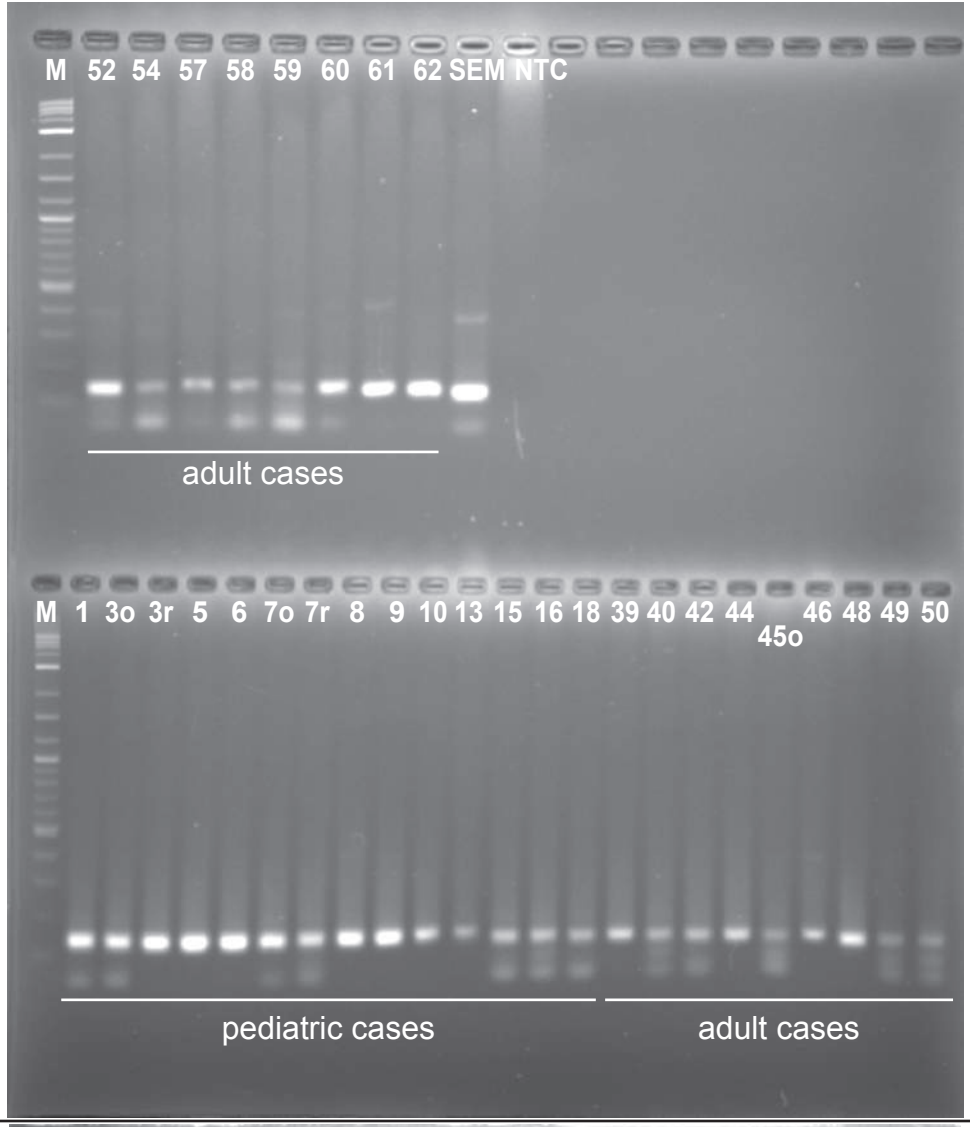

f-circRNAs with canonical *KMT2A* exon3::exon 4 splicing junction

B

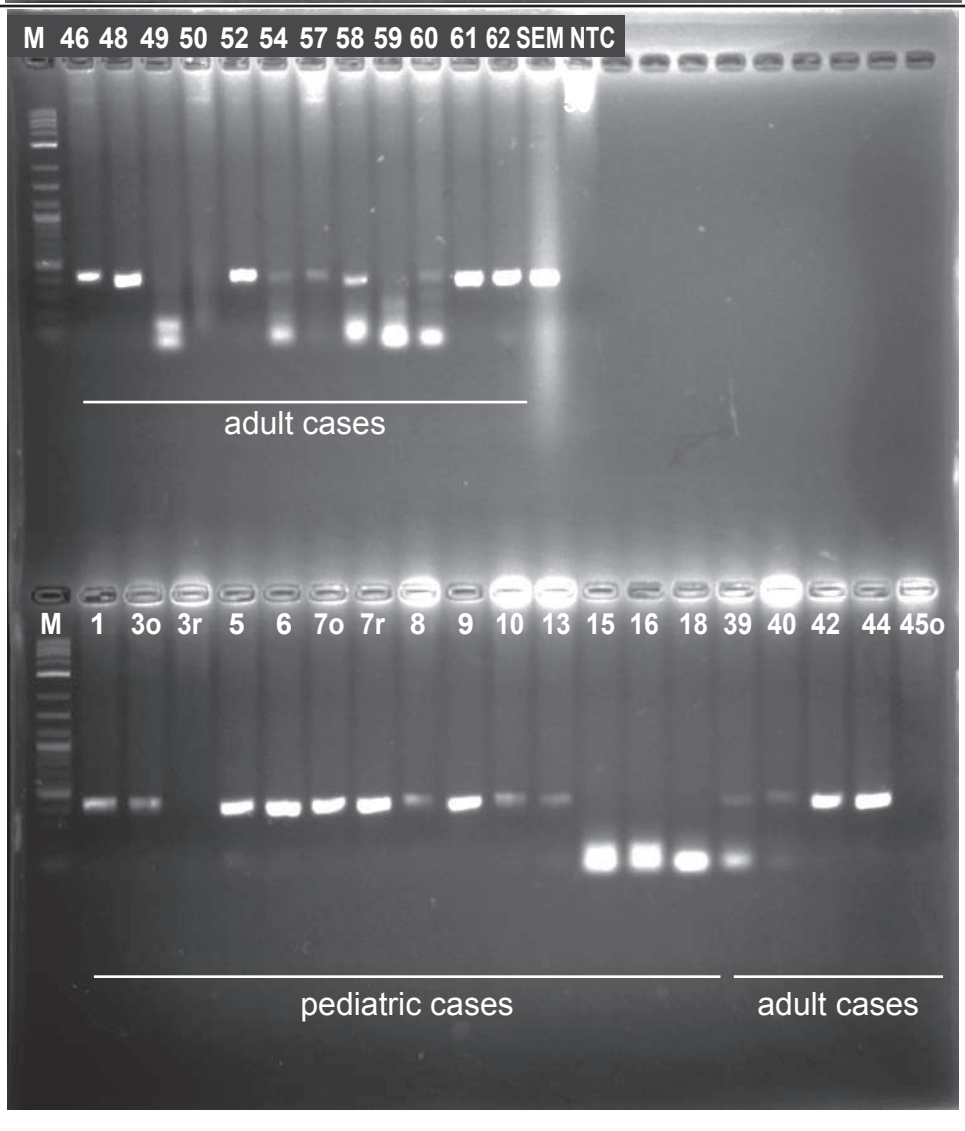

f-circRNAs with *KMT2A* exon 4 short variant

Supplementary Figure S6: RT-PCR results corresponding to the AK_7_3 isoforms in B-ALL patients with the t(4;11) translocation. A) RT-PCR results showing the occurrence of AK_7_3 harboring the canonical *KMT2A* exon3::exon 4 splicing junction (A) or the short *KMT2A* exon 4 variant (B) in all pediatric and adult patients positive for the t(4;11) translocation. The SEM sample was used as a positive control. NTC: Blank. M: Marker, 2-Log DNA ladder.

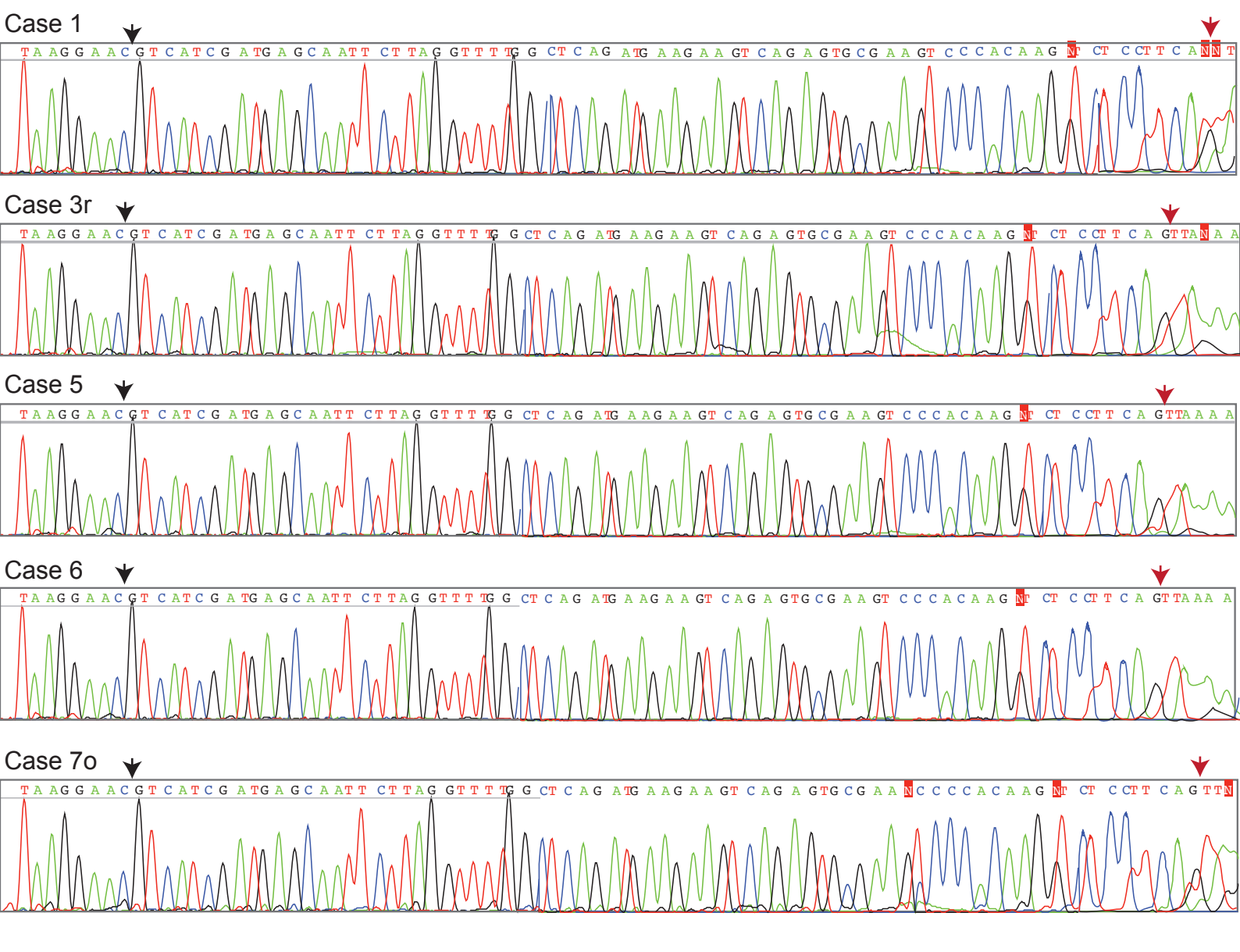
Case 1
TAAGGAACGTCATCGATGAGCAATTCTTAGGTTTTGGCTCAGATGAAGAAGTCAGAGTGCGAAGTCCCACAAGNTCTCCTTCANNT
Case 3r
TAAGGAACGTCATCGATGAGCAATTCTTAGGTTTTGGCTCAGATGAAGAAGTCAGAGTGCGAAGTCCCACAAGNTCTCCTTCAGTTANAA
Case 5
TAAGGAACGTCATCGATGAGCAATTCTTAGGTTTTGGCTCAGATGAAGAAGTCAGAGTGCGAAGTCCCACAAGNTCTCCTTCAGTTAAAA
Case 6
TAAGGAACGTCATCGATGAGCAATTCTTAGGTTTTGGCTCAGATGAAGAAGTCAGAGTGCGAAGTCCCACAAGNTCTCCTTCAGTTAAAA
Case 7o
TAAGGAACGTCATCGATGAGCAATTCTTAGGTTTTGGCTCAGATGAAGAAGTCAGAGTGCGAANCCCCACAAGNTCTCCTTCAGTTN

Supplementary Figure S7: Sanger sequencing of the AK_7_3 isoforms harboring the canonical *KMT2A* exon 3::exon 4 junctions in t(4;11)-positive B-ALL patients. Partial chromatograms, obtained from Sanger sequencing of some exemplificative RT-PCR products, showing the back-splicing junction and the canonical *KMT2A* exon 3::exon 4 splicing junction, indicated respectively with the black and red vertical arrows. (o) indicates the diagnostic sample of patient no.7, while (r) indicates the relapse sample from patients no. 3.

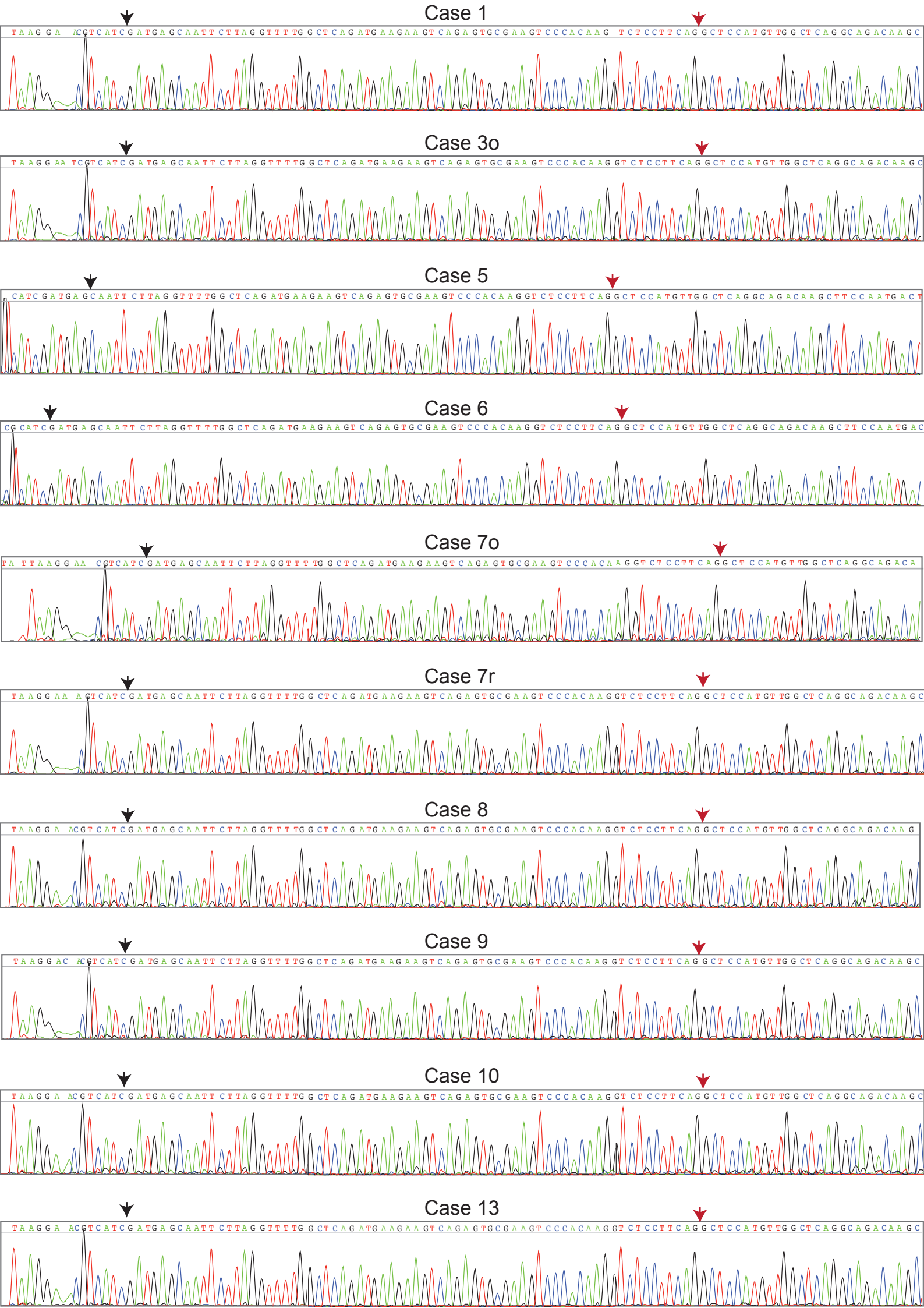
Case 1
Case 3o
Case 5
Case 6
Case 7o
Case 7r
Case 8
Case 9
Case 10
Case 13

Supplementary Figure S8: Sanger sequencing of the AK_7_3 sequences harboring the short *KMT2A* exon 4 variant in t(4;11)-positive pediatric B-ALL patients. Partial chromatograms, obtained from Sanger sequencing of the RT-qPCR products, showing the back-splicing junction and the *KMT2A* exon 3::exon 4 (short variant), indicated respectively with the black and red vertical arrows. The diagnostic and relapse samples from patient no. 7 are indicated, respectively, by (o) and (r); while (o) indicates the diagnostic sample from patient no. 3.

Case 39

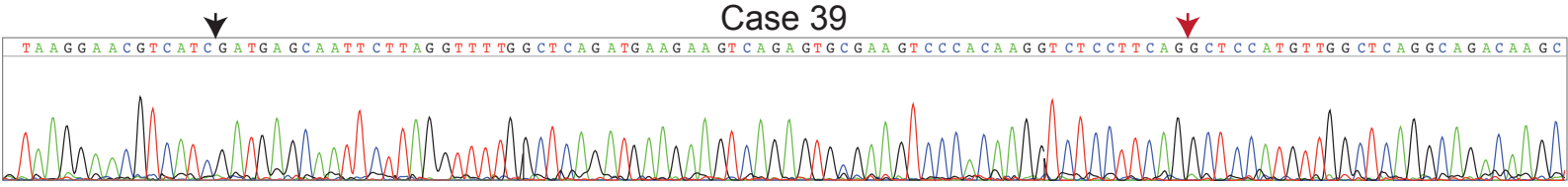

Case 40

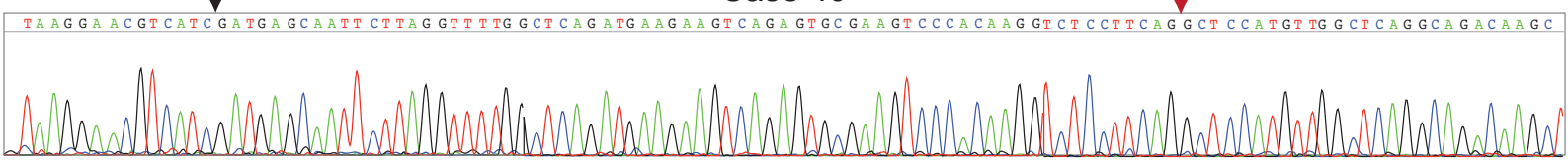

Case 42

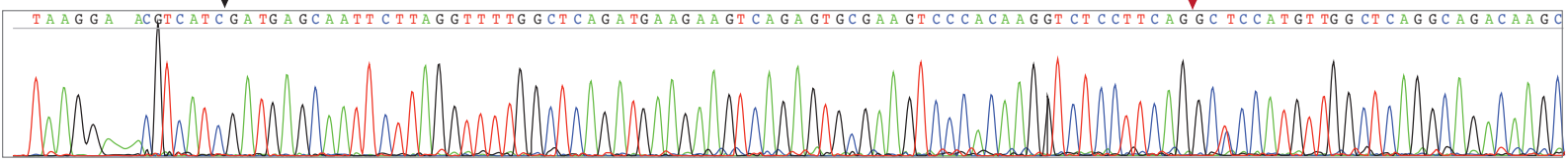

Case 44

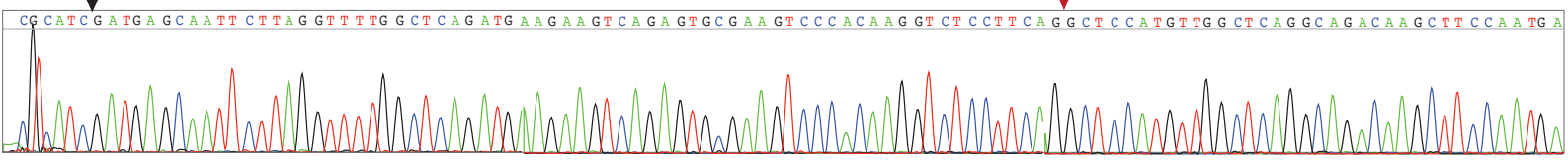

Case 46

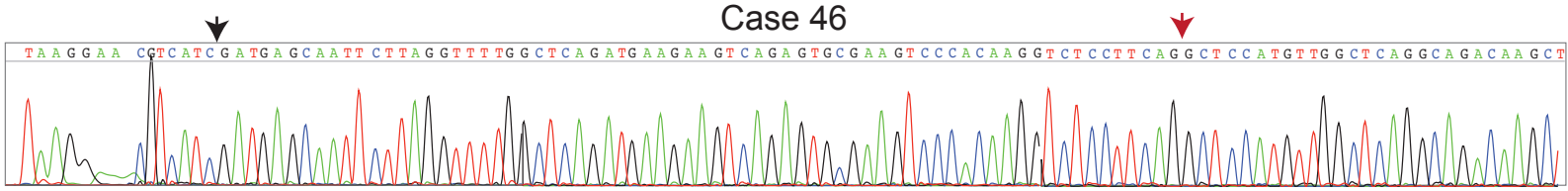

Case 48

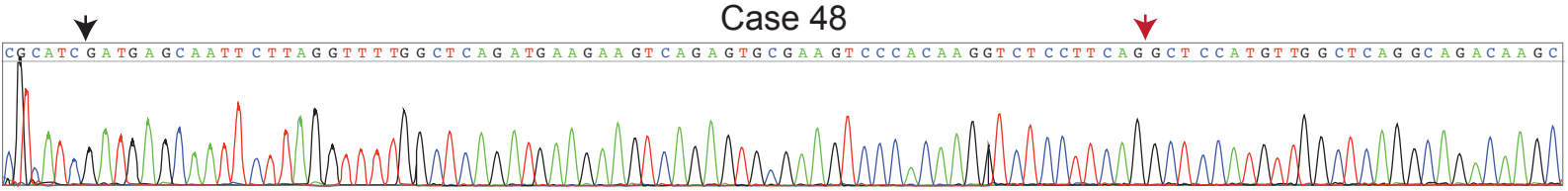

Case 52

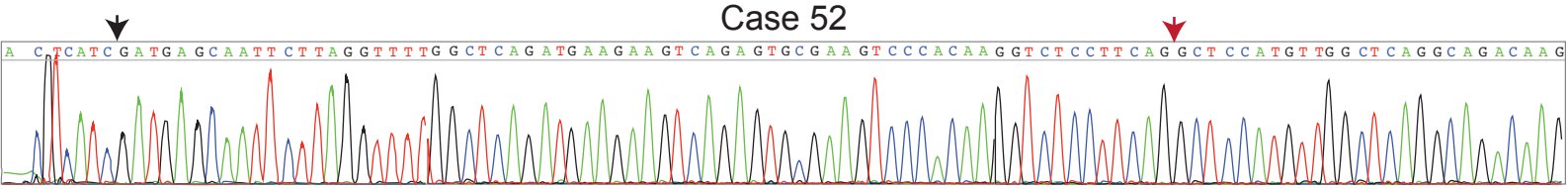

Case 57

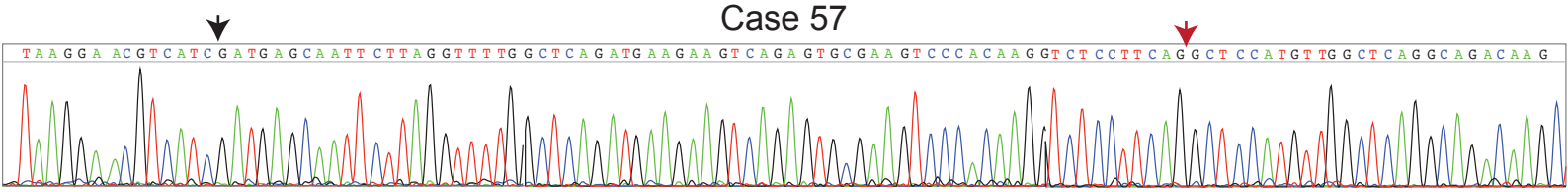

Case 58

Case 61

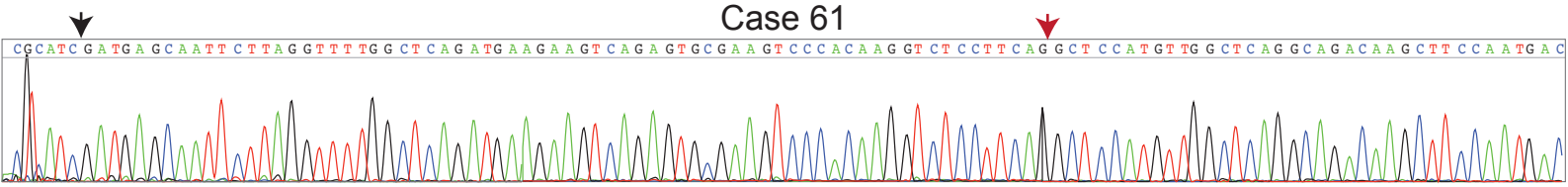

Case 62

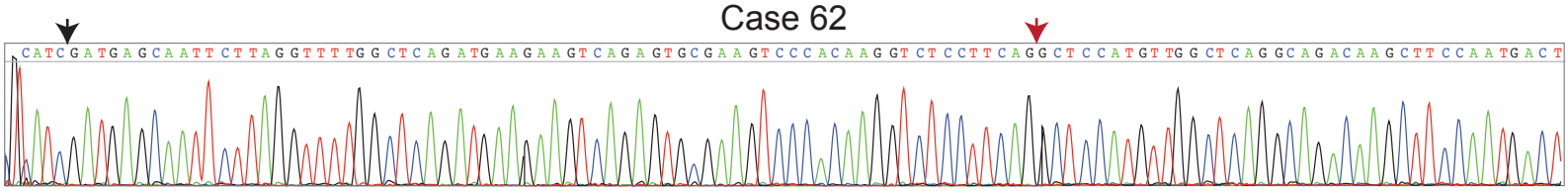

Supplementary Figure S9: Sanger sequencing of the AK_7_3 sequences harboring the short *KMT2A* exon 4 variant in t(4;11)-positive adult B-ALL patients. Partial chromatograms, obtained from Sanger sequencing of the RT-qPCR products, with the back-splicing junction and the *KMT2A* exon 3::exon 4 (short variant) are indicated respectively with the black and red vertical arrows.

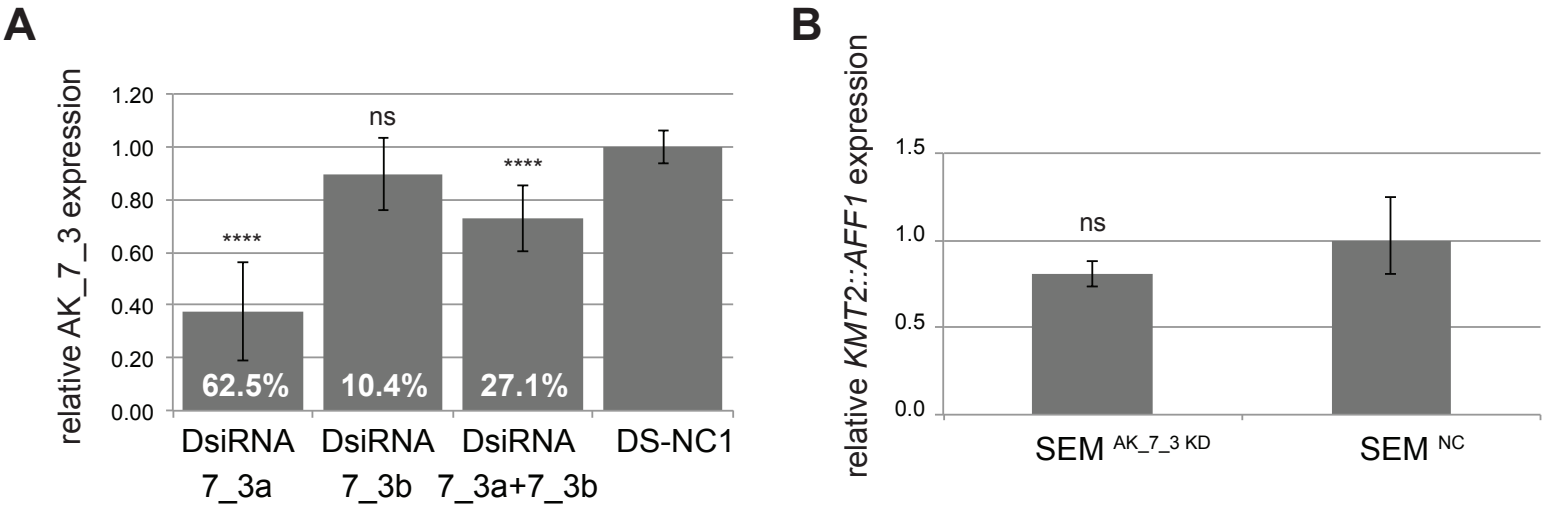
A
relative AK_7_3 expression
1.20
1.00
0.80
0.60
0.40
0.20
0.00
ns
****
****
62.5%
10.4%
27.1%
DsiRNA 7_3a
DsiRNA 7_3b
DsiRNA 7_3a+7_3b
DS-NC1
B
relative KMT2::AFF1 expression
1.5
1.0
0.5
0.0
ns
SEM AK_7_3 KD
SEM NC

Supplementary Figure S10: Transfection with 7_3a DsiRNA efficiently decreases AK_7_3 expression without affecting the expression of the *KMT2A::AFF1* fusion linear transcript. A) RT-qPCR results display a decrease in the AK_7_3 relative expression in the SEM cell line after transfection with specific DsiRNAs. DsiRNA 7_3a showed higher knockdown efficiency than 7_3b or the combined transfection of 7_3a and 7_3b, compared with the control sample (DS-NC1), used as a calibrator. For each condition, the percentage of silencing is reported. B) SEM cells do not show a significant decrease in the *KMT2A::AFF1* linear fusion relative expression after AK_7_3 silencing performed with DsiRNA 7_3a ($SEM^{AK\_7\_3\ KD}$) with respect to control (SEM^{NC}), used as a calibrator. Results are shown as mean ±SD.
****p<0.0001, ns: not significant (REST 2009 software).

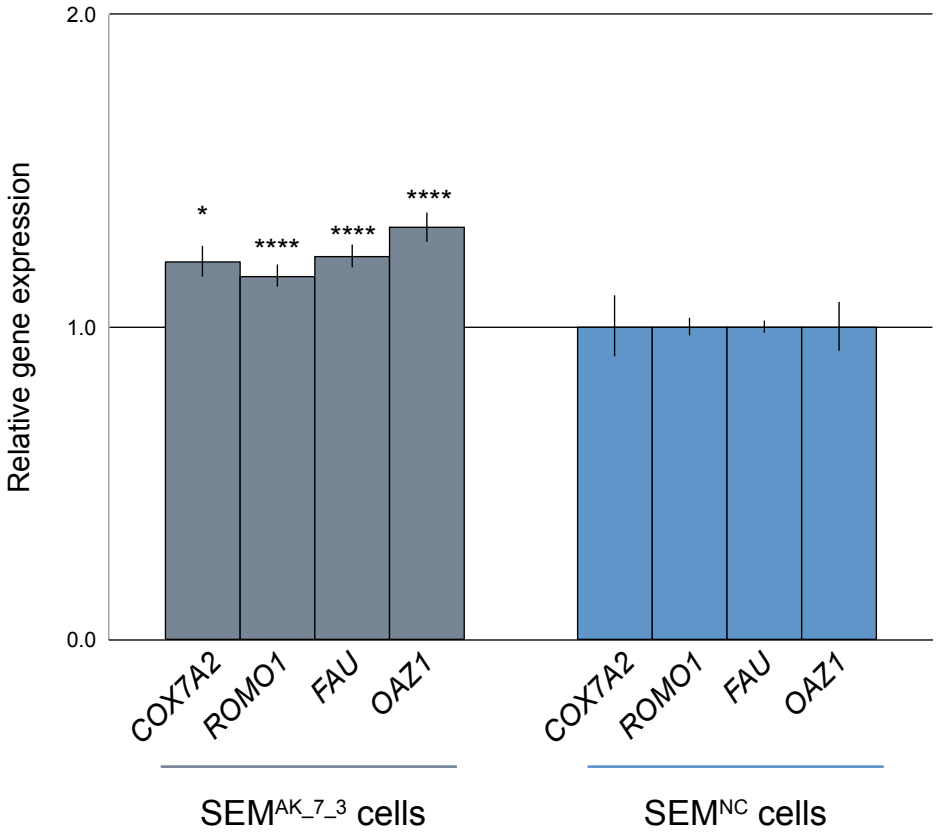
2.0
1.0
0.0
Relative gene expression
*
****
****
****
COX7A2
ROMO1
FAU
OAZ1
COX7A2
ROMO1
FAU
OAZ1
SEMAK_7_3 cells
SEMNC cells

Supplementary Figure S11: *COX7A2*, *ROMO1*, *FAU*, and *OAZ1* gene upregulation in SEM cells induced by AK_7_3 KD. RT-qPCR assays showing significant upregulation of *COX7A2*, *ROMO1*, *FAU*, and *OAZ1* in $SEM^{AK\_7\_3\ KD}$ vs. SEM^{NC}, the latter used as the calibrator. Results are shown as mean±SD. ****p<0.0001, *p<0.05 (REST 2009 software).

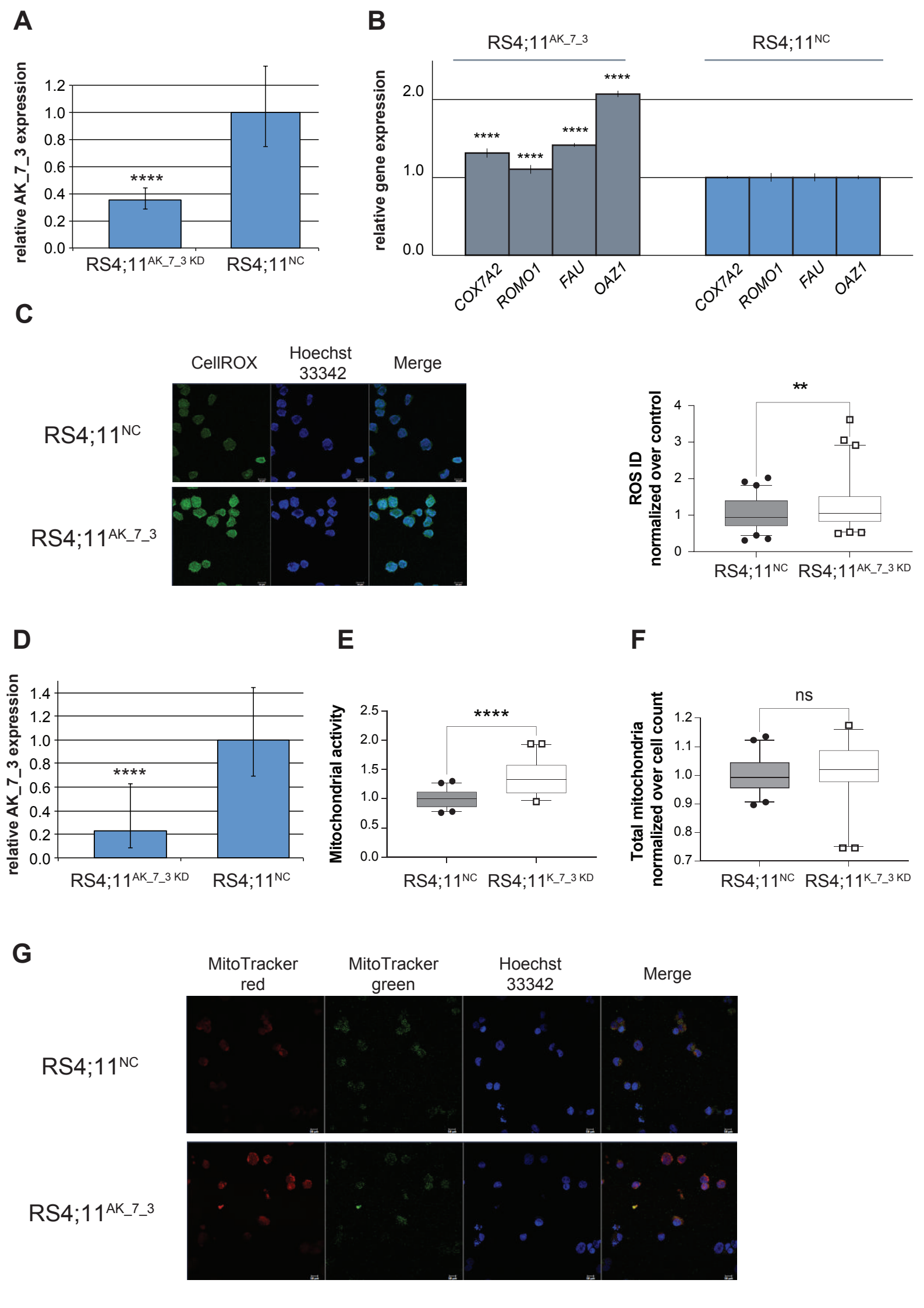
A
relative AK_7_3 expression
1.2
1.0
0.8
0.6
0.4
0.2
0.0
****
RS4;11AK_7_3 KD
RS4;11NC
B
RS4;11AK_7_3
RS4;11NC
relative gene expression
2.0
1.0
0.0
****
****
****
****
COX7A2
ROMO1
FAU
OAZ1
COX7A2
ROMO1
FAU
OAZ1
C
CellROX
Hoechst 33342
Merge
RS4;11NC
RS4;11AK_7_3
ROS ID normalized over control
**
4
3
2
1
0
RS4;11NC
RS4;11AK_7_3 KD
D
relative AK_7_3 expression
1.4
1.2
1.0
0.8
0.6
0.4
0.2
0.0
****
RS4;11AK_7_3 KD
RS4;11NC
E
Mitochondrial activity
2.5
2.0
1.5
1.0
0.5
0.0
****
RS4;11NC
RS4;11K_7_3 KD
F
Total mitochondria normalized over cell count
ns
1.2
1.1
1.0
0.9
0.8
0.7
RS4;11NC
RS4;11K_7_3 KD
G
MitoTracker red
MitoTracker green
Hoechst 33342
Merge
RS4;11NC
RS4;11AK_7_3

Supplementary Figure S12: AK_7_3 knockdown in RS4;11 cells corroborates its impact on mitochondrial functions. A) RT-qPCR results showing the decrease in the AK_7_3 relative expression in the RS4;11 cells used in RT-qPCR (panel B) and ROS (panel C) analyses, 48 hours after electroporation of the DsiRNA 7_3a as compared to control cells. Error bars refer to the SD. ****p<0.0001 (REST 2009 software). B) RT-qPCR assays showing significant upregulation of *COX7A2*, *ROMO1*, *FAU*, and *OAZ1* in RS4;11$^{AK_7_3\ KD}$ vs. RS4;11^{NC} (used as the calibrator). Results are shown as mean±SD. ****p<0.0001 (REST 2009 software). C) ROS confocal microscopy analysis in RS4;11$^{AK_7_3\ KD}$ and RS4;11^{NC} cells. On the left panel, images from one representative experiment are shown: green signal, CellROX; blue signal, Hoechst 33342. Bar graphs on the right report the quantification of ROS (mean green signal/mean blue signal) normalized to RS4;11^{NC}. **p<0.01 (Unpaired t-test). D) RT-qPCR results showing the decrease in the AK_7_3 relative expression in the RS4;11 cells used in mitochondrial membrane potential analyses, 72 hours after electroporation of the DsiRNA 7_3a as compared to RS4;11^{NC} cells. Error bars refer to the SD. ****p<0.0001 (REST 2009 software). E-G) Confocal analysis of mitochondrial membrane potential in RS4;11$^{AK_7_3\ KD}$ and RS4;11^{NC} by using MitoTracker red/green and Hoechst 33342. Bar graphs display the quantification of mitochondrial activity (mean red signal/mean green signal) as a measure of mitochondrial activity (panel E), and mitochondrial mass (mean green signal/mean blue signal) as a measure of total mitochondria (panel F). Data were normalized to RS4;11^{NC} cells. ****p<0.0001 (Unpaired t-test), ns: not significant. In panel G, images from one representative experiment are shown: red signal, MitoTracker red; green signal, MitoTracker green; blue signal, Hoechst 33342.

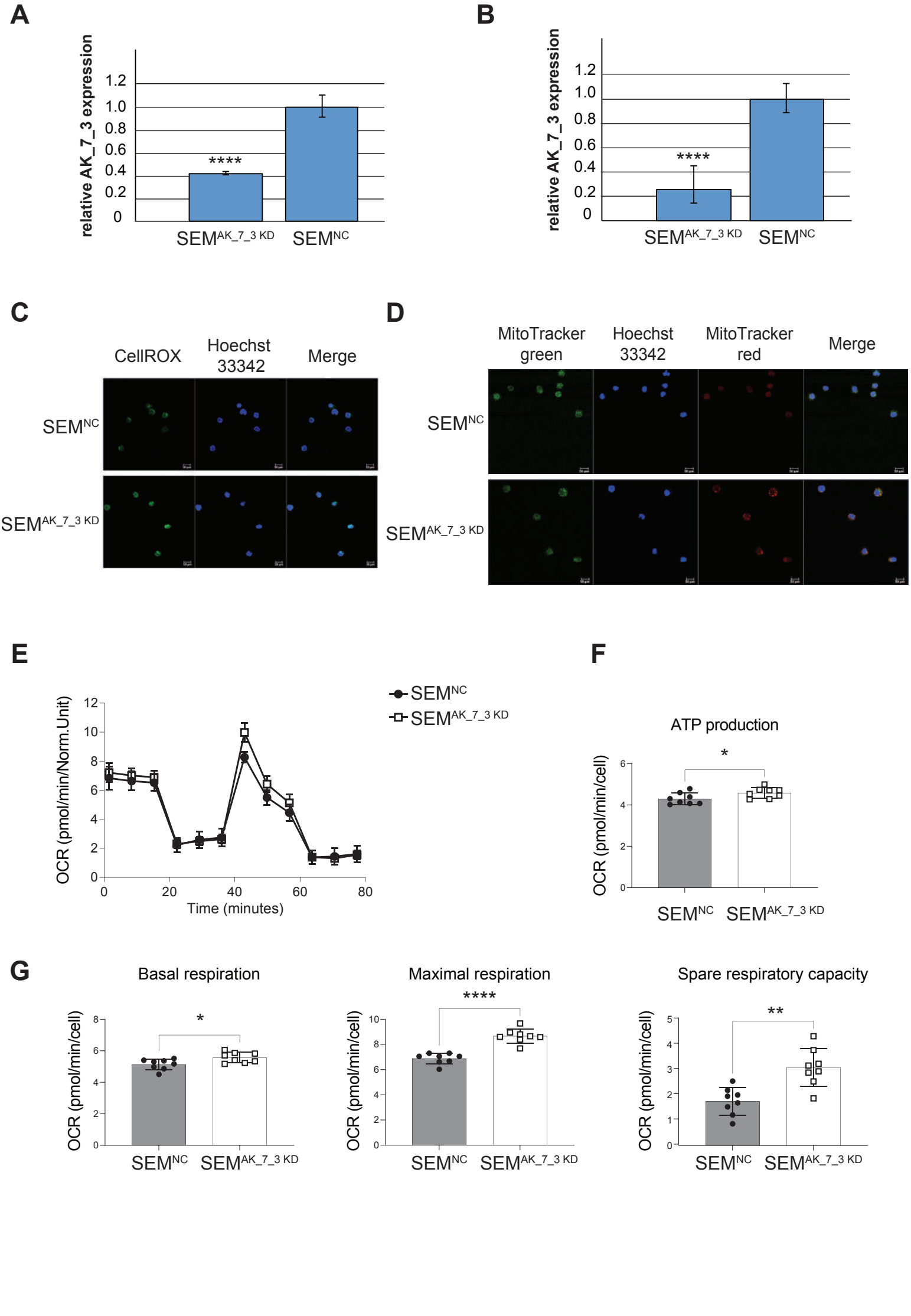
A
relative AK_7_3 expression
1.2
1.0
0.8
0.6
0.4
0.2
0
****
SEMAK_7_3 KD
SEMNC
B
relative AK_7_3 expression
1.2
1.0
0.8
0.6
0.4
0.2
0
****
SEMAK_7_3 KD
SEMNC
C
CellROX
Hoechst 33342
Merge
SEMNC
SEMAK_7_3 KD
D
MitoTracker green
Hoechst 33342
MitoTracker red
Merge
SEMNC
SEMAK_7_3 KD
E
SEMNC
SEMAK_7_3 KD
OCR (pmol/min/Norm.Unit)
12
10
8
6
4
2
0
0
20
40
60
80
Time (minutes)
F
ATP production
*
OCR (pmol/min/cell)
6
4
2
0
SEMNC
SEMAK_7_3 KD
G
Basal respiration
*
OCR (pmol/min/cell)
8
6
4
2
0
SEMNC
SEMAK_7_3 KD
Maximal respiration
****
OCR (pmol/min/cell)
10
8
6
4
2
0
SEMNC
SEMAK_7_3 KD
Spare respiratory capacity
**
OCR (pmol/min/cell)
5
4
3
2
1
0
SEMNC
SEMAK_7_3 KD

Supplementary Figure S13: AK_7_3 knockdown in SEM cells affects mitochondrial functions. A-B) RT-qPCR results showing the decrease in the AK_7_3 relative expression in the SEM cells used in confocal microscopy analyses and Seahorse bioenergetic profiling, 48 (A) and 72 (B) hours after transfection with the DsiRNA 7_3a as compared to control cells. Error bars refer to the SD. ****p<0.0001 (REST 2009 software). C) Confocal microscopy analysis of ROS in $SEM^{AK\_7\_3\ KD}$ and SEM^{NC} cells 48 hours after transfection. Green signal, CellROX; blue signal, Hoechst 33342. Images from one representative experiment are shown. D) Confocal microscopy analysis of mitochondrial membrane potential of $SEM^{AK\_7\_3\ KD}$ and SEM^{NC} cells 72 hours after transfection. Green signal, MitoTracker green; blue signal, Hoechst 33342; red signal, MitoTracker red. Images from one representative experiment are shown. E) Seahorse bioenergetic profiling of SEM cells 48 hours after transfection, by using the Seahorse XF Mito Stress Test. F) Total ATP produced by mitochondrial respiration. The bar graph reports the mean OCR values of eight replicates. *p<0.05 (Unpaired t-test). G) Histograms showing the basal (left) and maximal (middle) mitochondrial respiration, and the spare respiratory capacity (right). The bar graph shows the mean OCR values from eight replicates. *p<0.05 **p<0.01 ****p<0.0001 (Unpaired t-test).

Table S1: List of B-ALL patients analysed.

Case no.	Code	Age	Sex	Age subgroup (Pediatric/Adult)	Disease stage (Onset/Follow-up/Relapse)	Karyotype	Fusion transcript	Sample type	% blast percentage	AK_7_3 recurrence	AK_7_3 alternative exon 4 isofom
1	MD	4	m	Pediatric	Onset	46,XY,t(4;11)(q21;q23)[7]	*KMT2A::AFF1*	BM	95	Y	Y
2	PN	11	f	Pediatric	Onset	NA	*KMT2A::AFF1*	BM	93	N	NA
3o	CE	9	f	Pediatric	Onset	NA	*KMT2A::AFF1*	BM	94	Y	Y
3r				Pediatric	Relapse	46,XX,t(4;11)(q21;q23)[20]	*KMT2A::AFF1*	BM	84	Y	N
4	AA	7	m	Pediatric	Onset	53,XX,+?4,+21,+21,inc[3]/46,XX[15]	*KMT2A::AFF1*	BM	90	N	NA
5	OM	12	m	Pediatric	Onset	NA	*KMT2A::AFF1*	BM	93	Y	Y
6	PE	17	m	Pediatric	Onset	NA	*KMT2A::AFF1*	BM	90	Y	Y
7o	PV	1	f	Pediatric	Onset	46,XX,t(4;11)(q21;q23)[8]/46,XX[3]	*KMT2A::AFF1*	BM	65	Y	Y
7r					Relapse	NA		BM	80	Y	Y
8	1035417FS	1	f	Pediatric	Onset	NA	*KMT2A::AFF1*	BM	75	Y	Y
9	1037839FR	1	f	Pediatric	Onset	NA	*KMT2A::AFF1*	BM	89	Y	Y
10	1051489DGA	9	f	Pediatric	Onset	NA	*KMT2A::AFF1*	BM	86	Y	Y
11	14608	1	f	Pediatric	Onset	NA	*KMT2A::AFF1*	BM	62	N	NA
12	6065	8 months	m	Pediatric	Onset	NA	*KMT2A::AFF1*	BM	95	N	NA
13	F080905E	9mo	m	Pediatric	Onset	46,XX,t(4;11)(q21;q23)[3]/46,XX[7]	*KMT2A::AFF1*	PB	90	Y	Y
14	Z050913G	5mo	f	Pediatric	Onset	46,XX,t(4;11)(q21;q23)[22]	*KMT2A::AFF1*	BM	80	N	NA
15	F221216G	4mo	f	Pediatric	Onset	46,XX,t(4;11)(q21;q23)[13]	*KMT2A::AFF1*	BM	92	Y	N
16	R170519C	1mo	f	Pediatric	Onset	46,XX,ins(11;4)(q23;q21-q23?)[17]/46,XX[3]	*KMT2A::AFF1*	BM	88	Y	N
17	P130105A	15	m	Pediatric	Onset	NA	*KMT2A::AFF1*	BM	97	N	NA
18	C171000G	9	f	Pediatric	Onset	46,XX,t(4;11)(q21;q23)[10]	*KMT2A::AFF1*	BM	94	Y	N
19	AA	1	f	Pediatric	Onset	46,XX	None	BM	90	N	NA
20	BGS	16	m	Pediatric	Onset	NA	None	BM	90	N	NA
21	CG	3	m	Pediatric	Onset	48,XY,-13,der(16)t(13;16)(q14;p13),+21,+mar,inc[12]/46,XY[8]	None	BM	85	N	NA
22	PG	2	f	Pediatric	Onset	NA	None	BM	72	N	NA
23	SY	3	f	Pediatric	Onset	46,XX[20]	None	BM	90	N	NA
24	CD	5	m	Pediatric	Onset	NA	None	BM	87	N	NA
25	ZL	13	m	Pediatric	Onset	46,XY,add(9)(p?21),inc[6]/46,XY[2]	*ETV6::RUNX1*	BM	84	N	NA
26	FA	6	f	Pediatric	Onset	NA	*ETV6::RUNX1*	BM	76	N	NA
27	MB	2	m	Pediatric	Onset	46,XY[20]	*ETV6::RUNX1*	BM	77	N	NA
28	BLAE	6	m	Pediatric	Onset	44~45,XY,del(3)(p?12),-8,-10,?iso(10)(q11),-11,add(13)(p13),add(19)(p13),-21,+mar,inc[cp18]/46,XY[2]	*ETV6::RUNX1*	BM	80	N	NA
29	RL	5	m	Pediatric	Onset	NA	None	BM	90	N	NA
30	PP	9	m	Pediatric	Onset	46,XY[10]	None	BM	77	N	NA
31	MA	2	f	Pediatric	Onset	56~58,XX,+X,+4,+5,+6,+?9,+10,+?11,+18,+21,+21,inc[14]	None	BM	85	N	NA
32	MM	4	f	Pediatric	Onset	NA	None	BM	88	N	NA
33	SD	3	f	Pediatric	Onset	55,XX,+?5,+6,+8,+?10,+?15,+16,+18,der(19)t(1;19)(q23;p13),+21,+21[10]/46,XX[6]	None	BM	76	N	NA
34	MZ	3	f	Pediatric	Onset	52~54,XX,+?4,+?6,+21,inc[cp3]/46,XX[12]	None	BM	80	N	NA
35	PJ	17	m	Pediatric	Onset	NA	None	BM	77	N	NA
36	TF	14	m	Pediatric	Onset	NA	None	BM	56	N	NA
37	PAM	3	f	Pediatric	Onset	NA	None	BM	80	N	NA
38	SL	3	m	Pediatric	Onset	58~60,XY,+Y,+?12,+17,+18,+21,inc[19]/46,XY[5]	None	BM	70	N	NA
39	1210	50	m	Adult	Relapse	NA	*KMT2A::AFF1*	BM	50	Y	Y
40	2940	48	m	Adult	Relapse	NA	*KMT2A::AFF1*	BM	10	Y	Y
41	3057	49	m	Adult	Relapse	NA	*KMT2A::AFF1*	PB	73	N	NA
42	68098	21	m	Adult	Relapse	46,XX,t(4;11)(q21;q23),de17p13[20]	*KMT2A::AFF1*	BM	100	Y	Y
43o	1496/22	21	m	Adult	Onset	NA	*KMT2A::AFF1*	BM	NA	N	NA
43r	2388/23	21			Relapse	45,XY,t(4;11)(q21;q23),-9,-17,+mar[3]/46,XY[17]	*KMT2A::AFF1*	PB	50	N	NA
44	989/25	41	f	Adult	Onset	46,XX,t(4;11)(q21;q23)[7]/46,idem,i(7)(q10)[2]/46,XX[11]	*KMT2A::AFF1*	BM	74	Y	Y
45o	A230359LEdA	61	f	Adult	Onset	46,XX,t(4;11)(q21;q23),i(7)(q10)[13]	*KMT2A::AFF1*	BM	95	Y	N
45f (1)	A230359LEdAF1	61	f	Adult	Follow-up	46,XX[20]	*KMT2A::AFF1*	BM	0	N	NA
45f (10)	A230359LEdAF2	61	f	Adult	Follow-up	NA	*KMT2A::AFF1*	BM	0	N	NA
45f (11)	A230359LEdAF3	61	f	Adult	Follow-up	NA	*KMT2A::AFF1*	BM	0	N	NA
46	S181188A	29	f	Adult	Onset	46,XX,t(4;11)(q21;q23)[8]/46,XX,t(4;11)(q21;q23),i(7)(q10)[6]/46,XX[7]	*KMT2A::AFF1*	BM	90	Y	Y
47	FW291072CM	51	m	Adult	Onset	46,XY,t(4;11)(q21;q23)[24]/46,XY[4]	*KMT2A::AFF1*	PB	95	N	NA
48	989/22	62	f	Adult	Relapse	NA	*KMT2A::AFF1*	BM	86	Y	Y
49	49504	74	m	Adult	Onset	46,XY,t(4;11)(q21;q23)[18]/46,XY[5]	*KMT2A::AFF1*	PB	98	Y	N
50	49413	46	f	Adult	Onset	NA	*KMT2A::AFF1*	PB	93	Y	Y
51	34549	46	m	Adult	Onset	46 XY, t(4;11)(q21;q23)[11]/46 XY[3]	*KMT2A::AFF1*	PB	92	N	NA
52	37606	54	m	Adult	Onset	NA	*KMT2A::AFF1*	BM	NA	Y	Y
53	41391	48	f	Adult	Onset	46,XX,t(4;11)(q21;q23)[7]/46,XX[2]	*KMT2A::AFF1*	BM	60	N	NA
54	43034	68	f	Adult	Onset	46,XX,t(4;11)(q21;q23),i(7)(q10)[3]/46,XX[17]	*KMT2A::AFF1*	BM	93	Y	N
55	7494	41	f	Adult	Onset	NA	*KMT2A::AFF1*	PB	90	N	NA
56	2357	21	f	Adult	Onset	NA	*KMT2A::AFF1*	BM	90	N	NA
57	4519	60	m	Adult	Onset	46,XY,t(4;11)(q21;q23)[15]	*KMT2A::AFF1*	PB	80	Y	Y
58	4211	47	f	Adult	Onset	NA	*KMT2A::AFF1*	PB	95	Y	Y
59	44973	44	f	Adult	Onset	NA	*KMT2A::AFF1*	PB	95	Y	N
60	10739	28	m	Adult	Onset	NA	*KMT2A::AFF1*	BM	90	Y	N
61	32432	53	f	Adult	Onset	NA	*KMT2A::AFF1*	PB	90	Y	Y
62	32548	49	f	Adult	Onset	46,XX,t(4;11)(q21;q23)[2]/47,idem,+X[6]/46,XX[14]	*KMT2A::AFF1*	BM	90	Y	Y
63	4469	45	m	Adult	Onset	46,XY,del(9)(q?21q31-33)[9]/46,XY[11]	None	BM	95	N	NA
64	4593	65	m	Adult	Onset	47,XY,t(9;22)(q34-q11),+17[12]/46,XY[8]	*BCR::ABL1*	BM	31	N	NA
65	2082	61	m	Adult	Onset	46,XY[5]	None	BM	79	N	NA

NA: Not Available

o: onset

r: relapse

f: follow-up (months from onset)

Table S2: List of differentially expressed genes (DEGs) identified in SEM^{AK_7_3} KD cells vs. SEM^{NC} cells.

ENSG	baseMean	log2FoldChang	pvalue	padj	DEG	chr	start	end	genetype	genename	description
ENSG00000230629.2	5520.809995	0.573149293	1.13E-21	5.20E-18	up	chrX	70962964	70963293	processed_pseudogene	RPS23P8	ribosomal protein S23 pseudogene 8 [Source:HGNC Symbol;Acc:HGNC:35982]
ENSG00000233913.7	1110.36375	0.557876417	7.54E-07	0.000231771	up	chr5	168616352	168616996	processed_pseudogene	RPL10P9	ribosomal protein L10 pseudogene 9 [Source:HGNC Symbol;Acc:HGNC:35579]
ENSG00000224631.4	3433.007731	0.545300591	1.01E-15	9.32E-13	up	chr16	61055399	61055964	transcribed_processed_pseudogene	RPS27AP16	RPS27A pseudogene 16 [Source:HGNC Symbol;Acc:HGNC:36855]
ENSG00000185641.6	2508.916266	0.477410971	1.42E-05	0.00261244	up	chr5	116051917	116052289	processed_pseudogene	-	ribosomal protein S25 (RPS25) pseudogene
ENSG00000237550.7	11475.49028	0.47271254	1.46E-17	2.25E-14	up	chr15	82372196	82372916	transcribed_processed_pseudogene	-	ribosomal protein L9 pseudogene 9
ENSG00000198618.5	1299.779139	0.465022847	0.000212589	0.024500838	up	chr21	18857779	18858276	processed_pseudogene	PPIAP22	peptidylprolyl isomerase A pseudogene 22 [Source:HGNC Symbol;Acc:HGNC:17236]
ENSG00000242299.1	5878.938931	0.4512552	3.06E-11	2.01E-08	up	chr3	101576489	101576947	processed_pseudogene	RPS18P5	ribosomal protein S18 pseudogene 5 [Source:HGNC Symbol;Acc:HGNC:36287]
ENSG00000283498.1	2121.911046	0.417348706	0.001153605	0.094258632	up	chr5	118974586	118974670	miRNA	MIR1244-2	microRNA 1244-2 [Source:HGNC Symbol;Acc:HGNC:38321]
ENSG00000212802.4	5589.976572	0.40796142	7.04E-13	5.41E-10	up	chr6	12514110	12514724	processed_pseudogene	RPL15P3	ribosomal protein L15 pseudogene 3 [Source:HGNC Symbol;Acc:HGNC:21538]
ENSG00000233762.3	9851.889034	0.397436302	1.14E-16	1.32E-13	up	chr2	171517270	171517716	processed_pseudogene	RPS15P4	ribosomal protein S15 pseudogene 4 [Source:HGNC Symbol;Acc:HGNC:35712]
ENSG00000212664.5	1439.004704	0.392772336	3.94E-05	0.005857834	up	chr15	71341158	71341712	processed_pseudogene	RPL17P39	ribosomal protein L17 pseudogene 39 [Source:HGNC Symbol;Acc:HGNC:36427]
ENSG00000263266.2	8356.133979	0.377201539	4.28E-10	1.97E-07	up	chr17	28467822	28468406	processed_pseudogene	RPS7P1	ribosomal protein S7 pseudogene 1 [Source:HGNC Symbol;Acc:HGNC:17081]
ENSG00000235552.6	10539.25089	0.374502087	2.80E-10	1.43E-07	up	chr18	6462144	6463030	transcribed_processed_pseudogene	RPL6P27	ribosomal protein L6 pseudogene 27 [Source:HGNC Symbol;Acc:HGNC:36133]
ENSG00000137970.7	6520.069622	0.337926643	1.02E-10	5.88E-08	up	chr1	96678874	96679620	processed_pseudogene	RPL7P9	ribosomal protein L7 pseudogene 9 [Source:HGNC Symbol;Acc:HGNC:37028]
ENSG00000214389.2	4227.944595	0.334759063	5.32E-08	2.04E-05	up	chr7	98385801	98386584	processed_pseudogene	RPS3AP26	RPS3A pseudogene 26 [Source:HGNC Symbol;Acc:HGNC:36513]
ENSG00000125995.16	2403.926056	0.333444728	6.42E-05	0.008966798	up	chr20	35699272	35700984	protein_coding	ROMO1	reactive oxygen species modulator 1 [Source:HGNC Symbol;Acc:HGNC:16185]
ENSG00000232573.1	7488.850785	0.331584929	5.80E-10	2.43E-07	up	chr14	98972879	98973301	processed_pseudogene	RPL3P4	ribosomal protein L3 pseudogene 4 [Source:HGNC Symbol;Acc:HGNC:19805]
ENSG00000213741.11	28220.83339	0.319901121	1.15E-17	2.25E-14	up	chr14	49570984	49599164	protein_coding	RPS29	ribosomal protein S29 [Source:HGNC Symbol;Acc:HGNC:10419]
ENSG00000283041.1	4883.793667	0.311470912	1.23E-05	0.002372171	up	chr7	133034607	133035920	processed_pseudogene	-	eukaryotic translation elongation factor 1 gamma
ENSG00000115541.11	3103.512813	0.303351976	0.001146255	0.094258632	up	chr2	197500140	197503449	protein_coding	HSPE1	heat shock protein family E (Hsp10) member 1 [Source:HGNC Symbol;Acc:HGNC:5269]
ENSG00000240342.3	5353.216089	0.282292209	8.71E-06	0.001825949	up	chr12	118246084	118246962	processed_pseudogene	RPS2P5	ribosomal protein S2 pseudogene 5 [Source:HGNC Symbol;Acc:HGNC:31386]
ENSG00000071082.11	35562.70945	0.27879123	0.000207367	0.024500838	up	chr2	101002229	101024032	protein_coding	RPL31	ribosomal protein L31 [Source:HGNC Symbol;Acc:HGNC:10334]
ENSG00000142534.7	51313.51655	0.26397039	8.97E-07	0.000258453	up	chr19	49496365	49499708	protein_coding	RPS11	ribosomal protein S11 [Source:HGNC Symbol;Acc:HGNC:10384]
ENSG00000131469.15	23061.57424	0.253734519	1.94E-06	0.000470031	up	chr17	42998273	43002959	protein_coding	RPL27	ribosomal protein L27 [Source:HGNC Symbol;Acc:HGNC:10328]
ENSG00000173915.16	2459.366473	0.252089695	0.000849226	0.078298595	up	chr10	103389041	103396492	protein_coding	ATP5MK	ATP synthase membrane subunit k [Source:HGNC Symbol;Acc:HGNC:30889]
ENSG00000215030.5	6650.358576	0.244878994	1.40E-06	0.000357404	up	chr17	17383377	17384012	processed_pseudogene	RPL13P12	ribosomal protein L13 pseudogene 12 [Source:HGNC Symbol;Acc:HGNC:35701]
ENSG00000112695.13	3367.064058	0.231434304	0.00049581	0.049688763	up	chr6	75237675	75250323	protein_coding	COX7A2	cytochrome c oxidase subunit 7A2 [Source:HGNC Symbol;Acc:HGNC:2288]
ENSG00000165502.7	3632.416213	0.225688963	0.001165454	0.094258632	up	chr14	49618530	49620626	protein_coding	RPL36AL	ribosomal protein L36a like [Source:HGNC Symbol;Acc:HGNC:10346]
ENSG00000119705.10	2851.681663	0.224695467	0.000733445	0.070441238	up	chr14	77708071	77761104	protein_coding	SLIRP	SRA stem-loop interacting RNA binding protein [Source:HGNC Symbol;Acc:HGNC:20495]
ENSG00000135390.21	8695.439794	0.22437587	8.46E-06	0.001825949	up	chr12	53632726	53677408	protein_coding	ATP5MC2	ATP synthase membrane subunit c locus 2 [Source:HGNC Symbol;Acc:HGNC:842]
ENSG00000130255.13	15316.45198	0.214314711	1.77E-05	0.003024754	up	chr19	5674947	5691875	protein_coding	RPL36	ribosomal protein L36 [Source:HGNC Symbol;Acc:HGNC:13631]
ENSG00000100097.12	3558.690804	0.213424354	0.000712565	0.069892052	up	chr22	37675636	37679802	protein_coding	LGALS1	galectin 1 [Source:HGNC Symbol;Acc:HGNC:6561]
ENSG00000171858.18	17302.60394	0.213255297	1.08E-06	0.000291869	up	chr20	62387103	62388520	protein_coding	RPS21	ribosomal protein S21 [Source:HGNC Symbol;Acc:HGNC:10409]
ENSG00000110700.7	20783.67238	0.206848457	0.000480844	0.049259826	up	chr11	17074388	17077715	protein_coding	RPS13	ribosomal protein S13 [Source:HGNC Symbol;Acc:HGNC:10386]
ENSG00000149806.11	7414.140025	0.198786156	0.000150826	0.019314053	up	chr11	65120630	65122177	protein_coding	FAU	FAU ubiquitin like and ribosomal protein S30 fusion [Source:HGNC Symbol;Acc:HGNC:3597]
ENSG00000106153.13	7224.06562	0.193623196	0.000178374	0.022224425	up	chr7	56101573	56106476	protein_coding	CHCHD2	coiled-coil-helix-coiled-coil-helix domain containing 2 [Source:HGNC Symbol;Acc:HGNC:21645]
ENSG00000083845.9	20856.01162	0.184366239	1.66E-07	5.89E-05	up	chr19	58386400	58394806	protein_coding	RPS5	ribosomal protein S5 [Source:HGNC Symbol;Acc:HGNC:10426]
ENSG00000063177.13	20143.73015	0.174306246	5.33E-05	0.007682103	up	chr19	48615328	48619184	protein_coding	RPL18	ribosomal protein L18 [Source:HGNC Symbol;Acc:HGNC:10310]
ENSG00000019582.17	29250.38654	0.172509274	3.08E-05	0.004734462	up	chr5	150401637	150412969	protein_coding	CD74	CD74 molecule [Source:HGNC Symbol;Acc:HGNC:1697]
ENSG00000105372.8	22314.16042	0.171168268	8.00E-06	0.001825949	up	chr19	41860255	41872925	protein_coding	RPS19	ribosomal protein S19 [Source:HGNC Symbol;Acc:HGNC:10402]
ENSG00000204525.18	5622.30433	0.167445029	0.001149154	0.094258632	up	chr6	31268749	31272130	protein_coding	HLA-C	major histocompatibility complex, class I, C [Source:HGNC Symbol;Acc:HGNC:4933]
ENSG00000136942.15	22249.09302	0.159035651	9.85E-06	0.001974192	up	chr9	124857880	124861981	protein_coding	RPL35	ribosomal protein L35 [Source:HGNC Symbol;Acc:HGNC:10344]
ENSG00000234745.14	7545.360774	0.151670047	0.000904308	0.080170361	up	chr6	31353872	31367067	protein_coding	HLA-B	major histocompatibility complex, class I, B [Source:HGNC Symbol;Acc:HGNC:4932]
ENSG00000142676.14	40347.66902	0.151652065	2.31E-05	0.003670472	up	chr1	23691742	23696835	protein_coding	RPL11	ribosomal protein L11 [Source:HGNC Symbol;Acc:HGNC:10301]
ENSG00000104904.12	7836.776024	0.150786806	0.000872285	0.078847739	up	chr19	2269509	2273490	protein_coding	OAZ1	ornithine decarboxylase antizyme 1 [Source:HGNC Symbol;Acc:HGNC:8095]
ENSG00000178952.11	8413.90895	0.148516104	0.001212875	0.096402626	up	chr16	28842411	28846348	protein_coding	TUFM	Tu translation elongation factor, mitochondrial [Source:HGNC Symbol;Acc:HGNC:12420]
ENSG00000172809.13	15223.2909	0.141820711	0.000257216	0.028232502	up	chr17	74203582	74210655	protein_coding	RPL38	ribosomal protein L38 [Source:HGNC Symbol;Acc:HGNC:10349]
ENSG00000125691.14	28569.55426	0.141175366	0.000791899	0.074503108	up	chr17	38847860	38853764	protein_coding	RPL23	ribosomal protein L23 [Source:HGNC Symbol;Acc:HGNC:10316]
ENSG00000111348.9	18438.0354	0.14017984	0.000374502	0.040150046	up	chr12	14942031	14961728	protein_coding	ARHGDIB	Rho GDP dissociation inhibitor beta [Source:HGNC Symbol;Acc:HGNC:679]
ENSG00000149273.15	33730.67119	0.139021766	0.000149036	0.019314053	up	chr11	75399515	75422280	protein_coding	RPS3	ribosomal protein S3 [Source:HGNC Symbol;Acc:HGNC:10420]
ENSG00000167460.17	21304.4098	0.135709787	0.000200235	0.024291663	up	chr19	16067021	16103002	protein_coding	TPM4	tropomyosin 4 [Source:HGNC Symbol;Acc:HGNC:12013]
ENSG00000204628.12	30914.75723	0.130167074	0.000251379	0.028232502	up	chr5	181236897	181248096	protein_coding	RACK1	receptor for activated C kinase 1 [Source:HGNC Symbol;Acc:HGNC:4399]
ENSG00000144713.13	21243.08338	0.117845504	0.001155914	0.094258632	up	chr3	12834485	12841582	protein_coding	RPL32	ribosomal protein L32 [Source:HGNC Symbol;Acc:HGNC:10336]
ENSG00000263934.5	2255.170976	-0.378334944	0.000397301	0.041626345	down	chr17	19188016	19188714	snoRNA	SNORD3A	small nucleolar RNA, C/D box 3A [Source:HGNC Symbol;Acc:HGNC:33189]
ENSG00000200087.1	4694.170821	-0.459729741	0.000140222	0.019012412	down	chr1	28508559	28508762	snoRNA	SNORA73B	small nucleolar RNA, H/ACA box 73B [Source:HGNC Symbol;Acc:HGNC:10116]
ENSG00000263740.2	1014.267381	-0.56309123	1.76E-05	0.003024754	down	chr3	15738515	15738809	misc_RNA	RN7SL4P	RNA, 7SL, cytoplasmic 4, pseudogene [Source:HGNC Symbol;Acc:HGNC:10039]
ENSG00000202058.1	1464.414503	-0.731165223	1.92E-05	0.003153545	down	chr22	42565048	42565330	misc_RNA	RN7SKP80	RN7SK pseudogene 80 [Source:HGNC Symbol;Acc:HGNC:45804]
ENSG00000202538.1	1194.570537	-0.771421395	2.53E-07	8.34E-05	down	chr12	120291763	120291903	snRNA	RNU4-2	RNA, U4 small nuclear 2 [Source:HGNC Symbol;Acc:HGNC:10193]

Table S3: Functional enrichment analysis of identified DEGs.

Collection	Cluster	ID	Description	GeneRatio	BgRatio	pvalue	p.adjust	Count	geneID
GO-BP	up	GO:0002181	cytoplasmic translation	18/34	159/17116	1.92E-28	2.13E-25	18	RPS29/RPL31/RPS11/RPL27/RPL36/RPS21/RPS13/FAU/RPS5/RPL18/RPS19/RPL35/RPL11/RPL38/RPL23/RPS3/RACK1/RPL32
GO-BP	up	GO:0006412	translation	20/34	678/17116	5.69E-20	3.16E-17	20	RPS29/RPL31/RPS11/RPL27/RPL36AL/RPL36/RPS21/RPS13/FAU/RPS5/RPL18/RPS19/RPL35/RPL11/TUFM/RPL38/RPL23/RPS3/RACK1/RPL32
GO-BP	up	GO:0043043	peptide biosynthetic process	20/34	707/17116	1.30E-19	4.82E-17	20	RPS29/RPL31/RPS11/RPL27/RPL36AL/RPL36/RPS21/RPS13/FAU/RPS5/RPL18/RPS19/RPL35/RPL11/TUFM/RPL38/RPL23/RPS3/RACK1/RPL32
GO-BP	up	GO:0043604	amide biosynthetic process	20/34	839/17116	3.74E-18	1.04E-15	20	RPS29/RPL31/RPS11/RPL27/RPL36AL/RPL36/RPS21/RPS13/FAU/RPS5/RPL18/RPS19/RPL35/RPL11/TUFM/RPL38/RPL23/RPS3/RACK1/RPL32
GO-BP	up	GO:0006518	peptide metabolic process	20/34	861/17116	6.20E-18	1.38E-15	20	RPS29/RPL31/RPS11/RPL27/RPL36AL/RPL36/RPS21/RPS13/FAU/RPS5/RPL18/RPS19/RPL35/RPL11/TUFM/RPL38/RPL23/RPS3/RACK1/RPL32
GO-BP	up	GO:1901566	organonitrogen compound biosynthetic process	23/34	1712/17116	8.43E-16	1.56E-13	23	RPS29/RPL31/RPS11/RPL27/ATP5MK/RPL36AL/ATP5MC2/RPL36/RPS21/RPS13/FAU/RPS5/RPL18/RPS19/RPL35/RPL11/OAZ1/TUFM/RPL38/RPL23/RPS3/RACK1/RPL32
GO-BP	up	GO:0034645	cellular macromolecule biosynthetic process	20/34	1130/17116	1.20E-15	1.82E-13	20	RPS29/RPL31/RPS11/RPL27/RPL36AL/RPL36/RPS21/RPS13/FAU/RPS5/RPL18/RPS19/RPL35/RPL11/TUFM/RPL38/RPL23/RPS3/RACK1/RPL32
GO-BP	up	GO:0043603	cellular amide metabolic process	20/34	1135/17116	1.31E-15	1.82E-13	20	RPS29/RPL31/RPS11/RPL27/RPL36AL/RPL36/RPS21/RPS13/FAU/RPS5/RPL18/RPS19/RPL35/RPL11/TUFM/RPL38/RPL23/RPS3/RACK1/RPL32
GO-BP	up	GO:0042254	ribosome biogenesis	7/34	304/17116	1.86E-06	0.000229	7	RPL27/RPS21/RPS5/RPS19/RPL35/RPL11/RPL38
GO-BP	up	GO:0042255	ribosome assembly	4/34	59/17116	5.47E-06	0.000579	4	RPS5/RPS19/RPL11/RPL38
GO-BP	up	GO:0000028	ribosomal small subunit assembly	3/34	18/17116	5.73E-06	0.000579	3	RPS5/RPS19/RPL38
GO-BP	up	GO:0019883	antigen processing and presentation of endogenous antigen	3/34	25/17116	1.60E-05	0.001427	3	CD74/HLA-C/HLA-B
GO-BP	up	GO:0042274	ribosomal small subunit biogenesis	4/34	78/17116	1.67E-05	0.001427	4	RPS21/RPS5/RPS19/RPL38
GO-BP	up	GO:0022613	ribonucleoprotein complex biogenesis	7/34	469/17116	3.14E-05	0.002495	7	RPL27/RPS21/RPS5/RPS19/RPL35/RPL11/RPL38
GO-BP	up	GO:0006364	rRNA processing	5/34	224/17116	7.50E-05	0.005555	5	RPL27/RPS21/RPS19/RPL35/RPL11
GO-BP	up	GO:0002486	antigen processing and presentation of endogenous peptide antigen via MHC class I via ER pathway, TAP-independent	2/34	7/17116	7.99E-05	0.005555	2	HLA-C/HLA-B
GO-BP	up	GO:0002484	antigen processing and presentation of endogenous peptide antigen via MHC class I via ER pathway	2/34	8/17116	0.000106	0.006963	2	HLA-C/HLA-B
GO-BP	up	GO:0016072	rRNA metabolic process	5/34	263/17116	0.000159	0.009844	5	RPL27/RPS21/RPS19/RPL35/RPL11
GO-BP	up	GO:2001244	positive regulation of intrinsic apoptotic signaling pathway	3/34	61/17116	0.000238	0.013238	3	RPL11/RPS3/RACK1
GO-BP	up	GO:1904667	negative regulation of ubiquitin protein ligase activity	2/34	12/17116	0.00025	0.013238	2	RPL11/RPL23
GO-BP	up	GO:0048002	antigen processing and presentation of peptide antigen	3/34	62/17116	0.00025	0.013238	3	CD74/HLA-C/HLA-B
GO-BP	up	GO:2001242	regulation of intrinsic apoptotic signaling pathway	4/34	166/17116	0.000315	0.015273	4	CD74/RPL11/RPS3/RACK1
GO-BP	up	GO:0061844	antimicrobial humoral immune response mediated by antimicrobial peptide	3/34	69/17116	0.000343	0.015273	3	ROMO1/FAU/RPS19
GO-BP	up	GO:0046598	positive regulation of viral entry into host cell	2/34	14/17116	0.000343	0.015273	2	LGALS1/CD74
GO-BP	up	GO:0075294	positive regulation by symbiont of entry into host	2/34	14/17116	0.000343	0.015273	2	LGALS1/CD74
GO-BP	up	GO:0019885	antigen processing and presentation of endogenous peptide antigen via MHC class I	2/34	16/17116	0.000452	0.018779	2	HLA-C/HLA-B
GO-BP	up	GO:0042273	ribosomal large subunit biogenesis	3/34	76/17116	0.000456	0.018779	3	RPL35/RPL11/RPL38
GO-BP	up	GO:0031397	negative regulation of protein ubiquitination	3/34	82/17116	0.00057	0.022027	3	RPL11/RPL23/RPS3
GO-BP	up	GO:0002483	antigen processing and presentation of endogenous peptide antigen	2/34	18/17116	0.000574	0.022027	2	HLA-C/HLA-B
GO-BP	up	GO:1903321	negative regulation of protein modification by small protein conjugation or removal	3/34	92/17116	0.000797	0.029544	3	RPL11/RPL23/RPS3
GO-BP	up	GO:0051444	negative regulation of ubiquitin-protein transferase activity	2/34	22/17116	0.000863	0.030382	2	RPL11/RPL23
GO-BP	up	GO:0022618	ribonucleoprotein complex assembly	4/34	219/17116	0.000895	0.030382	4	RPS5/RPS19/RPL11/RPL38
GO-BP	up	GO:0140694	non-membrane-bounded organelle assembly	5/34	384/17116	0.000902	0.030382	5	RPS5/RPS19/RPL11/RPL38/RPS3
GO-BP	up	GO:1903902	positive regulation of viral life cycle	2/34	23/17116	0.000944	0.030874	2	LGALS1/CD74
GO-BP	up	GO:0071826	ribonucleoprotein complex subunit organization	4/34	227/17116	0.001022	0.03177	4	RPS5/RPS19/RPL11/RPL38
GO-BP	up	GO:1904666	regulation of ubiquitin protein ligase activity	2/34	24/17116	0.001029	0.03177	2	RPL11/RPL23
GO-BP	up	GO:0019882	antigen processing and presentation	3/34	104/17116	0.001137	0.033278	3	CD74/HLA-C/HLA-B
GO-BP	up	GO:1901796	regulation of signal transduction by p53 class mediator	3/34	104/17116	0.001137	0.033278	3	CD74/RPL11/RPL23
GO-BP	up	GO:0000027	ribosomal large subunit assembly	2/34	26/17116	0.001208	0.034447	2	RPL11/RPL38
GO-BP	up	GO:0019730	antimicrobial humoral response	3/34	109/17116	0.001302	0.0362	3	ROMO1/FAU/RPS19
GO-BP	up	GO:0034470	ncRNA processing	5/34	424/17116	0.001402	0.038018	5	RPL27/RPS21/RPS19/RPL35/RPL11
GO-BP	up	GO:0002474	antigen processing and presentation of peptide antigen via MHC class I	2/34	30/17116	0.001609	0.04161	2	HLA-C/HLA-B
GO-BP	up	GO:1901798	positive regulation of signal transduction by p53 class mediator	2/34	30/17116	0.001609	0.04161	2	RPL11/RPL23
GO-BP	up	GO:0051085	chaperone cofactor-dependent protein refolding	2/34	32/17116	0.00183	0.042479	2	HSPE1/CD74
GO-BP	up	GO:1902253	regulation of intrinsic apoptotic signaling pathway by p53 class mediator	2/34	32/17116	0.00183	0.042479	2	CD74/RPL11
GO-BP	up	GO:0043280	positive regulation of cysteine-type endopeptidase activity involved in apoptotic process	3/34	123/17116	0.001842	0.042479	3	HSPE1/RPS3/RACK1
GO-BP	up	GO:0031640	killing of cells of another organism	2/34	33/17116	0.001946	0.042479	2	ROMO1/RPS19
GO-BP	up	GO:0034599	cellular response to oxidative stress	4/34	271/17116	0.001961	0.042479	4	ROMO1/CHCHD2/RPS3/RACK1
GO-BP	up	GO:0000461	endonucleolytic cleavage to generate mature 3'-end of SSU-rRNA from (SSU-rRNA, 5.8S rRNA, LSU-rRNA)	1/34	1/17116	0.001986	0.042479	1	RPS21
GO-BP	up	GO:0034463	90S preribosome assembly	1/34	1/17116	0.001986	0.042479	1	RPL38
GO-BP	up	GO:0061481	response to TNF agonist	1/34	1/17116	0.001986	0.042479	1	RPS3
GO-BP	up	GO:1902546	positive regulation of DNA N-glycosylase activity	1/34	1/17116	0.001986	0.042479	1	RPS3
GO-BP	up	GO:2001235	positive regulation of apoptotic signaling pathway	3/34	129/17116	0.00211	0.04427	3	RPL11/RPS3/RACK1
GO-BP	down	GO:0000353	formation of quadruple SL/U4/U5/U6 snRNP	1/2	9/17116	0.001051	0.005958	1	RNU4-2
GO-BP	down	GO:0000365	mRNA trans splicing, via spliceosome	1/2	9/17116	0.001051	0.005958	1	RNU4-2
GO-BP	down	GO:0045291	mRNA trans splicing, SL addition	1/2	9/17116	0.001051	0.005958	1	RNU4-2
GO-BP	down	GO:0000244	spliceosomal tri-snRNP complex assembly	1/2	24/17116	0.002803	0.011911	1	RNU4-2
GO-BP	down	GO:0006396	RNA processing	2/2	1065/17116	0.003868	0.013152	2	SNORA73B/RNU4-2
GO-BP	down	GO:0000387	spliceosomal snRNP assembly	1/2	49/17116	0.005718	0.0162	1	RNU4-2
KEGG	up	hsa03010	Ribosome	18/26	134/8132	3.47E-27	1.56E-25	18	RPS29/RPL31/RPS11/RPL27/RPL36AL/RPL36/RPS21/RPS13/FAU/RPS5/RPL18/RPS19/RPL35/RPL11/RPL38/RPL23/RPS3/RPL32

Table S3: Functional enrichment analysis of identified DEGs.

KEGG	up	hsa05171	Coronavirus disease - COVID-19	18/26	216/8132	2.76E-23	6.21E-22	18	RPS29/RPL31/RPS11/RPL27/RPL36AL/RPL36/RPS21/RPS13/EFA
KEGG	up	hsa04612	Antigen processing and presentation	3/26	68/8132	0.001267	0.019006	3	CD74/HLA-C/HLA-B
KEGG	up	hsa05330	Allograft rejection	2/26	33/8132	0.004884	0.043545	2	HLA-C/HLA-B
KEGG	up	hsa05332	Graft-versus-host disease	2/26	36/8132	0.005793	0.043545	2	HLA-C/HLA-B
KEGG	up	hsa04940	Type I diabetes mellitus	2/26	39/8132	0.006774	0.043545	2	HLA-C/HLA-B
KEGG	up	hsa05320	Autoimmune thyroid disease	2/26	39/8132	0.006774	0.043545	2	HLA-C/HLA-B
KEGG	down	hsa03040	Spliceosome	1/1	157/8132	0.019306	0.019306	1	RNU4-2
MSIGDB-H	up	HALLMARK_MYC_TARGETS_V1	HALLMARK_MYC_TARGETS_V1	6/15	200/4350	3.10E-05	0.00031	6	HSPE1/RPS5/RPL18/TUFM/RPS3/RACK1
REACTOME	up	R-HSA-156902	Peptide chain elongation	17/29	87/10473	3.91E-29	1.84E-27	17	RPS29/RPL31/RPS11/RPL27/RPL36AL/RPL36/RPS21/RPS13/RPS5/RPL18/RPS19/RPL35/RPL11/RPL38/RPL23/RPS3/RPL32
REACTOME	up	R-HSA-192823	Viral mRNA Translation	17/29	87/10473	3.91E-29	1.84E-27	17	RPS29/RPL31/RPS11/RPL27/RPL36AL/RPL36/RPS21/RPS13/RPS5/RPL18/RPS19/RPL35/RPL11/RPL38/RPL23/RPS3/RPL32
REACTOME	up	R-HSA-156842	Eukaryotic Translation Elongation	17/29	90/10473	7.36E-29	1.84E-27	17	RPS29/RPL31/RPS11/RPL27/RPL36AL/RPL36/RPS21/RPS13/RPS5/RPL18/RPS19/RPL35/RPL11/RPL38/RPL23/RPS3/RPL32
REACTOME	up	R-HSA-2408557	Selenocysteine synthesis	17/29	91/10473	9.04E-29	1.84E-27	17	RPS29/RPL31/RPS11/RPL27/RPL36AL/RPL36/RPS21/RPS13/RPS5/RPL18/RPS19/RPL35/RPL11/RPL38/RPL23/RPS3/RPL32
REACTOME	up	R-HSA-72764	Eukaryotic Translation Termination	17/29	91/10473	9.04E-29	1.84E-27	17	RPS29/RPL31/RPS11/RPL27/RPL36AL/RPL36/RPS21/RPS13/RPS5/RPL18/RPS19/RPL35/RPL11/RPL38/RPL23/RPS3/RPL32
REACTOME	up	R-HSA-975956	Nonsense Mediated Decay (NMD) independent of the Exon Junction Complex (EJC)	17/29	93/10473	1.35E-28	2.30E-27	17	RPS29/RPL31/RPS11/RPL27/RPL36AL/RPL36/RPS21/RPS13/RPS5/RPL18/RPS19/RPL35/RPL11/RPL38/RPL23/RPS3/RPL32
REACTOME	up	R-HSA-72689	Formation of a pool of free 40S subunits	17/29	99/10473	4.30E-28	5.49E-27	17	RPS29/RPL31/RPS11/RPL27/RPL36AL/RPL36/RPS21/RPS13/RPS5/RPL18/RPS19/RPL35/RPL11/RPL38/RPL23/RPS3/RPL32
REACTOME	up	R-HSA-9633012	Response of EIF2AK4 (GCN2) to amino acid deficiency	17/29	99/10473	4.30E-28	5.49E-27	17	RPS29/RPL31/RPS11/RPL27/RPL36AL/RPL36/RPS21/RPS13/RPS5/RPL18/RPS19/RPL35/RPL11/RPL38/RPL23/RPS3/RPL32
REACTOME	up	R-HSA-156827	L13a-mediated translational silencing of Ceruloplasmin expression	17/29	109/10473	2.52E-27	2.76E-26	17	RPS29/RPL31/RPS11/RPL27/RPL36AL/RPL36/RPS21/RPS13/RPS5/RPL18/RPS19/RPL35/RPL11/RPL38/RPL23/RPS3/RPL32
REACTOME	up	R-HSA-1799339	SRP-dependent cotranslational protein targeting to membrane	17/29	110/10473	2.97E-27	2.76E-26	17	RPS29/RPL31/RPS11/RPL27/RPL36AL/RPL36/RPS21/RPS13/RPS5/RPL18/RPS19/RPL35/RPL11/RPL38/RPL23/RPS3/RPL32
REACTOME	up	R-HSA-72706	GTP hydrolysis and joining of the 60S ribosomal subunit	17/29	110/10473	2.97E-27	2.76E-26	17	RPS29/RPL31/RPS11/RPL27/RPL36AL/RPL36/RPS21/RPS13/RPS5/RPL18/RPS19/RPL35/RPL11/RPL38/RPL23/RPS3/RPL32
REACTOME	up	R-HSA-927802	Nonsense-Mediated Decay (NMD)	17/29	113/10473	4.86E-27	3.81E-26	17	RPS29/RPL31/RPS11/RPL27/RPL36AL/RPL36/RPS21/RPS13/RPS5/RPL18/RPS19/RPL35/RPL11/RPL38/RPL23/RPS3/RPL32
REACTOME	up	R-HSA-975957	Nonsense Mediated Decay (NMD) enhanced by the Exon Junction Complex (EJC)	17/29	113/10473	4.86E-27	3.81E-26	17	RPS29/RPL31/RPS11/RPL27/RPL36AL/RPL36/RPS21/RPS13/RPS5/RPL18/RPS19/RPL35/RPL11/RPL38/RPL23/RPS3/RPL32
REACTOME	up	R-HSA-2408522	Selenoamino acid metabolism	17/29	116/10473	7.82E-27	5.70E-26	17	RPS29/RPL31/RPS11/RPL27/RPL36AL/RPL36/RPS21/RPS13/RPS5/RPL18/RPS19/RPL35/RPL11/RPL38/RPL23/RPS3/RPL32
REACTOME	up	R-HSA-72613	Eukaryotic Translation Initiation	17/29	117/10473	9.14E-27	5.83E-26	17	RPS29/RPL31/RPS11/RPL27/RPL36AL/RPL36/RPS21/RPS13/RPS5/RPL18/RPS19/RPL35/RPL11/RPL38/RPL23/RPS3/RPL32
REACTOME	up	R-HSA-72737	Cap-dependent Translation Initiation	17/29	117/10473	9.14E-27	5.83E-26	17	RPS29/RPL31/RPS11/RPL27/RPL36AL/RPL36/RPS21/RPS13/RPS5/RPL18/RPS19/RPL35/RPL11/RPL38/RPL23/RPS3/RPL32
REACTOME	up	R-HSA-168273	Influenza Viral RNA Transcription and Replication	17/29	133/10473	9.26E-26	5.55E-25	17	RPS29/RPL31/RPS11/RPL27/RPL36AL/RPL36/RPS21/RPS13/RPS5/RPL18/RPS19/RPL35/RPL11/RPL38/RPL23/RPS3/RPL32
REACTOME	up	R-HSA-9711097	Cellular response to starvation	17/29	153/10473	1.13E-24	6.42E-24	17	RPS29/RPL31/RPS11/RPL27/RPL36AL/RPL36/RPS21/RPS13/RPS5/RPL18/RPS19/RPL35/RPL11/RPL38/RPL23/RPS3/RPL32
REACTOME	up	R-HSA-168255	Influenza Infection	17/29	154/10473	1.27E-24	6.83E-24	17	RPS29/RPL31/RPS11/RPL27/RPL36AL/RPL36/RPS21/RPS13/RPS5/RPL18/RPS19/RPL35/RPL11/RPL38/RPL23/RPS3/RPL32
REACTOME	up	R-HSA-9010553	Regulation of expression of SLITs and ROBOs	17/29	169/10473	6.61E-24	3.37E-23	17	RPS29/RPL31/RPS11/RPL27/RPL36AL/RPL36/RPS21/RPS13/RPS5/RPL18/RPS19/RPL35/RPL11/RPL38/RPL23/RPS3/RPL32
REACTOME	up	R-HSA-6791226	Major pathway of rRNA processing in the nucleolus and cytosol	17/29	179/10473	1.82E-23	8.85E-23	17	RPS29/RPL31/RPS11/RPL27/RPL36AL/RPL36/RPS21/RPS13/RPS5/RPL18/RPS19/RPL35/RPL11/RPL38/RPL23/RPS3/RPL32
REACTOME	up	R-HSA-8868773	rRNA processing in the nucleus and cytosol	17/29	189/10473	4.74E-23	2.20E-22	17	RPS29/RPL31/RPS11/RPL27/RPL36AL/RPL36/RPS21/RPS13/RPS5/RPL18/RPS19/RPL35/RPL11/RPL38/RPL23/RPS3/RPL32
REACTOME	up	R-HSA-72312	rRNA processing	17/29	199/10473	1.17E-22	5.19E-22	17	RPS29/RPL31/RPS11/RPL27/RPL36AL/RPL36/RPS21/RPS13/RPS5/RPL18/RPS19/RPL35/RPL11/RPL38/RPL23/RPS3/RPL32
REACTOME	up	R-HSA-376176	Signaling by ROBO receptors	17/29	216/10473	4.90E-22	2.08E-21	17	RPS29/RPL31/RPS11/RPL27/RPL36AL/RPL36/RPS21/RPS13/RPS5/RPL18/RPS19/RPL35/RPL11/RPL38/RPL23/RPS3/RPL32
REACTOME	up	R-HSA-72766	Translation	18/29	287/10473	1.18E-21	4.81E-21	18	RPS29/RPL31/RPS11/RPL27/RPL36AL/RPL36/RPS21/RPS13/RPS5/RPL18/RPS19/RPL35/RPL11/TUFM/RPL38/RPL23/RPS3/RPL32
REACTOME	up	R-HSA-71291	Metabolism of amino acids and derivatives	18/29	369/10473	1.13E-19	4.43E-19	18	RPS29/RPL31/RPS11/RPL27/RPL36AL/RPL36/RPS21/RPS13/RPS5/RPL18/RPS19/RPL35/RPL11/OAZ1/RPL38/RPL23/RPS3/RPL32
REACTOME	up	R-HSA-422475	Axon guidance	17/29	550/10473	3.98E-15	1.50E-14	17	RPS29/RPL31/RPS11/RPL27/RPL36AL/RPL36/RPS21/RPS13/RPS5/RPL18/RPS19/RPL35/RPL11/RPL38/RPL23/RPS3/RPL32
REACTOME	up	R-HSA-5663205	Infectious disease	20/29	942/10473	4.54E-15	1.65E-14	20	RPS29/RPL31/RPS11/RPL27/RPL36AL/RPL36/RPS21/RPS13/RPS5/RPL18/RPS19/HLA-C/RPL35/HLA-B/RPL11/TUFM/RPL38/RPL23/RPS3/RPL32
REACTOME	up	R-HSA-9675108	Nervous system development	17/29	575/10473	8.33E-15	2.93E-14	17	RPS29/RPL31/RPS11/RPL27/RPL36AL/RPL36/RPS21/RPS13/RPS5/RPL18/RPS19/RPL35/RPL11/RPL38/RPL23/RPS3/RPL32
REACTOME	up	R-HSA-8953854	Metabolism of RNA	17/29	667/10473	9.67E-14	3.29E-13	17	RPS29/RPL31/RPS11/RPL27/RPL36AL/RPL36/RPS21/RPS13/RPS5/RPL18/RPS19/RPL35/RPL11/RPL38/RPL23/RPS3/RPL32
REACTOME	up	R-HSA-2262752	Cellular responses to stress	17/29	772/10473	1.06E-12	3.48E-12	17	RPS29/RPL31/RPS11/RPL27/RPL36AL/RPL36/RPS21/RPS13/RPS5/RPL18/RPS19/RPL35/RPL11/RPL38/RPL23/RPS3/RPL32
REACTOME	up	R-HSA-8953897	Cellular responses to stimuli	17/29	784/10473	1.36E-12	4.33E-12	17	RPS29/RPL31/RPS11/RPL27/RPL36AL/RPL36/RPS21/RPS13/RPS5/RPL18/RPS19/RPL35/RPL11/RPL38/RPL23/RPS3/RPL32
REACTOME	up	R-HSA-9735869	SARS-CoV-1 modulates host translation machinery	7/29	34/10473	2.92E-12	9.02E-12	7	RPS29/RPS11/RPS21/RPS13/RPS5/RPS19/RPS3
REACTOME	up	R-HSA-1643685	Disease	21/29	1714/10473	3.15E-11	9.44E-11	21	RPS29/RPL31/RPS11/RPL27/RPL36AL/RPL36/RPS21/RPS13/RPS5/RPL18/RPS19/HLA-C/RPL35/HLA-B/RPL11/TUFM/RPL38/RPL23/RPS3/TPM4/RPL32
REACTOME	up	R-HSA-9754678	SARS-CoV-2 modulates host translation machinery	7/29	48/10473	3.89E-11	1.13E-10	7	RPS29/RPS11/RPS21/RPS13/RPS5/RPS19/RPS3
REACTOME	up	R-HSA-9705683	SARS-CoV-2-host interactions	10/29	189/10473	4.30E-11	1.22E-10	10	RPS29/RPS11/RPS21/RPS13/RPS5/RPS19/HLA-C/HLA-B/TUFM/RPS3
REACTOME	up	R-HSA-72695	Formation of the ternary complex, and subsequently, the 43S complex	7/29	49/10473	4.53E-11	1.25E-10	7	RPS29/RPS11/RPS21/RPS13/RPS5/RPS19/RPS3
REACTOME	up	R-HSA-72649	Translation initiation complex formation	7/29	56/10473	1.21E-10	3.16E-10	7	RPS29/RPS11/RPS21/RPS13/RPS5/RPS19/RPS3
REACTOME	up	R-HSA-72702	Ribosomal scanning and start codon recognition	7/29	56/10473	1.21E-10	3.16E-10	7	RPS29/RPS11/RPS21/RPS13/RPS5/RPS19/RPS3
REACTOME	up	R-HSA-72662	Activation of the mRNA upon binding of the cap-binding complex and eIFs, and subsequent binding to 43S	7/29	57/10473	1.38E-10	3.51E-10	7	RPS29/RPS11/RPS21/RPS13/RPS5/RPS19/RPS3
REACTOME	up	R-HSA-1266738	Developmental Biology	17/29	1070/10473	2.01E-10	5.00E-10	17	RPS29/RPL31/RPS11/RPL27/RPL36AL/RPL36/RPS21/RPS13/RPS5/RPL18/RPS19/RPL35/RPL11/RPL38/RPL23/RPS3/RPL32
REACTOME	up	R-HSA-9694516	SARS-CoV-2 Infection	10/29	285/10473	2.41E-09	5.86E-09	10	RPS29/RPS11/RPS21/RPS13/RPS5/RPS19/HLA-C/HLA-B/TUFM/RPS3
REACTOME	up	R-HSA-9692914	SARS-CoV-1-host interactions	7/29	93/10473	4.61E-09	1.09E-08	7	RPS29/RPS11/RPS21/RPS13/RPS5/RPS19/RPS3
REACTOME	up	R-HSA-392499	Metabolism of proteins	19/29	1915/10473	2.69E-08	6.24E-08	19	RPS29/RPL31/RPS11/RPL27/RPL36AL/RPL36/L/GALS1/RPS21/RPS13/RPS5/RPL18/RPS19/RPL35/RPL11/TUFM/RPL38/RPL23/RPS3/RPL32
REACTOME	up	R-HSA-9679506	SARS-CoV Infections	10/29	399/10473	6.03E-08	1.37E-07	10	RPS29/RPS11/RPS21/RPS13/RPS5/RPS19/HLA-C/HLA-B/TUFM/RPS3
REACTOME	up	R-HSA-9678108	SARS-CoV-1 Infection	7/29	139/10473	7.62E-08	1.69E-07	7	RPS29/RPS11/RPS21/RPS13/RPS5/RPS19/RPS3
REACTOME	up	R-HSA-1236977	Endosomal/Vacuolar pathway	2/29	11/10473	0.000401	0.00087	2	HLA-C/HLA-B
REACTOME	up	R-HSA-983170	Antigen Presentation: Folding, assembly and peptide loading of class I MHC	2/29	29/10473	0.00287	0.006098	2	HLA-C/HLA-B
REACTOME	up	R-HSA-2172127	DAP12 interactions	2/29	40/10473	0.00541	0.011263	2	HLA-C/HLA-B
REACTOME	up	R-HSA-909733	Interferon alpha/beta signaling	2/29	62/10473	0.012633	0.025771	2	HLA-C/HLA-B
REACTOME	up	R-HSA-5626978	TNFR1-mediated ceramide production	1/29	6/10473	0.016503	0.033007	1	RACK1
REACTOME	up	R-HSA-9013408	RHOG GTPase cycle	2/29	74/10473	0.017679	0.034678	2	HSPE1/ARHGDIB
REACTOME	up	R-HSA-877300	Interferon gamma signaling	2/29	88/10473	0.024466	0.047086	2	HLA-C/HLA-B
REACTOME	up	R-HSA-1236974	ER-Phagosome pathway	2/29	90/10473	0.025511	0.048187	2	HLA-C/HLA-B

Table S4: Primers used in RT-PCR and RT-qPCR experiments.

Primer name	Sequence	Map position (GRCh38/hg38)	References
AFF1_ex7_for	CTCAAATTCTCAGCAAGGAACG	chr4:87,094,943-87,094,964	
KMT2A_ex5_rev	TCCCATGGTAAGGCACTCAG	chr11:118,476,923-118,476,945	
AFF1_ex4_for	TGAAGTCCATTGTGTTGAAGAGA	chr4:87,084,134-87,084,156	
AK_7_3R	CCTAAGAATTGCTCATCGATG	back-splicing junction	
AK_7_3F	AAGGAACGTCATCGATGAGC	back-splicing junction	
KMT2A_4long_rev	AGCCACTTCTAGGTCTCCCA	chr11:118,471,687-118,471,706	
GAPDH_ for	GAAGGTGAAGGTCGGAGTCA	chr12:6,534,838-6,534,857	
GAPDH_ rev	GAAGATGGTGATGGGATTTC	chr12:6,536,766-6,536,785	
pre-GAPDH_for	CTGGGGGTAAGGAGATGCTG	chr12:6,645,547-6,645,566	
pre-GAPDH_rev	TTACCAGAGTTAAAAGCAGCCC	chr12:6,645,689-6,645,710	
KMT2A_ex3_for	GGTTTTGGCTCAGATGAAGAA	chr11:118,339,505-118,339,525	
AFF1_ex4_rev	TCTCTTCAACACAATGGACTTCA	chr4:87,084,134-87,084,156	
KMT2A_ex8_for	TACAGGACCGCCAAGAAAAG	chr11:118,482,013-118,482,032	
AFF1 exon 7-R	CGTTCCTTGCTGAGAATTTGAG	chr4:88,016,095-88,016,116	
FAU-F	CCAGGAGCTACACACCTTCG	chr11:65,121,774-65,121,793	doi: 10.21037/tcr.2019.05.05
FAU-R	GACTTGATCTTCCGGGGCAA	chr11:65,121,600-65,121,619	doi: 10.21037/tcr.2019.05.05
ROMO1-F	CTGTCTCAGGATCGGAATGCG	chr20:35,700,432-35,700,452	doi:10.1007/s11033-020-05702-1
ROMO1-R	CATCGGATGCCCATCCCAATG	chr20:35,700,882-35,700,902	doi:10.1007/s11033-020-05702-1
OAZ1-F	GGAACCGTAGACTCGCTCAT	chr19:2,273,168-2,273,187	doi:10.3390/medsci6020048
OAZ1-R	TCGGAGTGAGCGTTTATTTG	chr19:2,273,221-2,273,240	doi:10.3390/medsci6020048
COX7A2-F	CTATGGTTAGGAGCGCAAGC	chr6:75,243,864-75,243,883	doi:10.1007/s11060-017-2637-z
COX7A2-R	TTATCGTCCTCTGCCCAATC	chr6:75,241,235-75,241,254	doi:10.1007/s11060-017-2637-z

Table S5: NTA results for EVs isolated from cell lines.

Cell Line	Number of Vescicles (ul)	Mean (nm)	Std Dev (nm)	Mode	Std Dev (nm)
SEM	$6.42 * 10^8 \pm 3.68*10^7$	133.5	1.2	112.9	5
RS4;11	$4.39 * 10^8 \pm 2.4*10^7$	140.8	3.1	124.9	2.6

Table S6: GSEA Human Gene Sets of *KMT2A* target genes

GSEA Human Gene Set	*Systematic name*	*No. Genes*	*Source publication*	*Authors*
MULLIGHAN_MLL_SIGNATURE_1_DN	M18841	237	Pubmed: 17597811	Mullighan CG,Kennedy A,Zhou X,Radtke I,Phillips LA,Shurtleff SA,Downing JR
MULLIGHAN_MLL_SIGNATURE_1_UP	M17856	385		
MULLIGHAN_MLL_SIGNATURE_2_DN	M16867	278		
MULLIGHAN_MLL_SIGNATURE_2_UP	M3053	420		
GAUSSMANN_MLL_AF4_FUSION_TARGETS_A_DN	M1111	92	Pubmed: 17130830	Gaussmann A,Wenger T,Eberle I,Bursen A,Bracharz S,Herr I,Dingermann T,Marschalek R
GAUSSMANN_MLL_AF4_FUSION_TARGETS_A_UP	M1110	197		
GAUSSMANN_MLL_AF4_FUSION_TARGETS_B_DN	M9012	8		
GAUSSMANN_MLL_AF4_FUSION_TARGETS_B_UP	M14833	27		
GAUSSMANN_MLL_AF4_FUSION_TARGETS_C_DN	M1115	21		
GAUSSMANN_MLL_AF4_FUSION_TARGETS_C_UP	M1113	174		
GAUSSMANN_MLL_AF4_FUSION_TARGETS_D_DN	M527	9		
GAUSSMANN_MLL_AF4_FUSION_TARGETS_D_UP	M1801	38		
GAUSSMANN_MLL_AF4_FUSION_TARGETS_E_DN	M2039	22		
GAUSSMANN_MLL_AF4_FUSION_TARGETS_E_UP	M11319	98		
GAUSSMANN_MLL_AF4_FUSION_TARGETS_F_DN	M588	36		
GAUSSMANN_MLL_AF4_FUSION_TARGETS_F_UP	M8544	184		
GAUSSMANN_MLL_AF4_FUSION_TARGETS_G_DN	M11023	34		
GAUSSMANN_MLL_AF4_FUSION_TARGETS_G_UP	M18095	247		
SCHRAETS_MLL_TARGETS_DN	M1904	33	Pubmed: 12789274	Schraets D,Lehmann T,Dingermann T,Marschalek R
SCHRAETS_MLL_TARGETS_UP	M1902	33		
ROSS_LEUKEMIA_WITH_MLL_FUSIONS	M12695	79	Pubmed: 15226186	Ross ME,Mahfouz R,Onciu M,Liu HC,Zhou X,Song G,Shurtleff SA,Pounds S,Cheng C,Ma J,Ribeiro RC,Rubnitz JE,Girtman K,Williams WK,Raimondi SC,Liang DC,Shih LY,Pui CH,Downing JR
HESS_TARGETS_OF_HOXA9_AND_MEIS1_DN	M14829	84	Pubmed: 16507773	Hess JL,Bittner CB,Zeisig DT,Bach C,Fuchs U,Borkhardt A,Frampton J,Slany RK
HESS_TARGETS_OF_HOXA9_AND_MEIS1_UP	M1319	69		